RADIATION AND AEROSOL IN THE CONVECTIVE BOUNDARY LAYER

by

David Edward Warren, M.Sc. DIC

Submitted for the degree of Doctor of Philosophy
of the University of Edinburgh, February 1983

For the reasonings of mortals is unsure
and our designs are likely to fail....
We can hardly guess at what is on Earth
And what is at hand we find with labour
But who has traced out what is in the heavens?

Wisdom 9: 14,16

This thesis, which was composed by me, describes work that I carried out while a research student in the Department of Meteorology of the University of Edinburgh between October 1978 and November 1981.

TABLE OF CONTENTS

ACKNOWLEDGEMENTS

I should like to thank all the members of the Department of Meteorology for the assistance, encouragement and friendship they gave me while I was in Edinburgh, especially Keith Weston who supervised the work described in this thesis.

My thanks also to my family and friends who have continued to encourage me, in one way or another, during the over-lengthy process of writing-up; to Mrs Dorothy Trueland for typing and to the Natural Environment Research Council for financial support.

ABSTRACT

The daily evolution of the convective boundary layer is described and current ideas about the mechanisms by which the development proceeds are reviewed. Some parameterizations of the entrainment process are described and contrasted. The majority of these parameterizations are based on the turbulent kinetic energy budget applied either to the whole of the well mixed layer beneath the inversion at which the entrainment takes place, or at a single level just beneath the inversion. The underlying view of entrainment is that it proceeds by dissipating the turbulent kinetic energy which has not been dissipated by other processes within the mixed layer.

It is suggested that diabatic heating within the mixed layer caused by the absorption of incoming solar radiation, tends to stabilise the layer and modifies the rate at which turbulent kinetic energy is generated, thereby altering the rate at which entrainment deepens the mixed layer.

A much simplified model of the developing convective boundary layer is described and some of its implications are explored before describing a more detailed numerical model.

Comparison of the results of some integrations of the numerical model with various values of the parameters are then presented.

These show that the entrainment rate is reduced by the additional heating and that the effect is most marked in the early morning and late afternoon when the sun's elevation is low. This implies that when the boundary layer contains a high aerosol loading dispersion of the aerosol by the deepening of the layer is slower than would be inferred from studies of the unpolluted boundary layer.

LIST OF SYMBOLS

a_{oz}	ozone path length
a_{wv}	scaled water vapour path length
A	entrained heat flux ratio for a non-turbid layer
A'	entrained heat flux ratio for a turbid layer
b	aerosol backscattering coefficient
c_p	specific heat of dry air at constant pressure
C_u, C_θ	drag coefficient and heat transfer coefficient
$C_{uN}, C_{\theta N}$	turbulent transfer coefficients in neutral stability
D	soil damping depth
E(z)	water vapour flux
E_T, E_L	sensible and latent energy content of the mixed layer
F_r, F_f	direct and diffuse solar irradiance at top of mixed layer
g	acceleration due to gravity; aerosol asymmetry factor
G	geostrophic wind speed
G(z)	heat flux within the soil
$G(\tau,\mu)$	normalised shortwave global irradiance in a Rayleigh atmosphere
h(t)	depth of the mixed layer
H(z)	sensible heat flux
$I(\tau,\mu,\phi)$	diffuse solar radiance
$I^+(\tau), I^-(\tau)$	hemispheric integrals of shortwave irradiance
$I_o(\lambda)$	solar spectral irradiance at the top of the atmosphere
J(z)	initial soil temperature profile
k	thermal conductivity of the soil
k	fraction of buoyancy generated turbulent kinetic energy dissipated by entrainment
ℓ	scaled water vapour path length
L	Monin Obukhov length scale
L(z)	downward infra-red irradiance

m	air mass number
$p(z)$	atmospheric pressure
$p(\mu,\phi;\mu',\phi')$	aerosol scattering phase function
$P(Re,Pr)$	Zilitinkevich's function defining temperature difference between earth's surface and height z_o
Pr	Prandtl number
r_s	albedo of the surface
R	gas constant for dry air
Re	Reynolds number
Ri	Richardson number
R_N	net radiation at the surface
Si	shortwave irradiance at the top of the mixed layer
$S(z)$	net shortwave irradiance
$S(\tau)$	function defined by Chandrasekhar (see appendix)
t	time
$t(\ell)$	longwave transmittance of the mixed layer
T	temperature
u_i	velocity fluctuations
U_i	mean velocity components
u_*	friction velocity
w	angular frequency
w_o	aerosol single scattering albedo
w_*	free convection scaling velocity
z_o	roughness length
z_*	height at which turbulent heat flux vanishes
$Z(\tau,\mu)$	function defined by Chandrasekhar (see appendix)

β	Bowen ratio
γ	potential temperature gradient
Γ	dry adiabatic lapse rate
δ	solar declination
$\Delta\theta$	potential temperature jump at the top of the mixed layer
Δq	water-vapour mixing ratio jump at the top of the mixed layer
ϵ	ratio of sensible heat flux to absorbed solar energy at surface
ζ	non-dimensional height z/h
$\theta(z)$	potential temperature
θ_*	convective scaling temperature
κ	von Karman's constant
κ	thermal diffusivity of the soil
λ	wavelength
μ	cosine of the solar zenith angle
ν	kinematic viscosity of dry air
ρ	density of dry air
σ	Stefan's constant
σ_w	vertical velocity variance
τ	optical depth
$\tau_R(\lambda)$	optical depth in a Rayleigh atmosphere
ϕ_u, ϕ_θ	diabatic influence functions for momentum and heat
Φ	latitude
ψ_u, ψ_θ	integrated stability functions for momentum and heat

Subscripts (unless otherwise defined)

a refers to the value of a variable at the top of the surface layer

d refers to the value of a variable at the bottom of the soil layer

m refers to the value of a variable in the mixed layer

s refers to the value of a variable at the earth's surface

CHAPTER 1

INTRODUCTION

1.1 THE CONVECTIVE BOUNDARY LAYER

The exchange of momentum, heat and water-vapour between the surface of the earth and the free atmosphere is carried out across the Planetary Boundary Layer by a number of physical mechanisms whose relative importance changes over the course of twenty-four hours as a result of varying conditions in the atmosphere and the underlying soil. The response of the boundary layer to changes in external conditions is complex and may modify those conditions; for example, the development of convective cloud within the boundary layer depends on the depth of the layer and on the temperature and moisture at the surface. Once such cloud has formed its presence alters the radiation balance at the surface, which in turn affects not only the surface fluxes of temperature and moisture but also the subsequent development of the layer.

Over the past quarter of a century, a great deal of effort has been expended in studying the development of the atmospheric boundary layer and the physical processes which are responsible for that development. This interest has been stimulated partly by the importance to general circulation models of accurate parameterizations of the energy and momentum transfers from the surface to the free atmosphere.

Models designed to reproduce observational results using fundamental theory are, of necessity, solved numerically. Deardorff (1974) describes a three-dimensional numerical model of the boundary layer which explicitly calculates turbulence quantities for all scales greater than the grid spacing. The model covers an area 5 km square

to a height 2 km above the surface, with a resolution of about 10 m. Even on one of the faster computers available, the time integration of this model ran roughly ten times slower than nature itself.

Fortunately it has proved to be possible to use much simpler parameterizations profitably in studying and attempting to understand individual processes and in predicting larger-scale details.

The present work describes a theoretical study of the effect of heating a convectively mixed layer throughout its depth, rather than just at the surface. The motivation for such a study arises from considering the radiative divergence across the planetary boundary layer, in particular on occasions when the lower atmosphere carries a large aerosol loading. Under such conditions the solar irradiance at the surface is reduced and therefore the surface heating of the boundary layer is lessened. If, as actually happens, the aerosol predominantly absorbs rather than scatters the sunlight, it will warm the air directly, so that it is possible that there will be little net effect on the air temperature. However, if the aerosol is distributed uniformly with height, the direct heating will be greatest at the top of the absorbing layer. This will increase the static stability of the layer and inhibit the turbulence which is directly responsible for the deepening of the convective boundary layer, and for maintaining the well mixed profiles.

A simple one-dimensional boundary layer model is described and the effects of radiative divergence are included. This model is used to study the effect that varying the aerosol loading has on the development of a convective boundary layer (CBL), during the daytime.

After describing the physical processes that are of importance

in the boundary layer and the typical course of its diurnal evolution this first chapter describes some recent experimental results which have been reported in the literature and concludes with a review of boundary layer modelling, noting especially those attempts to include the effects of radiation in the simpler types of model, and some of the conclusions that have been drawn from such studies.

Chapter 2 describes some results that have been obtained from a very simple analytic model which, while being quite unrealistic, in that all of the external parameters are held constant, illustrates the effects of diabatic heating throughout the layer and allows the effect of individual mechanisms to be easily appreciated.

A more realistic model is described in the following chapter. This model is intended to to reproduce the behaviour of the convective boundary layer with a realistic aerosol loading over the course of the daylight hours. The results obtained from this detailed model are presented and discussed in the final chapter.

1.2 DIURNAL DEVELOPMENT OF THE CBL

The atmospheric boundary layer is that part of the atmosphere which is modified within a few hours by vertical transfers of heat, momentum and moisture from the surface. This very general definition may be usefully applied in all conditions, although in the vicinity of cumulo nimbus towers it may imply that the whole of the troposphere is included in the boundary layer. It should be pointed out that the depths of the boundary layers for heat, moisture and momentum need not be the same, but that in convective conditions vertical transfer is limited by a stable layer the base of which defines the top of the

boundary layers for each of these quantities.

For much of the time the atmospheric boundary layer is characterised by a turbulent flow, in contrast to the free atmosphere above where the flow is laminar. The major exception to this occurs at night when the air near the earth's surface is stable, turbulence is suppressed and any vertical exchange with the surface is limited to the lowest 100 m or so.

During the daytime when the surface heat flux is sufficiently large turbulent motions generated within the boundary layer might be expected to result in potential temperature, water-vapour mixing ratio and wind velocity profiles which are very nearly constant with height, except very close to the surface. Observations are most likely to be in accord with these notions about the idealised well-mixed layer if they are made at a site with a uniform, flat ground surface extending to a distance upwind which is several times the height at which the highest measurement is to be made. Light steady winds and a cloudless sky assist in easing the interpretation of such observations.

A typical tropospheric temperature sounding is slightly stable to dry ascent, so that mixing a layer adiabatically to a uniform potential temperature will result in a discontinuity of potential temperature at the top of the mixed layer, the air above being warmer. Observations show that convective boundary layers are normally capped by temperature inversions or stable layers. The conditions described above, appropriate for the formation of convective layers, are associated with anticyclonic conditions. The subsidence to be expected in an anticyclone will tend to intensify the potential temperature difference across the capping layer as well as inhibiting the deepening

of the mixed layer.

Figure 1.1 illustrates these features over a period of twenty-four hours. By midnight a nocturnal surface inversion has developed beneath the mixed layer in the period since the surface heat flux changed sign shortly before sunset. The potential temperature above this surface inversion layer is still very nearly independent of height. The water-vapour profile is not so well mixed. The mixed layer of the previous day had reached a depth of about 1250 m. The air above this height is much drier than that below, having a relative humidity of 20% compared to 60% lower down. The potential temperature distribution shows a similar feature. The air above 1250 m is 8 K warmer than that below.

By 0325 local time the depth of the mixed layer has decreased to about 1100 m due to large scale subsidence, and the surface inversion has intensified and deepened from 150 m to 300 m as the surface has continued to cool by long-wave radiative loss. The cooling of the surface, the deepening of the surface inversion layer and the decrease in the depth of the 'old' mixed layer continue until 0610 at least. It is apparent from the sounding that the cooling of the lowest 100 m or so has been sufficient to saturate the air with formation of fog reported. By 0900 the surface has started to warm up and a new mixed layer has formed, although it has only reached a depth of 50 m. The dispersion of the previous day's mixed layer continued at higher levels. Between 0900 and midday the convection increases, the overnight inversion layer is destroyed and a new mixed layer develops to a height of 1100 m. The surface temperature increases more rapidly than that of the mixed layer and a super-adiabatic layer forms close to the ground.

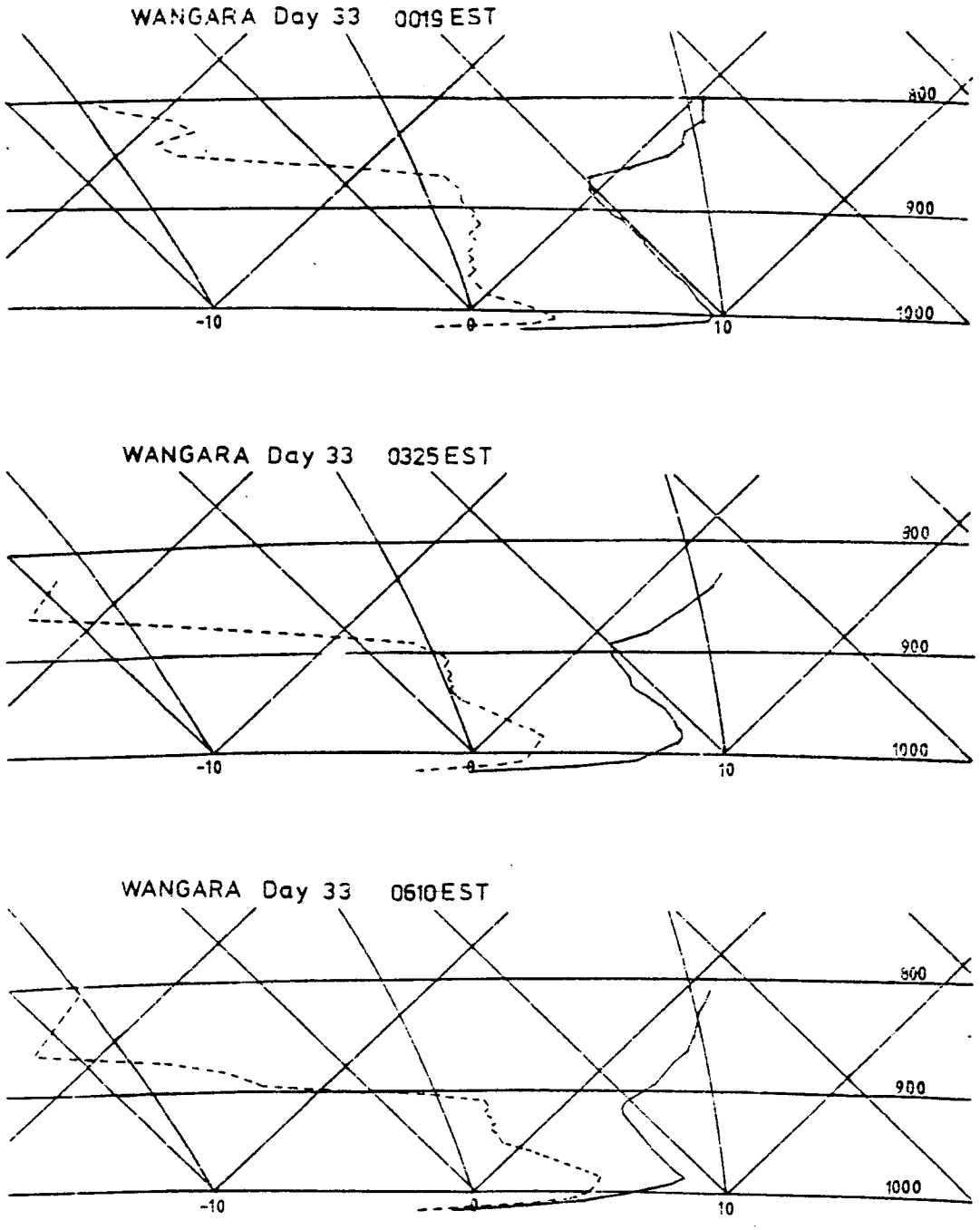

Figure 1.1 Convective Boundary Layer Development. Temperature (——) and humidity (---) soundings at three hourly intervals. (Drawn from data published by Clarke et al, 1971)

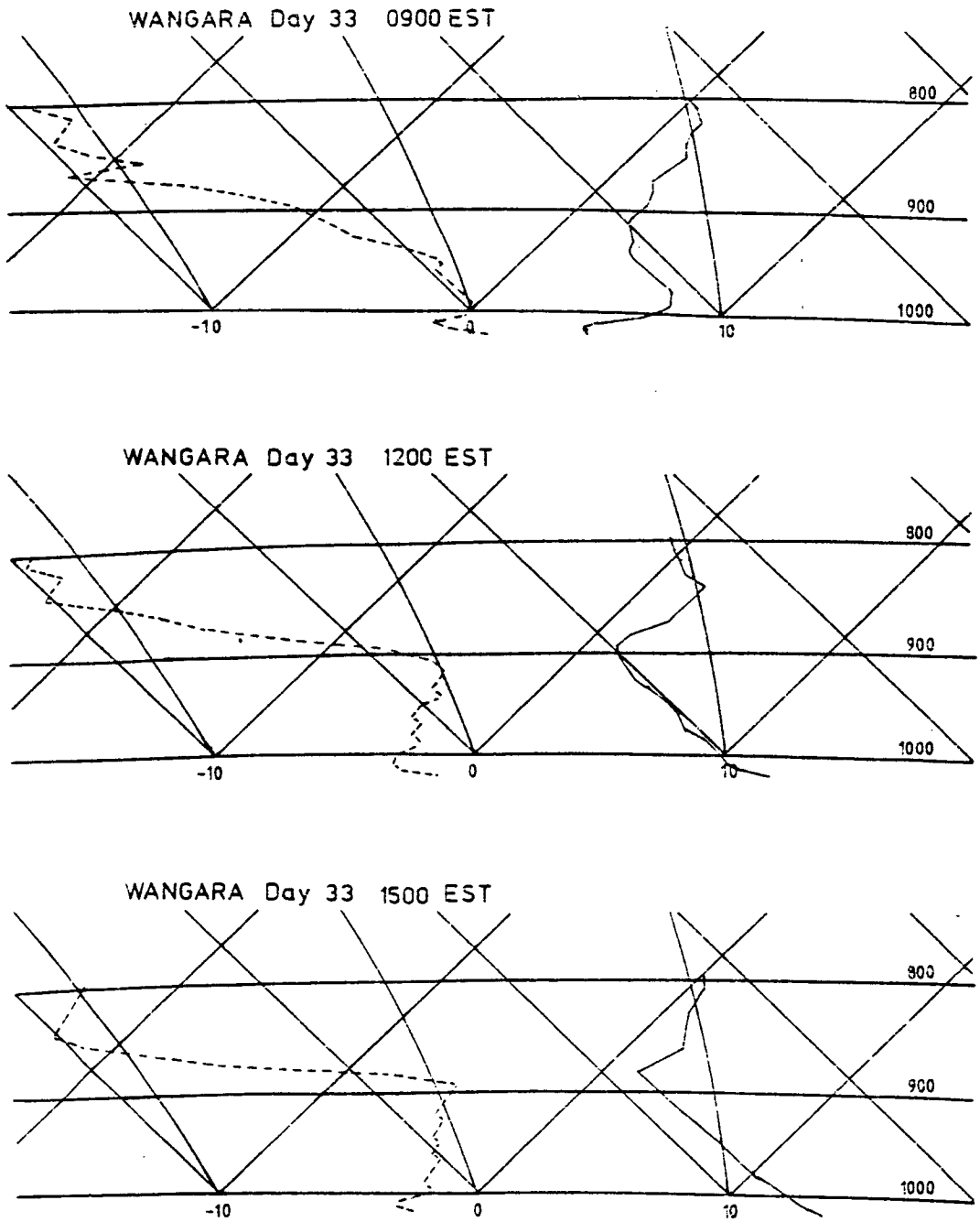
WANGARA Day 33 0900 EST
800
900
1000
-10
0
10
WANGARA Day 33 1200 EST
800
900
1000
-10
0
10
WANGARA Day 33 1500 EST
800
900
1000
-10
0
10

Figure 1.1

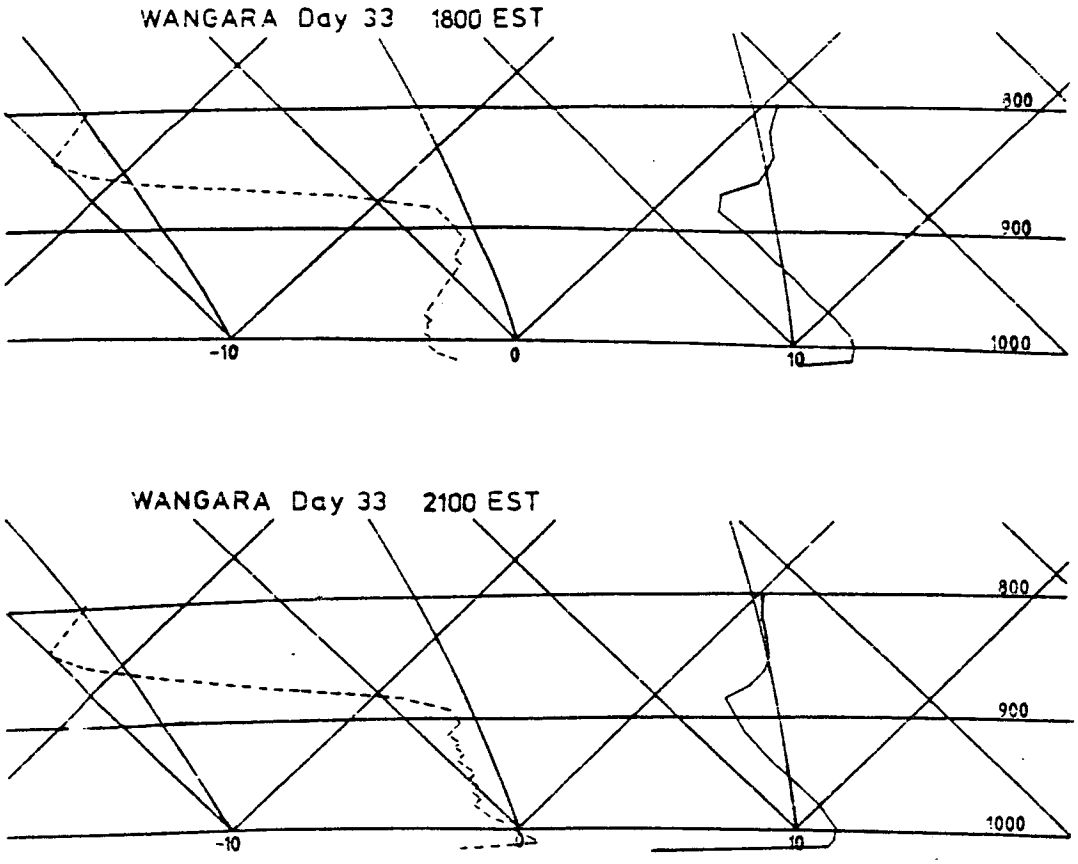
WANGARA Day 33 1800 EST
800
900
1000
-10
0
10
WANGARA Day 33 2100 EST
800
900
1000
-10
0
10

Figure 1.1

In fact the lowest level represented in these soundings is the screen height, and the true surface temperature is likely to be higher than the screen temperature while the surface is warming and lower while the surface is cooling off.

The warming and deepening of the mixed layer continue until some time between 1500 and 1800 after which the surface begins to cool and the surface inversion layer is re-established. This is already evident in the 1800 sounding and even more dramatically in that made at 2100.

1.3 RADIATION

a) Solar Radiation

The basic energy input to the Earth-Atmosphere system is short-wave radiation from the sun. In passing through the atmosphere, and the boundary layer in particular, absorption by water-vapour and carbon-dioxide are important in modifying the existing temperature profile and in reducing the radiant energy incident at the surface. Over the troposphere as a whole the estimated heating rate by short wave radiation absorption is of the order of 1 K day^{-1} (Lacis and Hansen, 1974). Various estimates of the shortwave convergence across the boundary layer have been made. Direct measurements and indirect estimates range from 20 - 80 Wm^{-2} across layers of between one and three kilometres deep, which correspond to a heating rate of from 0.5 to 6.0 K day^{-1} (Glazier, Monteith and Unsworth, 1976).

Diffuse reflection of the incoming solar radiation at the earth's surface depends predominantly on the nature of the surface. This may of course vary seasonally as the vegetation grows and decays and as the moisture content of the soil varies. There is also a variation of

the surface reflectance depending on the zenith angle of the sun. The variation is largest over water whose surface is undisturbed. For shortwave radiation incident nearly normally the reflection coefficient is about 5%; this increases to more than 30% as the angle of incidence increases to 80° or more.

Most natural surfaces have albedos of 20 - 30%. The shortwave radiation which is absorbed by the surface, along with the absorbed longwave component, are balanced by a heat flux into the soil, which results in the soil warming up, turbulent fluxes of heat and moisture into the atmosphere and a longwave radiative emission from the surface.

Figure 1.2 represents the interactions between the various radiative processes which affect the development of the boundary layer. Both the long and shortwave radiation streams may be modified by material which is present within the boundary layer itself. Clouds are the most obvious examples. Convective cloud forms within the boundary layer in amounts which depend on the distribution of heat and moisture. The presence of cloud alters the net radiation at the earth's surface by changing both the solar and terrestrial components.

Modelling the interaction between the boundary layer and convective cloud will be difficult until a satisfactory parameterization is available to relate the cloud fraction to the temperature and moisture parameters. A parameterization of this type is described by Benoit (1976) in which the cloud fraction is related to the relative positions of the base of the capping inversion and the lifting condensation level of the surface air.

The primary effect of aerosol is to reduce the solar radiation reaching the ground and to warm the air directly. A secondary effect

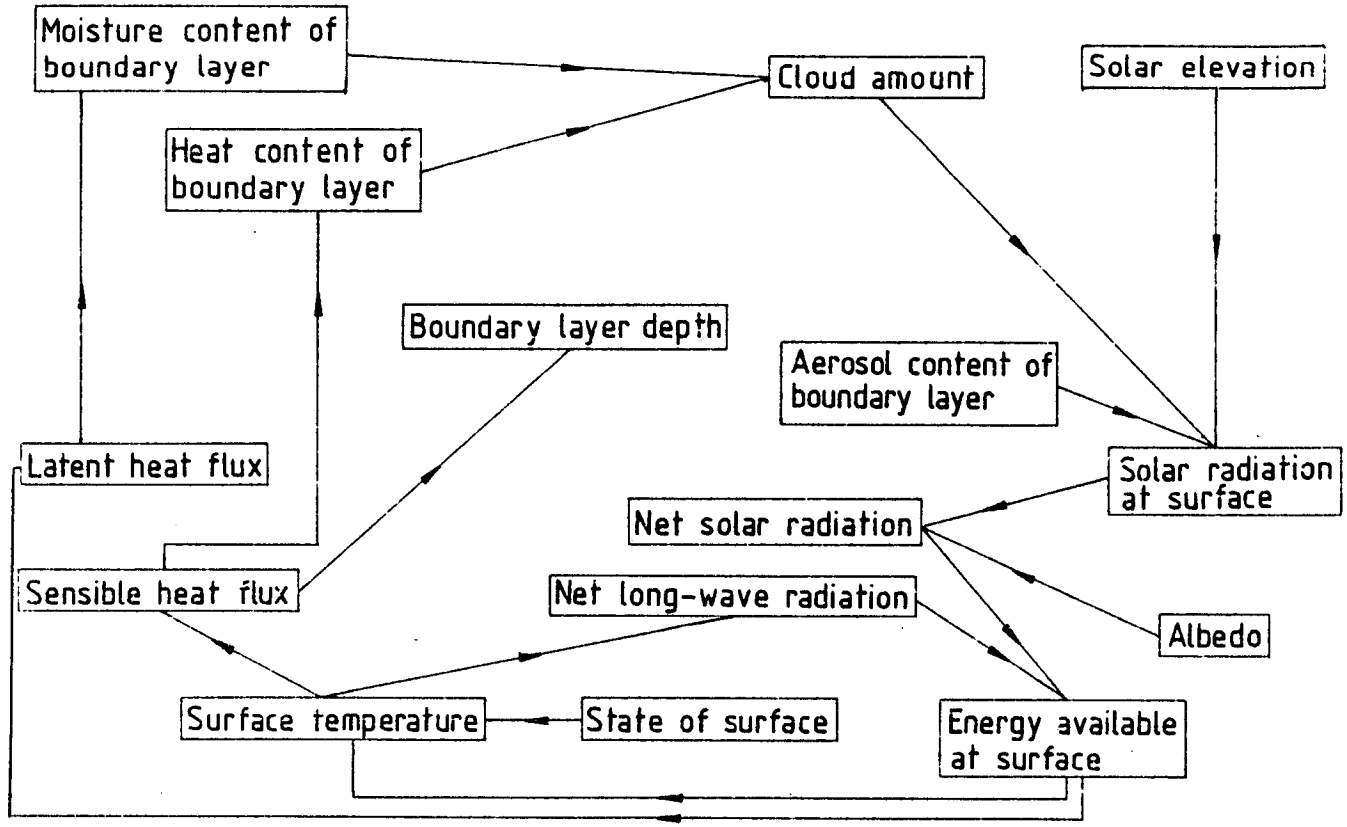

Figure 1.2 Interactions Between Radiation Streams and the Boundary Layer and Soil Surface. (after Smith and Carson, 1977)

is to modify entrainment at the base of inversion layer by increasing the stability of the mixed layer, thus reducing the amount of turbulent kinetic energy which is available to perform the entrainment. The primary aim of this study is to determine the relative importance of this mechanism in the growth of a convective boundary layer during the day.

b) Longwave Radiation

Most of the energy emitted by the sun, 97.6%, is radiated at wavelengths between 0.25 μm and 3 μm whereas at temperatures around 290 K, typical of the atmosphere and the surface of the earth, most of the energy radiated by a black-body is confined to wavelengths between 3 μm and 100 μm. Within this wavelength interval radiation from a gas arises from transitions in the rotational state of the radiating molecule. Only those constituents of the atmosphere which are composed of triatomic molecules radiate at these wavelengths; water-vapour, carbon-dioxide and ozone are the three most important atmospheric components in this respect. Water-vapour is the most abundant and is largely confined to the troposphere where it is the major source of longwave divergence. The longwave radiative cooling averaged over the troposphere amounts to 1 - 2 K day^{-1}, although in the lowest few hundreds of metres the cooling is about twice this value.

The surfaces of the earth and of lakes and seas behave very nearly as black-bodies in the longwave region of the spectrum. The emissivity of most bare soil or rock varies from 0.9 to 0.95 depending on its exact constitution. A surface covered by vegetation has a longwave emissivity of 0.93 - 0.99 and water surfaces have emissivities greater than 0.99.

1.4 TURBULENCE

The vertical transfers of momentum, heat and moisture within the atmospheric boundary layer, and in particular the entrainment of air which occurs at the base of the capping inversion, are mediated by the turbulent motion within the layer, a feature which distinguishes the boundary layer from the free atmosphere above, in which the flow is largely laminar.

Because of the complexity of a complete mathematical description of turbulent motions, various attempts have been made to parameterize the turbulent fluxes in terms of the appropriate gradient and empirically determined coefficients of eddy diffusivity. The formulation is modelled on the theory of molecular diffusion; however, the coefficients of eddy diffusivity are functions of such things as the vertical gradients of temperature and wind-speed and although, in principle, the exchanges could be described in this way, the behaviour of the diffusion coefficients is complicated and their introduction is artificial without leading to any great simplifications.

By splitting the temperature, velocity and moisture fields each into a mean part, which is simply the mean-value over a "suitable" time interval, and a fluctuating part, which is the difference between the actual field and the mean part, the theoretical treatment of the turbulent flow is made much easier. Some physical justification for this partitioning can be found when the power spectrum of the motion displays a local minimum in the middle part of the frequency range. The frequency at which the minimum occurs provides a natural definition of the averaging time. The motions which contribute to the high-frequency end of the spectrum are considered to be the turbulent part

of the motion. In other cases the partition is, to a certain extent, arbitrary.

Splitting the fields in this way leads to equations describing the evolution of the mean fields which include a term involving the covariances of the turbulent fluctuations - the Reynolds stresses and the turbulent fluxes. An equation for the time derivative of these terms can be derived, but because of the non-linear advective term in the equation of motion, the resulting equation will involve third-order covariances. In principle this would lead to an infinite hierarchy of equations to be solved to completely describe a turbulent flow. In practice it is hoped that, in considering a particular situation, it will be possible to express the nth order covariances in terms of the (n-1)th order covariances. It may be that the covariances of sufficiently high order behave in a relatively simple fashion and that the details of the assumed relationship will not have too large an effect on the final results. Direct experimental data to justify this type of closure assumption are not available; the best that can be achieved is to justify the assumption a posteriori if the resulting predictions agree well with measured flows.

The specification of eddy diffusion coefficients is equivalent to parameterizing the second order covariances in terms of the gradients of the mean-quantities.

Typical energy spectra of the velocity components in a convective boundary layer do not display a bi-modal form which could lead to a natural partition into mean and fluctuating parts. Mahrt (1979) suggested that in studying penetrative convection the buoyant plumes should be considered as part of the mean motion although they contribute

to the energy spectrum at all wavenumbers. He deems this to be necessary to properly account for the interaction of plumes with the smaller scales of motion which he feels may not be adequately described by the conventional energy cascade processes.

The budget of the turbulent kinetic energy, TKE, of a fluid is described by an equation derived from the momentum equation which may be written

$$\underset{\text{I}}{\frac{\partial}{\partial t}(\text{TKE})} = \underset{\text{IIa}}{-U_j\frac{\partial}{\partial x_j}(\text{TKE})} \underset{\text{IIb}}{-\frac{\partial}{\partial x_j}\overline{u_j(\text{TKE})}} \underset{\text{III}}{-\overline{u_i u_j}\frac{\partial U_i}{\partial x_j}} + \underset{\text{IV}}{\frac{g}{\Theta}\overline{\Theta' u_i}\,\delta_{i3}}$$

$$\underset{\text{V}}{-\frac{\partial}{\partial x_j}\left(\frac{1}{\rho}\overline{pu}_j\right)} + \underset{\text{VI}}{\nu\, u_i\frac{\partial^2 u_i}{\partial x_j^2}} \qquad \text{equation 1.1}$$

(See, for example Tennekes 1969, Turner 1973, Townsend 1956, etc.) where U_j represents the jth component of the mean velocity vector; u_j the turbulent fluctuation of the velocity; Θ and Θ' represent the mean and turbulent parts of the potential temperature field, g is the acceleration due to gravity and ν is the kinematic viscosity. The Boussinesq approximation has been made. The mean density is represented by ρ and fluctuations of pressure are represented by p. δ_{ij} is the Kronecker delta and the Einstein summation convention is implicit.

The details of the equation need not concern us. The rate of change of TKE of an element of the fluid (term I) is equated to the advection of TKE by the mean flow, IIa, and the turbulence, IIb; generation of TKE by shear in the mean wind field, III, by buoyancy, IV; transport by an interaction with the fluctuations of the pressure field, V, and dissipation of TKE by viscous forces, VI.

Experimental techniques for measuring the velocity and temperature of a fluid at frequencies high enough to resolve the turbulent fluctuations have become available during the last fifteen years and a small number of experiments have been carried out using these techniques to study the structure of the turbulence within the atmospheric boundary layer.

Two articles (Caughey and Wyngaard, 1979; Caughey and Palmer, 1979) describe the results from a series of measurements made over flat uniform surfaces, one in Minnesota, one at Ashchurch in Worcestershire, during convective conditions.

The magnitudes of the individual terms of the TKE budget are shown in Figure 1.3, scaled with respect to the depth, h (metres), of the convective layer and a convective scaling speed,

$$w_* = \left(h \frac{g}{T} \frac{H(o)}{\rho c_p} \right)^{1/3} \quad ms^{-1}$$

The function H(z) (Wm^{-2}) represents the vertical sensible heat flux at a height z metres above the surface. The specific heat, at constant pressure of dry air is denoted by c_p measured in units of J kg^{-1} K^{-1}. The combination g/T is a buoyancy parameter where T (K) is the absolute temperature.

The sites at which the measurements were made and the conditions at the time were horizontally homogeneous, so that the advection by the mean flow is zero and only the vertical divergences in terms IIb, III and V of the TKE equation are non-zero. The buoyancy production, mechanical generation, viscous dissipation and vertical transport were all measured, and it was assumed that the local rate of change of TKE would be small compared to the other terms, except during the early

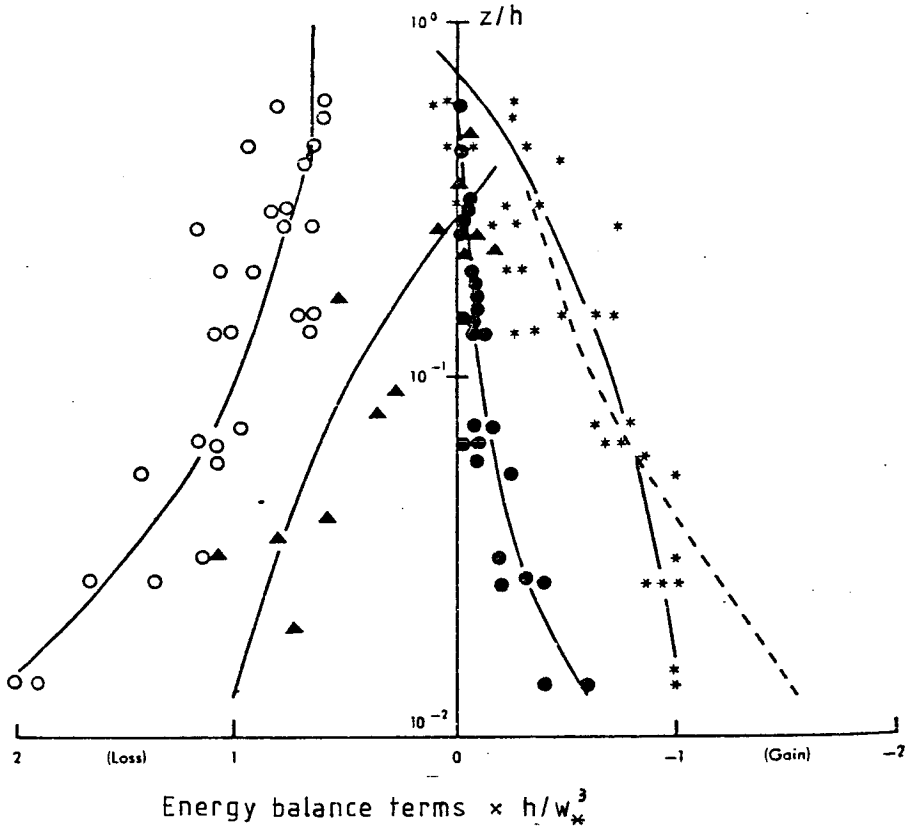

Figure 1.3 The Non-Dimensional Turbulent Kinetic Energy Budget in a Convective Boundary Layer. The measurements were made at two sites under a variety of unstable conditions. The buoyancy production (✱), mechanical production (●) vertical transport (▲) and viscous dissipation (o) were all measured. The residue is represented by the dashed line. (from Caughey and Wyngaard, 1979)

morning and late afternoon when convection was beginning or dying away.

The buoyancy production decreases upwards becoming negative somewhere above 0.5 h, although above 0.1 h the scatter of the data points become larger. Certainly towards the level of the inversion the effect of entrainment becomes evident. This can be seen very clearly in the profile of the temperature variances shown in Figure 1.4. The mechanical production term also decreases with height being half the size of the buoyancy generation term at the lowest level and more or less vanishing above 0.1 h.

The viscous dissipation was estimated from the slope of the spectrum of the vertical velocity fluctuations between 0.1 and 1 Hz which was assumed to be the inertial subrange. The viscous dissipation is greatest closest to the surface, above about 0.3 h it is very nearly constant up to the inversion base. This is more obvious in Figure 1.5. The imbalance in the measured terms was identified with the pressure transport term.

The turbulent heat flux can be calculated from a series of simultaneous measurements of the air temperature and velocity components. The vertical heat flux deduced from measurements of this kind made during the experiments at Ashchurch and in Minnesota are shown in Figure 1.6 together with aircraft measurements made some years earlier in an unrelated experiment described by Lenschow (1970). The heat fluxes are normalised by the surface heat flux and the heights are expressed as fractions of the mixed layer depth. There is a close agreement between the two profiles in the lower part of the mixed layer, notwithstanding the large scatter of the measurements in what is, after all, a turbulent fluid.

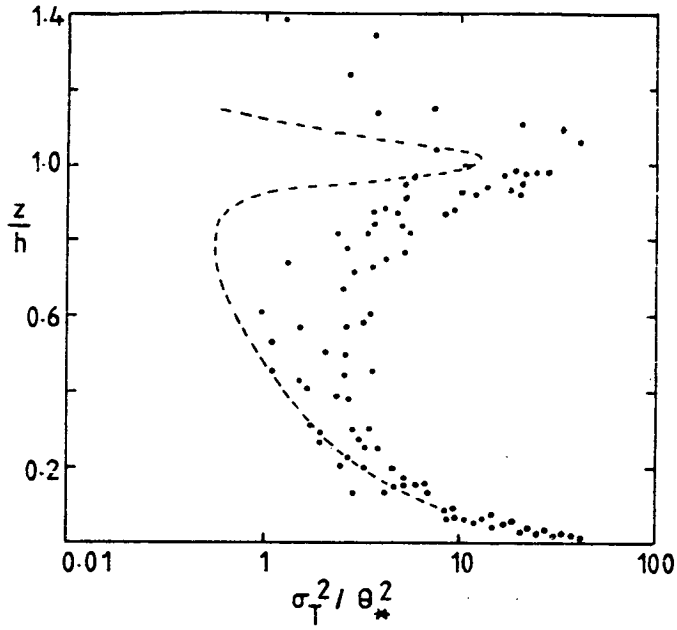

Figure 1.4 The Non-Dimensional Temperature Variance Within the Convective Boundary Layer.
The dashed line represents the results from a numerical simulation by Willis and Deardorff (1974).
(from Caughey and Palmer 1979)

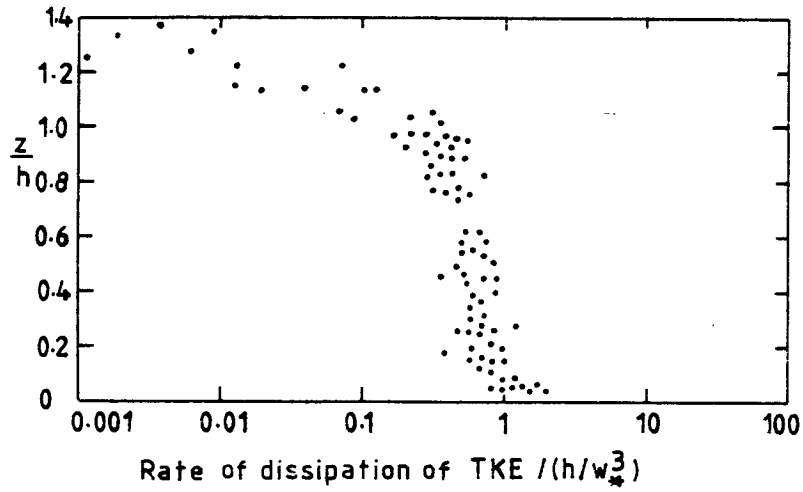

Figure 1.5 The Non-Dimensional Rate of Dissipation of Turbulent Kinetic Energy
(from Caughey and Palmer 1979)

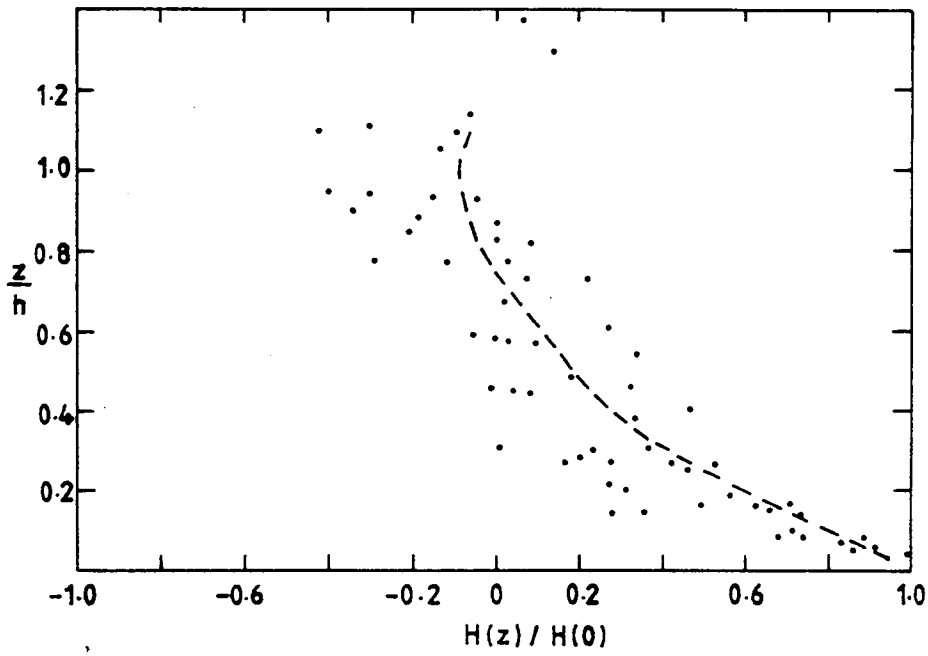

Figure 1.6 The Vertical Turbulent Heat Flux Measured during the Minnesota and Ashchurch Experiments (•). The dashed line represents the measurements made by Lenschow (1970). (From Caughey and Palmer 1979)

The heat flux changes sign near to a height of 0.8 h and the entrained heat flux at the top of the layer is between 10% and 30% of the flux at the surface. However, the flux profile departs significantly from a linear form.

1.5 TURBULENT ENTRAINMENT AT THE TOP OF THE CONVECTIVE BOUNDARY LAYER

The mixed layer deepens by entraining warmer drier air from above the capping inversion into the turbulent air below. The details of the process are difficult to observe directly and must be inferred from observation of their overall effects. The turbulent flow within the boundary layer is critical. Indeed there are other well known situations (jets and plumes) where a turbulent flow which is confined to a part of an otherwise laminar fluid increases in extent by entraining the laminar fluid. The turbulence may be generated either mechanically, as in a jet or by buoyancy, as in a plume. However the presence of the capping inversion makes an important difference.

In the boundary layer the smaller scale turbulent eddies, generated mainly by buoyancy, which maintain the well-mixed profiles beneath the inversion, deepen the mixed layer at the expense of the inversion layer but do little to entrain air from above the inversion. This mechanism is the same as that by which jets and plumes entrain their environments, but a different process is needed to account for the rise of the inversion layer.

Readings et al (1973) and Carson (1973) suggested a two-stage mechanism as a result of a case-study of a convective boundary layer. They proposed that rising thermals which have diameters much larger than the depth of the inversion layer deform and stretch it

rather than break through. In stretching, the inversion layer becomes thinner, decreasing the local Richardson number until it is likely that Kelvin-Helmholtz billows will form and grow, entraining air into the inversion layer from above and below.

The combination of the intermittent thickening of the inversion layer and the continual erosion at its lower boundary allows the mixed layer to deepen. The thickness of the inversion layer obviously depends on the difference in the rates at which the two processes proceed. One of the earliest theoretical studies of the way the convective layer grows during the daytime was carried out by Ball (1960). The influence this paper has had on both theoretical and observational studies is considerable. In Ball's study the lower atmosphere is represented by a layer of uniform potential temperature, Θ_m, which extends from the surface to a height h. The inversion layer is represented by a discontinuity, $\Delta\Theta$, in the potential temperature at h. Above the discontinuity the potential temperature is linear, $\Theta(z)=\theta_o+\theta z$. There are only two unknowns in this very simple model of dry convection, namely Θ_m and H. One equation involving the time derivatives of both unknowns and the model parameters can be easily obtained by considering the sensible heat budget of the mixed layer. To derive a second equation, Ball started with the budget of turbulent kinetic energy (TKE), which may be written schematically as

$$\text{Change in storage} = \text{advection} + \text{mechanical generation} + \text{buoyant generation} - \text{dissipation}$$

Ball assumed that the change in the storage term was small enough over a few hours to be neglected. Since the surface layer is the only region in which there is appreciable wind-shear, mechanical generation

of TKE is limited to the lowest 10 metres or so and therefore this component of the TKE budget is injected in the form of eddies of a relatively small scale. Thermal generation on the other hand is effective throughout the convective layer and will therefore generate eddies on a larger scale, of the order of 100 m.

Viscous dissipation is most effective at small scales and, following a suggestion made by Taylor in 1952, Ball supposed that the small-scale, mechanically-generated TKE is dissipated locally by viscosity. Then the thermal component of the TKE must be destroyed in increasing the potential energy of the mixed layer by entraining warm air from above.

If all of the thermally generated TKE is dissipated in this way then the downward heat flux across the inversion is equal in magnitude to the upward sensible heat flux at the surface. If, conversely, all the thermally-generated TKE is dissipated by viscous forces, there will be no entrainment and no entrained heat flux. Between these two extremes an entrainment coefficient or flux ratio, A, may be defined

$$A = - H(h)/H(o)$$

where H(z) is the vertical, sensible heat flux at height z.

It is relatively easy to estimate the mean value of the flux ratio over a period from observations of the changes in the potential temperature profile.

Carson (1973) used data from the Wangara experiment (Clarke et al, 1971) to examine the way in which the flux ratio varies during the day. He found that once the convection had started, about one hour after sunrise a well-mixed layer formed, but that it grew only slowly

until the nocturnal inversion had been eroded and during that time the flux ratio was close to zero. Afterwards the flux ratio increased until the surface heat flux was close to its maximum when the entrained flux was approximately half the magnitude of the surface flux. This period when the flux ratio is at its greatest lasted from about noon until about 1600 local time. Subsequently, with the surface heating decreasing, the mixed layer ceased to deepen and the flux ratio was again close to zero. Finally the surface heat flux changed sign and the nocturnal inversion was re-established from the surface.

The profile of the vertical heat transfer within the mixed layer is more-or-less linear. Such a profile is needed to maintain the uniform potential temperature. The flux ratio is then reflected in the height at which the vertical heat flux changes sign.

Rayment and Readings, in the case-study already referred to, estimated the mean flux ratio over the period when the surface heat flux was directed upwards to be approximately $\frac{1}{4}$, but during the period when the inversion was rising, between 1038 and 1334 GMT, the flux ratio was 0.4. Another study by Cattle and Weston (1975) obtained values of 0.29 and 0.31 for the flux ratio on two occasions between 1000 GMT and about 1400 GMT. Many other estimates of the flux ratio have been published. The range of values is from 0.04 (Lenschow, 1973) to 0.9 (Lenschow and Johnson, 1968), but the vast majority fall between 0.1 and 0.3.

In general the fluxes are not measured directly but evaluated from the change in the potential temperature profile. The mean value of the entrained heat flux over a period of time is found from the temperature difference across the inversion and the change in the

depth of the mixed layer. Any heat source within the mixed layer, in particular radiative convergence, will result in an overestimate of the surface heat flux and an underestimate of the flux ratio.

Since about 1970, it has become possible to measure turbulent fluxes directly. Observations reported by Caughey and Kaimal (1977) show that about an hour before sunset, when the surface heat flux is decreasing, the level at which the heat-flux profile changes sign descends to the surface in about fifteen minutes. This implies that the flux ratio increases dramatically as convection ceases. The simplest interpretation being that the entrained heat flux remains more-or-less constant as the surface flux decreases.

Curran (1978) proposed a model of the entrainment mechanism which differed from Rayment and Readings' version, but which elegantly explains Caughey and Kaimal's observation. Curran pointed out that it is normally assumed that the rate at which thermals thicken the inversion layer determines the rate at which entrainment proceeds and that there is sufficient small scale TKE within the mixed layer to erode the base of the inversion. In fact Rayment and Readings estimated the entrainment rate from statistics of the spatial distribution and frequency at which thermals arrived at the inversion. Curran postulated that it is the rate at which the lower boundary of the inversion layer is eroded which determines the overall rate of entrainment. He argued that since the major sources of TKE are found near the surface, the small scale eddies responsible for eroding the inversion must be transported vertically. The transport of TKE from the surface to the top of the mixed layer is analogous to the transport of heat or water-vapour and can be modelled by a diffusion process. Thus the TKE density

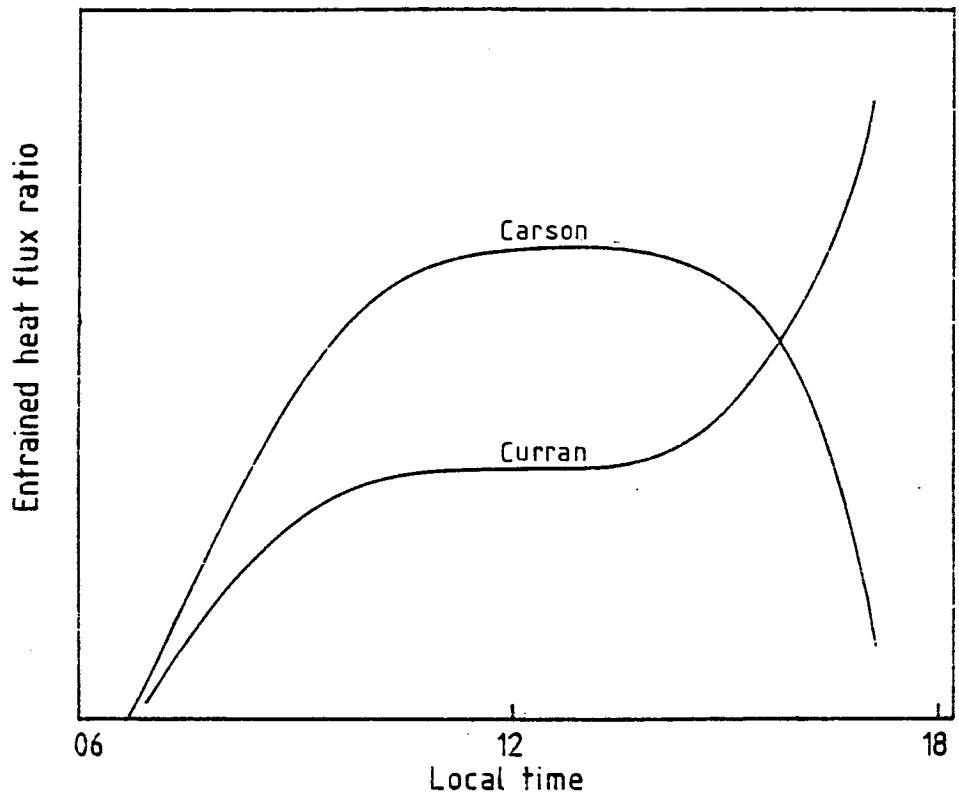

Figure 1.7 The Form of the Variation of the Entrained Flux Ratio According to Curran (1978) and Carson (1973).

at the top of the mixed layer is likely to be characteristic of the surface heat flux at some time previously. Curran estimated that the time lag would be up to about 45 minutes. During most of the day this will make little difference, but when the surface flux is changing quickly the effect on the flux ratio will be quite dramatic. When the surface heat flux decreases quickly the flux ratio will increase as observed by Caughey and Kaimal.

Although the models of the entrainment ratio proposed by Curran and Carson differ as dramatically as they do, predictions of the depth of the well-mixed layer, for example, are insensitive to which model is chosen because during the period when the difference between the predicted entrainment ratios is greatest, that is towards the sunset, the surface heat flux is small and decreasing, and consequently little further growth of the layer takes place.

Balls' model of dry convection was extended by Lilly (1968) to describe moist convection within a layer in which there is a complete cloud-deck immediately beneath the inversion layer. The inclusion of water-vapour and clouds necessitates a number of complications. Firstly, whereas the potential temperature is a measure of density and enthalpy in the dry model, when water-vapour is included two separate variables are needed, the virtual potential temperature as the density variable and the wet-bulb potential temperature as the enthalpy variable. Secondly the effect of the longwave radiative divergence at cloud-top is included as a discontinuity of the radiative flux profile, at the same height as the temperature discontinuity. The correct method of parameterizing this cloud-top radiative divergence has been the subject of a number of more recent papers (Kahn and Businger, 1979; Randall, 1980; Deardorff, 1980).

Lilly uses a closure hypothesis equivalent to Ball's and finds steady state solutions to the equations for a maximum entrainment condition, when the entrained flux of virtual potential temperature at the inversion is equal to that at the surface, and a minimum entrainment condition. The minimum entrainment condition in Ball's dry convection model implies that the entrained heat flux is zero. In the moist model Lilly requires that the flux of virtual potential temperature should have a minimum value of zero but that its integral over the layer should be positive. Such a condition includes the dry convection model as a special case.

Lilly compared the results of his model with observations of strato-cumulus capped convective layers which persist off the coast of California and in the South Atlantic. In both these areas the convective layers persist for days evolving only slowly; any growth of the layer beneath the inversion is suppressed by the subsidence induced by the subtropical anticyclones, on whose flanks these systems form.

The steady state solutions obtained demonstrated that, in this case at least, the predicted growth of the convection layer is not very sensitive to the entrainment assumption.

Reference has already been made to Deardorff's three-dimensional model (Deardorff, 1974) of the boundary layer. Having successfully simulated the evolution of the lower atmosphere during Day 33 of the Wangara experiment by reproducing the temperature, and humidity profiles observed every three hours and the wind profiles measured every hour, Deardorff used the model to investigate the structure of the atmosphere in greater detail than is practical in making the observations. For example the model can provide profiles of the vertical

turbulent fluxes with a vertical resolution of the order of 100 m at each six second time step. In this sense this particular model is almost a tool for analysis rather than prediction. The simulated mixed layer depth for Day 33 was summarised in the same paper by means of a "rate-equation".

An alternative method of parameterizing the entrained heat flux was suggested by Manins and Turner (1978). They proposed that the ratio of the increase in the potential energy of the mixed layer due to redistribution of the original density profile to the total potential energy made available by surface heating is more "physically relevant" than the flux ratio most commonly used. It is easy to show that for dry convection this approach is equivalent to the more conventional treatment. However Manins and Turner maintain that their definition permits an interpretation which is in better accord with the observed facts. Their objection to the use of the energy ratio is that it implies that fumigation of the mixed layer is impossible since the entrained heat is wholly and solely responsible for heating the air between the base of the inversion and the level at which the heat flux changes sign.

This seems to be an unnecessarily rigid interpretation of the flux ratio parameterization. However, it does seem that a potential energy formulation of the entrainment hypothesis might have advantages in practice, particularly when heat sources other than the surface heat flux are introduced. In studying the effect of radiative convergence within the mixed layer, it would seem to be reasonable to regard the instantaneous effect of the radiative heating as being to modify the initially well-mixed potential temperature profile; TKE is then dissipated in remixing the modified profile, thus reducing the TKE available

for entrainment. It seems that this scheme fits quite naturally into the potential energy ratio defined by Manins and Turner.

An attempt to model the entrained heat flux at the inversion in a more general manner was made in a series of articles by Tennekes (1973), Zilitenkevich (1975) and Zeman and Tennekes (1977). Their strategy was to parameterize each term in the TKE budget for a level just below the inversion in terms of a scaling velocity and a length scale.

The divergence terms of the turbulent kinetic energy budget (terms IIb and V of equation 1.1) were treated together. Observations of homogeneous shear flows show that the pressure correlation term $\overline{pw}/\rho$ is directly proportional to the third order mean velocity product $\overline{w\ TKE}$. The square root of the variance of the vertical velocity fluctuations, σ_w, is taken as a scaling velocity and the depth of the mixed layer is used as a length scale so that the divergence term is

$$\frac{\partial}{\partial z}\left(\overline{w\ TKE} + \frac{\overline{pw}}{\rho} \right)\Bigg|_{z=h} = C_D \frac{\sigma_w^3}{h}$$

The storage term, I, is modelled by taking $(\frac{1}{h}\frac{dh}{dt})^{-1}$ as the appropriate time scale for the change in the TKE, and since the rate at which the mixed layer deepens is equal to $H(h)/\rho c_p \Delta\theta$ the term is expressed as

$$\left(\frac{d\ \overline{TKE}}{dt} \right)_{z=h} = C_T \frac{1}{h} \frac{H(h)}{\rho c_p} \frac{\sigma_w^2}{\Delta\theta}$$

If the length scale for the viscous dissipation is proportional to h, then the parameterized expression for term VI can be included in that for the divergence term. Modelling of the dissipation of TKE in increasing the potential energy of the mixed layer by entraining warm air downwards is less simple. Zeman and Tennekes used the distance, d, thermals

overshoot into the stable air. If $\Delta\Theta$ is small this distance is determined largely by the potential temperature gradient γ in the stable air

$$d = \sigma_w/(g\gamma/T)^{\frac{1}{2}}$$

If, alternatively, the overshoot is determined by the potential temperature difference across the inversion, then $d \sim \sigma_w^2/(\Delta\Theta g/T)$.

When mechanical generation of TKE at the top of the mixed layer is small, that is to say when there is little or no wind-shear across the inversion, then σ_w is proportional to the free convection scaling velocity $w_* = (g/T)h\ H(o)/\rho c_p)^{1/3}$; and by substituting this for σ_w and rearranging the parameterized TKE equation, the heat flux ratio can be written

$$-\frac{H(h)}{H(o)} = \frac{C_F + C_D\ h/d}{1 + C_T\ w_*^2/(h\Delta\Theta g/T)}$$

here the values of the three constants, C_F, C_D and C_T are determined from experimental measurements.

A similarly detailed expression for the entrainment velocity $w_e = dh/dt$ was derived by Stull (1973)

$$\frac{dh}{dt} = \frac{2\Theta_m}{gd\Delta\Theta}\ (c_1 w_*^3 + c_2 u_*^3 + c_3(\Delta u)^3 - GW)$$

where u_* is the friction velocity; Δu the difference in wind speed across the inversion layer and 'GW' represents the transport of TKE by gravity waves excited on the inversion.

A more comprehensive comaprison of four models of the heat flux ratio was carried out by Artaz and André (1980). By expressing each formulation in terms of a single non-dimensional variable

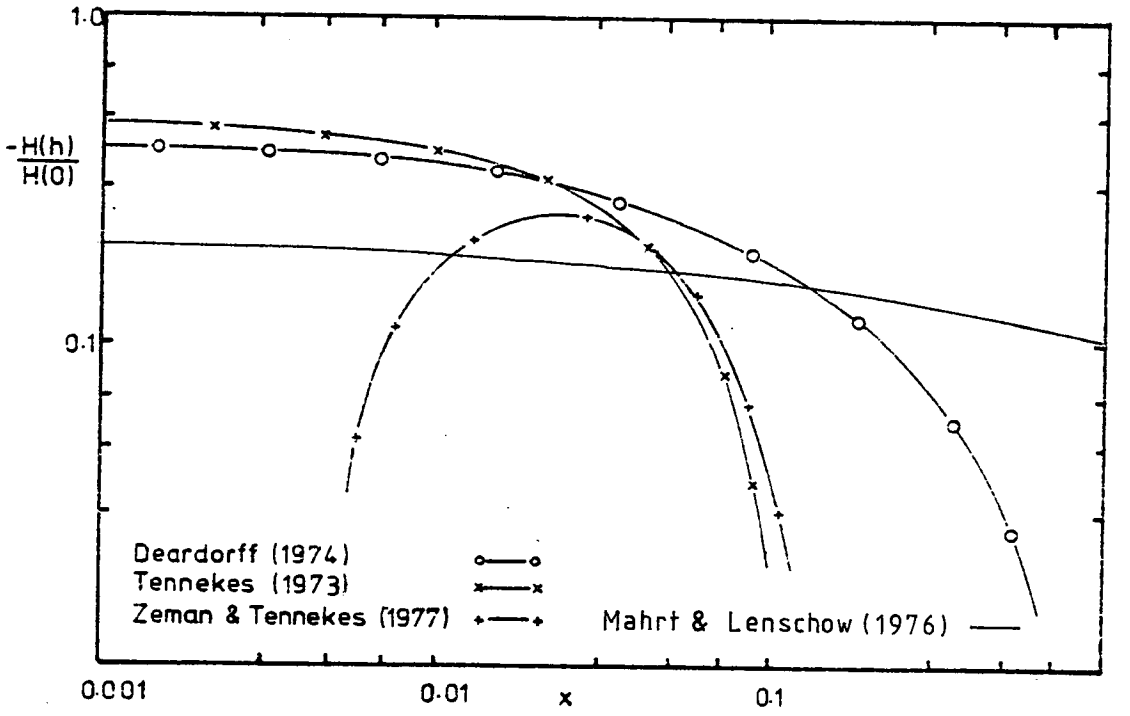

Figure 1.8 The Entrained Heat Flux Ratio Predicted from the Models of Tennekes (1973), Zeman and Tennekes (1977), Deardorff (1974) and Mahrt and Lenschow (1976). The similarity co-ordinate x is defined on page 35 (after Artaz and André, 1980).

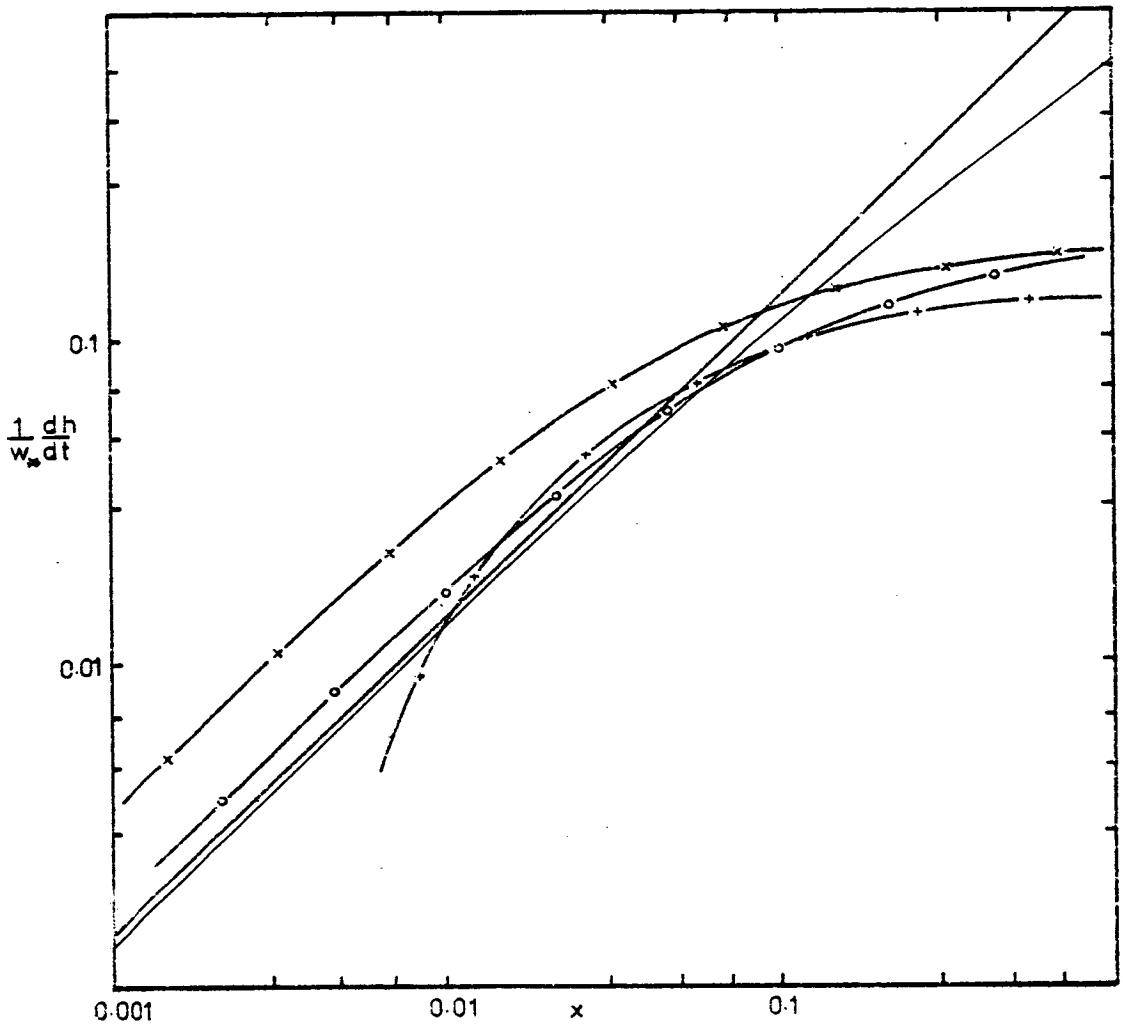

Figure 1.9 a) The Rate of Growth of the Mixed Layer Predicted by the Models Referred to in Figure 1.8. These theoretical results may be compared with atmospheric measurements plotted in Figure 1.9b.

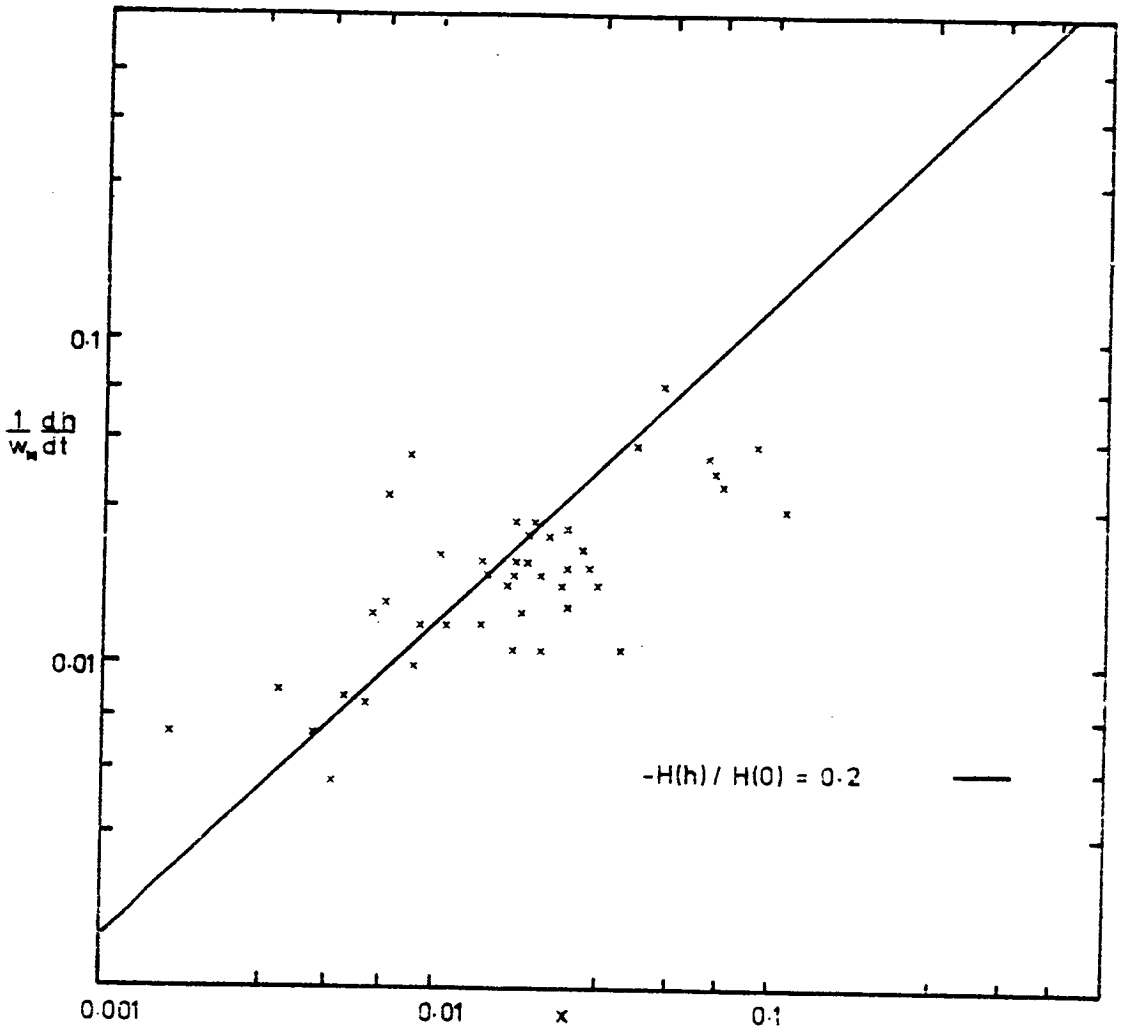

Figure 1.9 b) Atmospheric Measurements of the Mixed Layer Growth Rate
after Artaz and André (1980)

$x = \left[(H(o)/\rho c_p)^2/(\gamma^3 h^4 g/T)\right]^{1/3}$ they first of all compared the behaviour of different parameterizations one with another. Apart from five different versions of Zeman and Tennekes expression, Artaz and André include a result derived by Deardorff to summarise the results of a numerical simulation (Deardorff, 1974) and one due to Mahrt and Lenschow (1976), arrived at by considering the thermodynamic and TKE equations integrated from the earth's surface to a level well above the inversion layer.

The predicted heat flux ratios are shown in Figure 1.8. Apart from the constant heat flux ratio model there is a decrease in the ratio as the parameter x increases. It is also evident that the final form of Zeman and Tennekes' model decreases at small x as well. The resulting rates at which the mixed layer deepens are shown in Figure 1.9. The differences between each formulation are much less evident. Normally x has a value less than 0.1 and for predicting the growth of the mixed layer there is little to be gained from using anything more complicated than a constant entrainment flux ratio, although such a formulation cannot reproduce the decrease in the flux ratio which Artaz and André describe as the surface heat flux increases. This agrees very well with the findings reported by Dubosclard (1980). These consisted of comparisons of values of the entrainment flux ratio obtained from "sodar" measurements and concurrent temperature soundings with predictions deduced from the parameterizations of Zeman and Tennekes and that of Stull.

The results of these comparisons were inconclusive. When Stull's expression was compared with the observed values the correlation coefficient was high, 0.93, but the predictions were approximately half of the observed values.

The agreement between the observations and the values deduced from Zeman and Tennekes parameterization was not as good. The scatter was much larger, although the best fit line was more nearly of unit slope.

Of more interest was the correlation described by Dubosclard between the observed entrainment flux ratio and the ratio between the Monin-Obukhov length and the depth of the mixed layer. This demonstrates that when an appreciable fraction of the turbulent kinetic energy is generated mechanically the entrainment flux ratio is larger than would be expected in conditions of free convection. This effect is likely to be of importance particularly in the early morning and late afternoon when the buoyancy flux is most likely to be small.

1.6 AEROSOL

In the remainder of this work the aerosol in the boundary layer is characterised solely by its bulk optical properties. Here some representative measurements of the size, distribution, composition, concentration and individual optical parameters are described to provide a context within which these bulk values can be appreciated. Twomey (1969) gives a detailed account of aerosol properties.

Dry aerosol in the atmosphere consists largely of particles with radii in the range 10^{-9} m to 10^{-5} m. At and beyond the lower end of this interval particles coagulate quickly to form larger agglomerates. At the upper end of the size spectrum particle fall speeds are of the order of 1.0 cm s^{-1}; fast enough to permit rapid settling out.

The most widely used description of the size distribution of the natural aerosol is the Junge inverse power law. From direct observations

of particle sizes between 10^{-7} m and about 10^{-5} m Junge deduced that equal volumes of particulate matter are contained within equal logarithmic intervals of particle radius. This observation implies that the size distribution function is inversely proportional to the fourth power of the radius. Other indirect observations of particles in continental air masses over larger size intervals have been made and distributions of this type fitted to the results by allowing the exponent to vary. Not all natural aerosols follow this type of distribution. Salt particles in maritime air are a notable exception. In theoretical examinations of aerosols Junge type distribution functions are often used; they are very easy to manipulate mathematically. However some authors (e.g. Atwater, 1971; Kondratyev et al, 1981) have used modified Gamma distributions.

In the cleanest low-level air there may be less than 10^8 particles m^{-3}, while at highly polluted urban sites concentrations as high as 10^{12} m^{-3} may be encountered. The interpretation of these figures in terms of mass concentrations depends on the size distribution of the particles. The total mass of particulate matter distributed according to a Junge distribution is given by an integral which diverges as the lower limit tends to zero. The result of any calculation is therefore very sensitive to the radius assumed for the smallest particles present. If the exponent in the distribution function takes the value 4 then the calculated mass is sensitive to the upper limit in a similar way. Nevertheless fairly clean urban air may be expected to contain about 10 $\mu g\ m^{-3}$ of solid material, corresponding to about 10^9 or 10^{10} particles m^{-3} (Twomey, 1969).

In moist air aerosol particles may act as condensation nucleii

for water vapour. The equilibrium radius of the droplets which form on such centres depends mainly on the environmental relative humidity. As water vapour condenses on the particle, apart from the increase in radius there will also be a change in the optical properties of the particle or droplet. As the droplet grows its refractive-index approaches that of water.

There have been a few experimental studies of the importance of the atmospheric aerosol to the energy budget of the lower atmosphere. Glazier, Monteith and Unsworth (1976) estimated the size of the components of the sensible heat budget of the boundary layer during daylight hours on five days in summer at a rural site near Nottingham. They partitioned the observed heating into five components arising from the sensible heat flux originating at the earth's surface, the convergence of shortwave radiation caused by atmospheric gas, the shortwave convergence due to aerosol and the two corresponding longwave convergences.

Their results indicate that the gaseous absorption is very nearly balanced by the longwave emission and, more interestingly, that the heating due to aerosol-induced shortwave absorption can be as much as 40% of the overall heating due to the sensible heat input at the surface during the day. This means that the heating of the convective layer by aerosol absorption is comparable in size to that caused by the entrained heat flux at the top of the layer.

From a theoretical model described in the same paper, the authors predict that the net effect of the aerosol absorption on the heating of the boundary layer depends on the surface moisture content. Over water surfaces or vegetated surfaces which have a plentiful supply of water

the aerosol decreases the overall albedo of the earth and lower atmosphere, while over dry surfaces where the latent heat flux is small the aerosol increases the albedo.

The surface moisture is quantified in terms of the appropriate surface resistance. There is a critical value of the resistance which distinguishes a "wet" surface, which causes aerosol absorption to decrease the overall albedo from a dry one. The value of this critical resistance depends on the bulk backscattering ratio of the aerosol. In their experimental study Glazier et al measured the mean turbidity over a period of about 10 hours and used an empirical expression to derive the absorption and backscattering coefficients. Their derived values for the absorption coefficient vary from 0.14 to 0.22 and the backscattering ratio varies between 0.04 and 0.06.

A theoretical investigation of the interaction between aerosol and the dynamics of the boundary layer has been described by Zdunkowski, Welch and Paegle (1976). They put together a very detailed radiation model (Welch and Zdunkowski, 1976) and a one-dimensional boundary layer model to investigate the effects that industrial pollutants in the form of aerosol particles and nitrogen dioxide, have on the development of a surface inversion layer.

The shortwave part of their radiation scheme solves the radiative transfer equation by expressing the scattering phase function in terms of Legendre polynomials and the shortwave radiance in terms of spherical harmonics. This is equivalent to the two-stream method (Meador and Weaver, 1980).

The shortwave spectrum is treated in three parts. The water vapour absorption bands are taken together and the average transmission

function for water-vapour is calculated from empirical expressions in terms of the water-vapour path length. The absorption by nitrogen dioxide is calculated in a similar manner. Scattering by atmospheric gases and aerosol, and absorption by aerosol, are calculated independently over the entire solar spectrum.

In contrast to many other similar studies Zdunkowski et al attempt to account for the variation of aerosol size and refractive index with the relative humidity. They do this by making use of experimental determinations of the extinction, scattering and absorption coefficients of a Junge distribution of particles with radii between 0.4 μm and 20.0 μm.

The interaction of aerosol with the longwave radiation stream is neglected over most of the infra-red spectrum where it is much smaller than the strong absorption due to water-vapour and carbon dioxide. However in the window between 8.75 μm and 12.25 μm there are no strong absorption bands and in this region of the spectrum the emission by aerosol is calculated. The temperature change due to longwave emission by aerosol in the window alone can be as large as 0.5 K hr^{-1} according to the results from this model. This is comparable with the total calculated cooling due to longwave divergence.

The calculated effects of allowing the optical properties of the aerosol to vary with the environmental relative humidity are substantial. The heating rate at the top of the inversion layer doubles on doubling the relative humidity throughout the layer. The computed net solar flux at the earth's surface changes by 40% if the humidity effect on the aerosol is disregarded. The cooling due to longwave divergence changes by a similar proportion under these circumstances.

The aerosol loading and nitrogen dioxide concentration used in the comparisons were intended to reproduce extreme conditions likely to be encountered in an urban environment. The concentration of nitrogen dioxide was set at 1.0 ppm and the aerosol concentration at 700 $\mu g\ m^{-3}$ or $6 \times 10^{10}\ m^{-3}$ to represent "polluted" conditions, and these were reduced to 0.01 ppm and $5 \times 10^{9}\ m^{-3}$ respectively to represent clear air. The boundary layer model described in this paper uses 50 grid points in the vertical, spaced at equal logarithmic intervals to simulate the lower atmosphere up to a height of 3 km. The temperature at the top of the model is fixed at 256.5 K and that at a depth of 1 m at 276 K. The initial air temperature profile consists of an inversion layer from the surface to 500 m and a linear profile above. The relative humidity is fixed at 50% throughout the model. Aerosol is confined to the inversion layer.

The equations are integrated numerically until the "daily temperature wave at a given height becomes effectively periodic".

The turbulent fluxes throughout the model are computed from one of three semi-empirical surface layer formulations. This is an unjustified extrapolation of these formulae, and although it is pointed out by the authors that there is very little difference between the results obtained using each of these expressions, this cannot be taken as justifying their use.

As might be expected, the greatest differences between the "clear" and "polluted" models occur at the earth's surface. In the lowest 500 m of the model the inclusion of aerosol leads to a decrease in both the minimum and maximum temperatures reached during a twenty-four hour period and also in the range of temperature experienced

during the same period.

At the surace itself the extreme temperatures developed in the clear conditions are 263 K and 283 K and with the pollution added these fell to 258 K and 265 K.

Above the top of the surface inversion, the aerosol causes a warming, although the effect of a fixed temperature at the top of the model seems to be important down to 1000 m, so that interpretation of this result is not straightforward.

A surface based inversion does not develop in the same way as a convective layer so that these results are not directly comparable with the rest of this thesis, although they do serve to illustrate the type of effects likely to occur and give an idea of their likely magnitude.

The authors state that the particular choice of expression for the eddy diffusivities does not have a great effect on the calculated depth of the inversion. Without the aerosol the inversion begins to grow from the surface about two hours after the maximum surface temperature is reached and continues to deepen for about sixteen hours, eventually reaching a height of some 250 m.

In the final state of the model the polluted inversion grows to a maximum depth of about 800 m but its diurnal variation is small.

The temperature difference across the inversion layer does seem to be sensitive to the eddy difussivity model chosen, varying between 16 K and 17.5 K in the polluted case, but hardly at all in the clear case.

The effect of the relative humidity can be large. The attenuation of the solar beam increases by a factor of five as the relative

humidity in the lowest 50 m increases from 50% to 95% and by a further factor of five in increasing to 99%.

A numerical model of a convective boundary layer, including aerosol and its effect on the radiation streams, is described by Venkatram and Viskanta (1979). Their model includes a well-mixed layer in which the potential temperature is constant. The growth of this layer is determined by an entrainment assumption due to Zilitinkevich and Tennekes which has already been mentioned. The solar radiation is treated by a two-stream technique and the aerosol's optical properties are prescribed simply in terms of a single scattering albedo and a backscattering fraction. The effect of relative humidity and nitrogen dioxide are not treated.

The paper describes the results from three pairs of integrations of this model. In one of each pair, the aerosol, although present, does not interact with the shortwave radiation stream. The second pair of integrations is carried out with the soil moisture content doubled, and then in the third the albedo of the surface is doubled.

The results demonstrate the importance of both the soil moisture and the surface albedo in determining the effect that the aerosol absorption has on the overall albedo of the boundary layer and soil. The authors also point out that to a large extent the boundary layer develops in such a way as to minimise the effect of the radiative divergence within it. The aerosol absorbs solar radiation which warms the mixed layer directly but decreases the surface fluxes. The decreased surface fluxes by themselves lead to a decrease in the rate at which the mixed layer deepens but the direct heating of the mixed layer by the aerosol decreases the temperature discontinuity and increases the

mass entrainment at the inversion.

It is likely that the direct warming of the mixed layer will affect the entrainment at the inversion base by instantaneously increasing the potential energy of the layer. Such possibilities have been ignored up to now and the work described in the following chapters attempts to make an estimate of the likely size of such an effect.

CHAPTER 2

A SIMPLE ANALYTIC MODEL

2.1 INTRODUCTION

Before going on to describe the results obtained from the numerical model specified in the next chapter it is worth investigating some of its details using a simpler analytic model. In fact the boundary layer model itself is identical in both the analytic treatment and the numerical calculations. The simplification necessary to obtain analytic solutions to the equations is achieved by simplifying the specifications of the shortwave radiation profile and the turbulent heat flux at the surface.

In both the analytic and numerical treatments therefore, the boundary layer itself extends from the surface to a height h (metres). Within this layer the potential temperature, θ_m (K), the water-vapour mixing ratio, r_m (g/kg), and the wind speed, u_m (m s^{-1}), are each independent of the vertical coordinate, z. Each of the quantities θ_m, r_m, u_m and h is a function of time.

The profiles of potential temperature and water-vapour mixing ratio are linear at heights greater than h and are held constant throughout the model integration. At the top of the mixed layer (z=h) the profiles may be discontinuous. The temperature discontinuity is an idealised representation of an inversion layer or stable layer which normally limits the vertical extent of a convective boundary layer.

The entrainment of air from above the temperature discontinuity into the mixed layer is parameterized by assuming that the rate at

which turbulent kinetic energy is dissipated by the entrainment process is a constant fraction of the rate of generation of TKE by buoyancy within the mixed layer.

The assumption that the potential temperature remains independent of height implies that the divergence of the enthalpy flux is also independent of height within the mixed layer. If the radiative flux profiles are known or can be calculated, then this condition on the flux divergence, together with the entrainment assumption, can be used to calculate the profile of the turbulent sensible-heat flux throughout the mixed layer. In particular the sensible heat flux at the top of the mixed layer, the entrained heat flux, can be found and in this way the effect of absorption of radiation within the layer on the rate of entrainment can be investigated.

2.2 THE LIMPID CONVECTIVE LAYER

(a) The Mixed Layer Model and a Simple Solution

The development of a transparent, dry convective boundary layer bounded above by an inversion layer or stable layer has been modelled by a number of authors (for example, Ball, 1960; Carson, 1974; Heidt, 1977; Stull, 1976; Deardorff, 1974) using various forms of the simple slab model which was outlined in the introduction to chapter two. It is quite straightforward to derive an analytic solution to the equations which describe this type of model. Such a solution provides a convenient reference, with which the results from a more complex model, which includes aerosol absorption, can be compared.

The first of the fundamental equations is the conservation of enthalpy, which, in the absence of any large-scale vertical motion,

is

$$\frac{d}{dt}\left[\int_{o}^{z_t}\theta(z)\,dz\right] = \frac{H(o)}{\rho c_p}$$

where z_t is an arbitrary height, above the top of the mixed layer, where the potential temperature is constant. The Boussinesq approximation has been made so that here, and in the rest of this study, the density is treated as independent of height, except when it appears in combination with the acceleration due to gravity.

The only heat source is assumed, for the moment, to be the sensible heat flux at the surface, $H(0)\,(Wm^{-2})$. The sensible heat flux, $H(z)$, may vary with time. There is no need to include a latent energy term since layers in which cloud forms will not be considered. However when absorption of radiation is included in the model an extra term describing the heating which results, will appear on the right hand side of this equation.

There is often a general subsidence observed when conditions are suitable for the formation of the type of convective layers being considered here. Subsidence slows the rate at which the mixed layer deepens, most noticeably towards late afternoon when the mixed layer is growing relatively slowly. Once the surface heat flux changes sign the capping inversion is forced downwards by the descending air, although only very slowly, at a rate of a few cm s^{-1}. In what follows the large scale vertical velocity is set to zero. This simplifies the equations slightly without greatly altering the form of the solutions.

The potential temperature profile is defined by

$$\theta(z) = \begin{cases} \theta_m(t) & z < h(t) \\ \theta_o + \gamma z & z > h(t) \end{cases}$$

where θ_o and γ are constants which define the profile above the mixed layer. The potential temperature gradient above the mixed layer, γ, is a constant only because it has been assumed that there is no vertical motion.

The discontinuity in the potential temperature profile at the top of the model's mixed layer simulates the effect of the stable layers, of non-zero thickness, which limit real convective layers. Manton (1977) described a convective layer model in which, having specified the temperature profile within the mixed layer and that above in the free atmosphere, the potential temperature within the capping stable layer was specified by imposing continuity of both the temperature and its first derivative at the boundaries of the stable layer. In fact, Manton defined the top of the mixed layer to be that level above which the turbulent heat flux is negative. However most other authors have used a temperature discontinuity model and have obtained equally good results, at least in predicting mixed layer layer depths. The discontinuity model does permit a very simple expression to be used to calculate the sensible heat flux at the base of the inversion layer, namely

$$\frac{H(h)}{\rho c_p} = - \Delta\theta \frac{dh}{dt}$$

where $\Delta\theta = \theta_o + \gamma h - \theta_m$.

Substituting the definition of $\theta(z)$ into the enthalpy equation and using the definition of $\Delta\theta$ leads to

$$\frac{H(o)}{\rho c_p} = \gamma h(t) \frac{dh}{dt} - \frac{d}{dt} (\Delta\theta(t) h(t)) \qquad \text{equation 2.1}$$

This can be integrated to give

$$\int_{t_1}^{t_2} \frac{H(o)}{\rho c_p}\, dt = \left(\frac{1}{2}\gamma h^2(t) - \Delta\theta(t)h(t)\right)\Big|_{t_1}^{t} \qquad \text{equation 2.2}$$

A second integral to equation 2.1 can be obtained by eliminating the surface heat flux. By assuming that entrainment of air into the mixed layer dissipates a constant fraction of the turbulent kinetic energy generated by the buoyancy flux within the mixed layer, it is possible to show that the entrained buoyancy flux at the top of the mixed layer is a constant fraction, A, of that at the surface. In a dry layer the buoyancy flux is proportional to the sensible flux and so

$$\frac{H(o)}{\rho c_p} = -\frac{1}{A}\frac{H(h)}{\rho c_p} = \frac{\Delta\theta(t)}{A}\frac{dh}{dt}$$

Substituting this expression into equation 2.1 and integrating gives the second integral.

$$\left[\gamma\left(\frac{A}{1+2A}\right) h(t) - \Delta\theta(t)\right](h(t))^{(1+A)/A}\Big|_{t_1}^{t} = 0 \qquad \text{equation 2.3}$$

$\Delta\theta(t_2)$ can be eliminated from these two equations, 2.2 and 2.3, to produce an equation which can be solved for the depth of the mixed layer as a function of time, given initial values $\Delta\theta(t_1)$ and $h(t_1)$.

The solution is easier to manipulate in terms of a variable $Z(t) = h(t)/h(t_1)$ which has to satisfy the condition

$$F(Z) = Z^{\frac{1}{A}}\left[Z^2 + (1+2A)\left(\frac{2\Delta\theta(t_1)}{\gamma h(t_1)} - 1 - \frac{2}{\gamma h^2(t_1)}\int_{t_1}^{t}\frac{H(o)}{\rho c_p}\, dt\right)\right]$$

$$+(1+2A)\left[\frac{2A}{1+2A} - \frac{2\Delta\theta(t_1)}{\gamma h(t_1)}\right] = 0 \qquad \text{equation 2.4}$$

If the initial conditions are such that

$$\Delta\theta(t_1) = \left(\frac{A}{1+2A}\right) \gamma\, h(t_1)$$

then the second term of equation 2.4 vanishes and the solutions for $h(t)$ and $\Delta\theta(t)$ take a particularly simple form, namely

$$h(t) = \sqrt{h^2(t_1) + \frac{2(1+2A)}{\gamma} \int_{t_1}^{t} \frac{H(o)}{\rho c_p}\, dt} \qquad \text{equation 2.5a}$$

$$\Delta\theta(t) = \gamma \left(\frac{A}{1+2A}\right) h(t) \qquad \text{equation 2.5b}$$

These solutions were derived in a similar manner by Carson (1974).

The non-dimensionalised solution for the inversion height (equation 2.5a) is shown in Figure 2.1 for a constant surface heat flux and also for a sinusoidal heat flux which has a twenty-four hour period and an amplitude $\frac{1}{2}\pi$ times the value of the constant heat flux. This choice ensures that the total energy input to the mixed layer is the same in both calculations.

b) Development from Arbitrary Initial Conditions

The development of a convective layer from an arbitrary set of initial conditions is described by the zeroes of the function $F(Z)$ defined in equation 2.4. This function has the form

$$F(Z) = Z^{\alpha} (Z^2 + b(t)) + c$$

The exponent α is identical to the reciprocal of the entrained buoyancy flux ratio A. Since the latter is necessarily restricted to values between zero and one, α may take any positive, real value greater

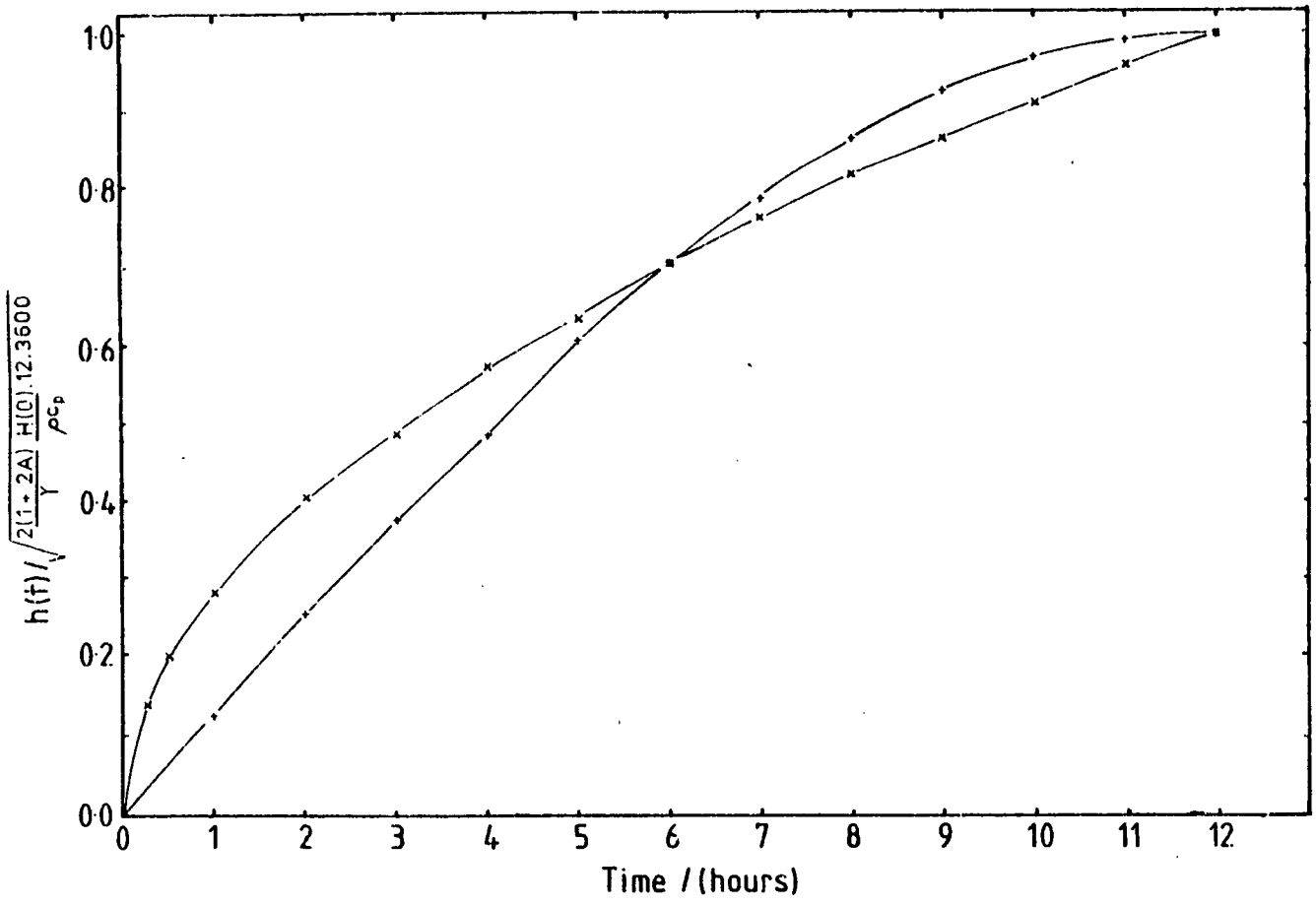

Figure 2.1 The 'Simple' Solution for the Mixed Layer Depth Calculated Assuming

i) a constant surface heat flux, H(0), (×)

ii) a sinusoidal surface heat flux, (+)

$H(0,t) = \frac{1}{2}\pi H(0)\sin(\Omega t - \frac{1}{4}\pi)$

t is the time, in hours, and $\Omega = \pi/12$ rad hr^{-1}

than or equal to one. The behaviour of F(Z) may be gauged from that of the polynomial functions defined by assigning integral values to α. Since the great majority of observational evidence implies that the buoyancy flux ratio lies between 0.1 and 0.3, only values of α between three and ten need to be considered. This suggests that there may be between five and twelve complex zeroes of F(Z). Fortunately the form of the function limits the number of zeroes to no more than four no matter how large α becomes. Of these four zeroes only two can lie in the positive half plane and have any physical significance.

The form of the first and second derivatives of F(Z) depend on the value of α. However if, as has already been assumed, α is greater than three the derived functions can be written as

$$F'(Z) = Z^{\alpha-1}((2+\alpha)Z^2 + \alpha b(t))$$

$$F''(Z) = Z^{\alpha-2}((2+\alpha)(1+\alpha)Z^2 + \alpha(\alpha-1)b(t)) \qquad \text{equation 2.6}$$

at $Z = 0$ $F(0) = C$ and $F'(0) = F''(0) = 0$

Furthermore $F'(Z)$ has zeroes at the points $Z = \pm (-\alpha b(t)/(2+\alpha))^{\frac{1}{2}}$ which are real if and only if $b(t)$ is negative.

The stationary value of F(Z) in the positive half plane corresponds to a minimum. The sign of the second derivative is determined by that of the factor in brackets in equation 2.6, substituting for Z this becomes

$$(2+\alpha)(1+\alpha)\frac{(-\alpha b(t))}{(2+\alpha)} + \alpha(\alpha-1)b(t) = -2\alpha b(t)$$

which is positive, since $b(t)$ is, in this instance, negative.

From these general considerations it is easy to deduce the form

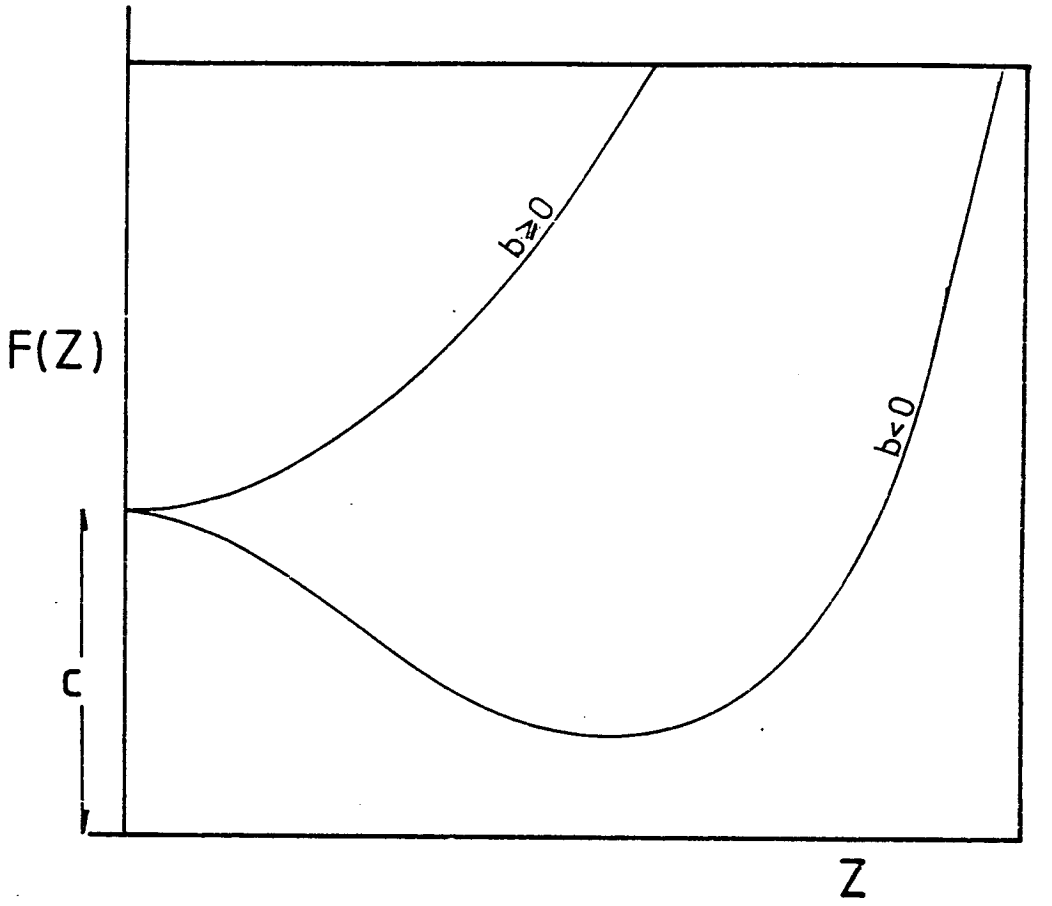

Figure 2.2 The Function $F(Z) = Z^{\alpha}(Z^2+b(t)) + c$

	b < 0	b ≥ 0
c < 0	1	1
c ≥ 0	0,1,2	0

Table 2.1 The Number of Zeroes of the Function F(Z).

of the function and the number of roots that exist for different values of the coefficients b(t) and c. Figure 2.2 shows the form of the function for positive or negative values of b(t).

Table 2.1 shows how the number of zeroes of F(Z) there are for positive values of Z and how the number of zeroes depends on the signs of b(t) and c.

If c is positive then there is only one zero no matter what value b(t) takes. If c and b(t) are both non-negative F(Z) has no real positive zeroes. However it is easy to see that this can never occur, since, from the definitions of b(t) and c

$$b(t) = (1+2A)\left(\frac{2\Delta\theta(t_1)}{\gamma h(t_1)} - 1 - \frac{2}{\gamma h^2(t_1)}\int_{t_1}^{t}\frac{H(o)}{\rho c_p}\,dt\right)$$

$$c = -(1+2A)\left(\frac{2\Delta\theta(t_1)}{\gamma h(t_1)} - \frac{2A}{1+2A}\right)$$

and $$c = -\,b(t) - 1 - \frac{2}{\gamma h^2(t_1)}\int_{t_1}^{t}\frac{H(o)}{\rho c_p}\,dt$$

Hence if b(t) is positive or zero then c must be negative.

To demonstrate that the model will only generate one solution it is only necessary to point out that, from these definitions

$$c = -\,b(0) - 1$$

and hence, at the initial instant, t_1, there is always a zero of F(Z) at Z = 1. When b(t) is negative F(Z) has a local minimum at which

$$F(Z) = \left(\sqrt{\frac{-\,b(t)}{(2+\alpha)}}\right)^{\alpha}\frac{2}{2+\alpha}\,b(t) - b(0) - 1$$

This value decreases as time goes on and therefore it is not

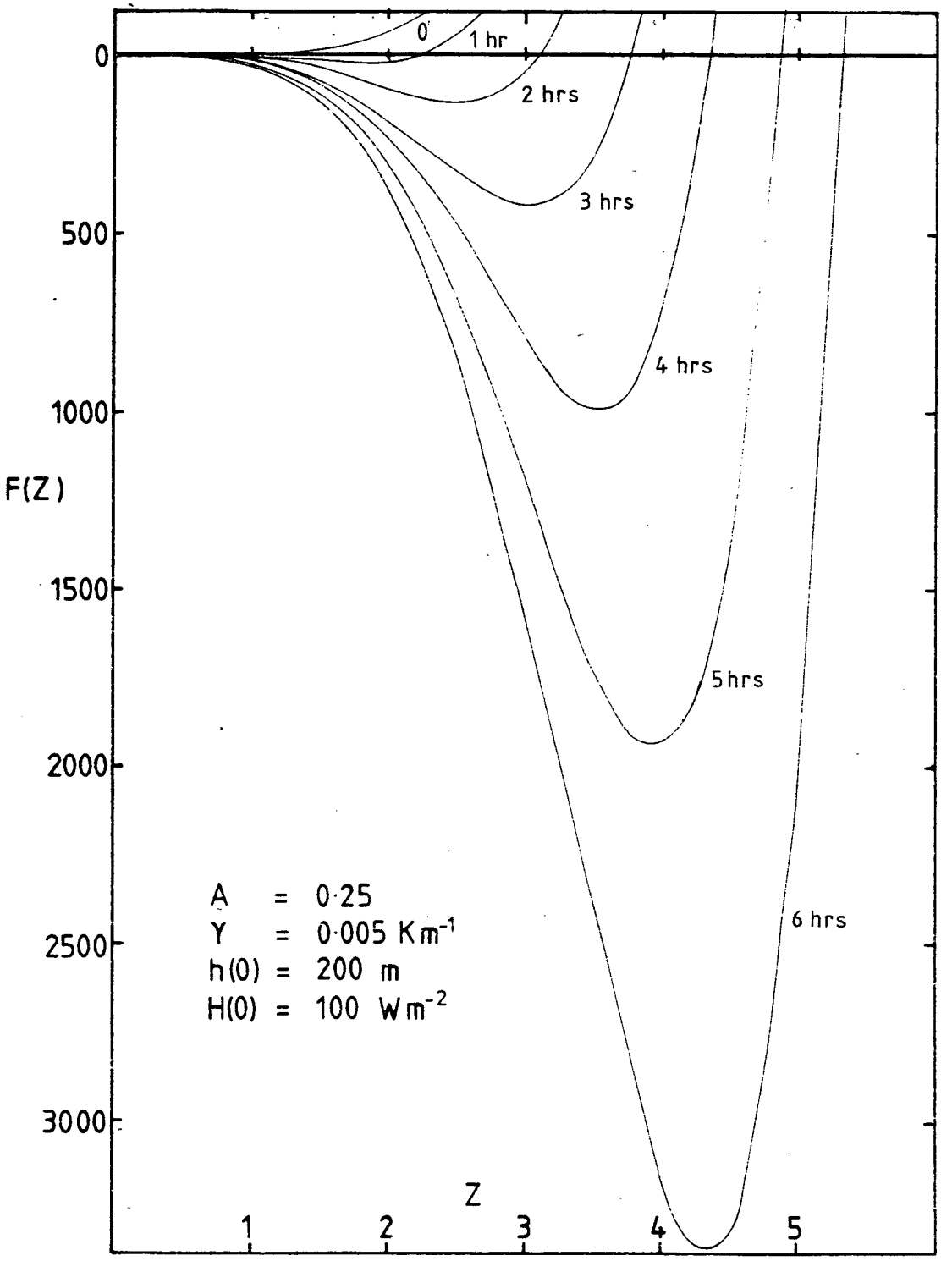

Figure 2.3 F(Z) Calculation at Hourly Intervals

possible for either situation in which F(Z) has no positive zeroes to arise.

It now only remains to show that there is one and only one zero of F(Z) at or to the right of Z = 1. If c is negative this is equivalent to requiring that F(1) is negative or zero. But

$$F(1) = 1 + b(t) + c = b(t) - b(o)$$

which is less than or equal to zero because b(t) is a decreasing function of time. Equality is only possible at the initial instant. If c is positive there may be two positive zeroes of F(Z). However since F(1) is zero or less there can only be one zero of F(Z) to the right of Z = 1.

Figure 2.3 shows how F(Z) changes over a period of six hours and the corresponding graph showing the depth of the mixed layer as a function of time is shown in Figure 2.4.

The 'simple' solution obtained when the initial conditions are such that the second term on the right hand side of equation 2.4 vanishes is not as limited in its application as might be thought at first. In fact no matter what the actual initial conditions are the solution to equation 2.4 approaches the 'simple' solution as time goes by. To demonstrate this the second solution to the basic equations (equation 2.3) need simply be re-written as

$$\left[\frac{\Delta\theta(t)}{\gamma h(t)} - \frac{A}{1+2A}\right] = \left[\frac{\Delta\theta(t_1)}{\gamma h(t_1)} - \frac{A}{1+2A}\right]\left[\frac{h(t_1)}{h(t)}\right]^{(1+2A)/A}$$

Obviously the left-hand side tends to zero as the depth of the mixed layer increases. The time required for the two solutions to converge

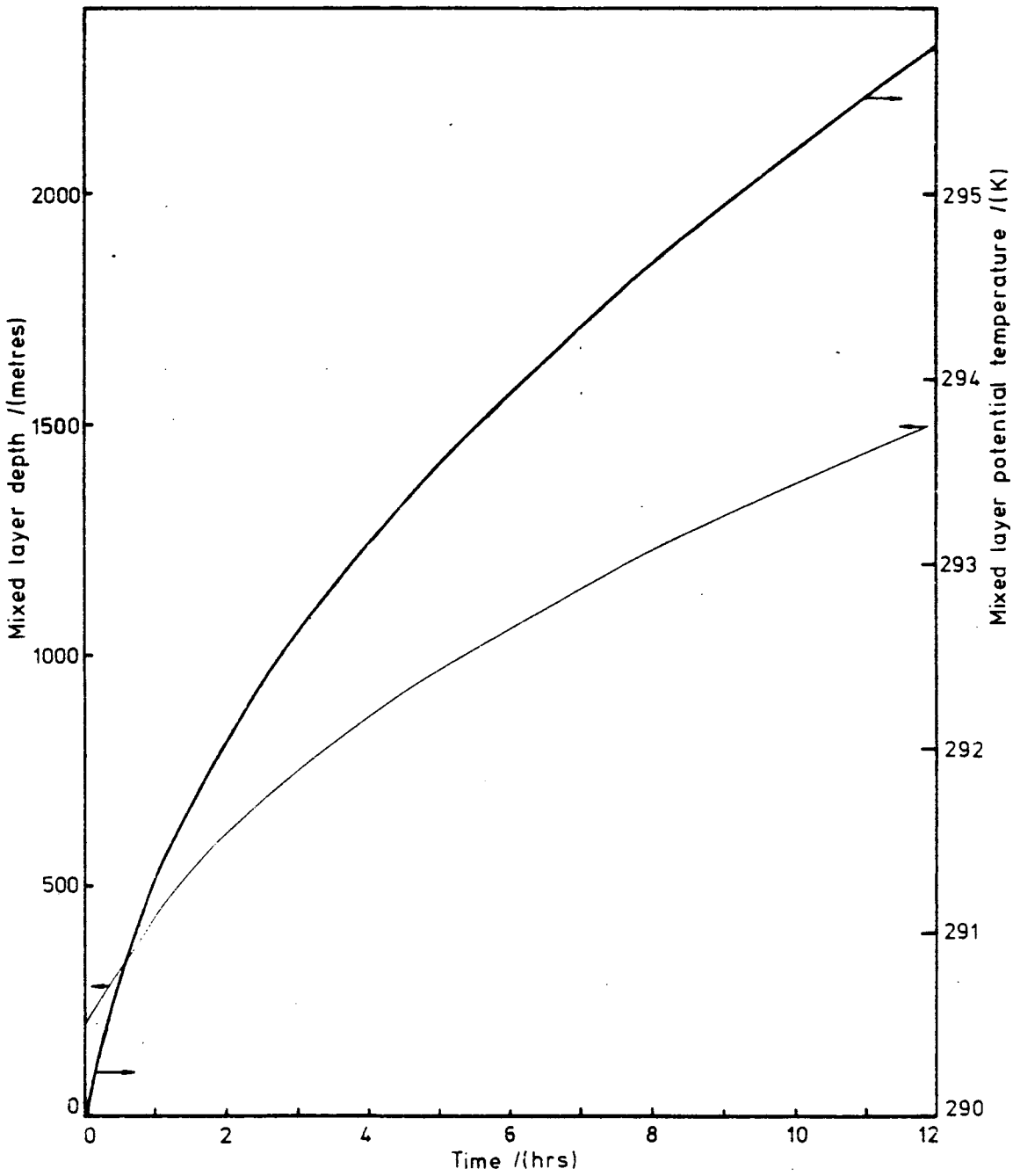

Figure 2.4 a) The Development of the Mixed Layer

b) The Mixed Layer Potential Temperature

Both calculated for the same parameters as those detailed in Figure 2.3

depends on the particular initial conditions and on the size of the surface heat flux. Figure 2.5 shows how the solution to equation 2.4 tends towards the simple solution which is represented by the straight line passing through the origin.

If the initial state arises by adiabatic mixing of the lowest part of the atmosphere which initially has a linear potential temperature profile then $\frac{\Delta\theta(t_1)}{\gamma h(t_1)}$ has the value 0.5 and smaller values of this ratio reflect the quantity of heat added to the layer as it grows.

Assuming a value of 0.25 for the entrainment coefficient A means that $\frac{\Delta\theta(t_\infty)}{\gamma h(t_\infty)}$ should tend to a limiting value of $\frac{1}{6}$.

The behaviour of the potential temperature jump, $\Delta\theta$, as a function of time, plotted in Figure 2.6, illustrates how quickly solutions to the full equation, starting from arbitrary initial conditions, approach the simple solutions. When the initial temperature jump is greater than that predicted by equation 2.5b the mixed layer grows at a much reduced rate, and the temperature jump decreases to a minimum value. As the minimum temperature jump is reached the rate of growth of the mixed layer increases and shortly thereafter the solution conforms to equations 2.5a and 2.5b. The speed with which the solutions adjust depends on the magnitude of the surface heat flux. The initial conditions used in the calculations whose results are shown in Figures 2.5 and 2.6 result in the initial temperature jump being up to ten times that expected from equation 2.5b, yet after, at most, two hours the actual solutions are indistinguishable from the simple ones.

2.3 THE PARTITION OF ENERGY WITHIN THE CONVECTIVE LAYER

The total energy content of the convective layer is partitioned

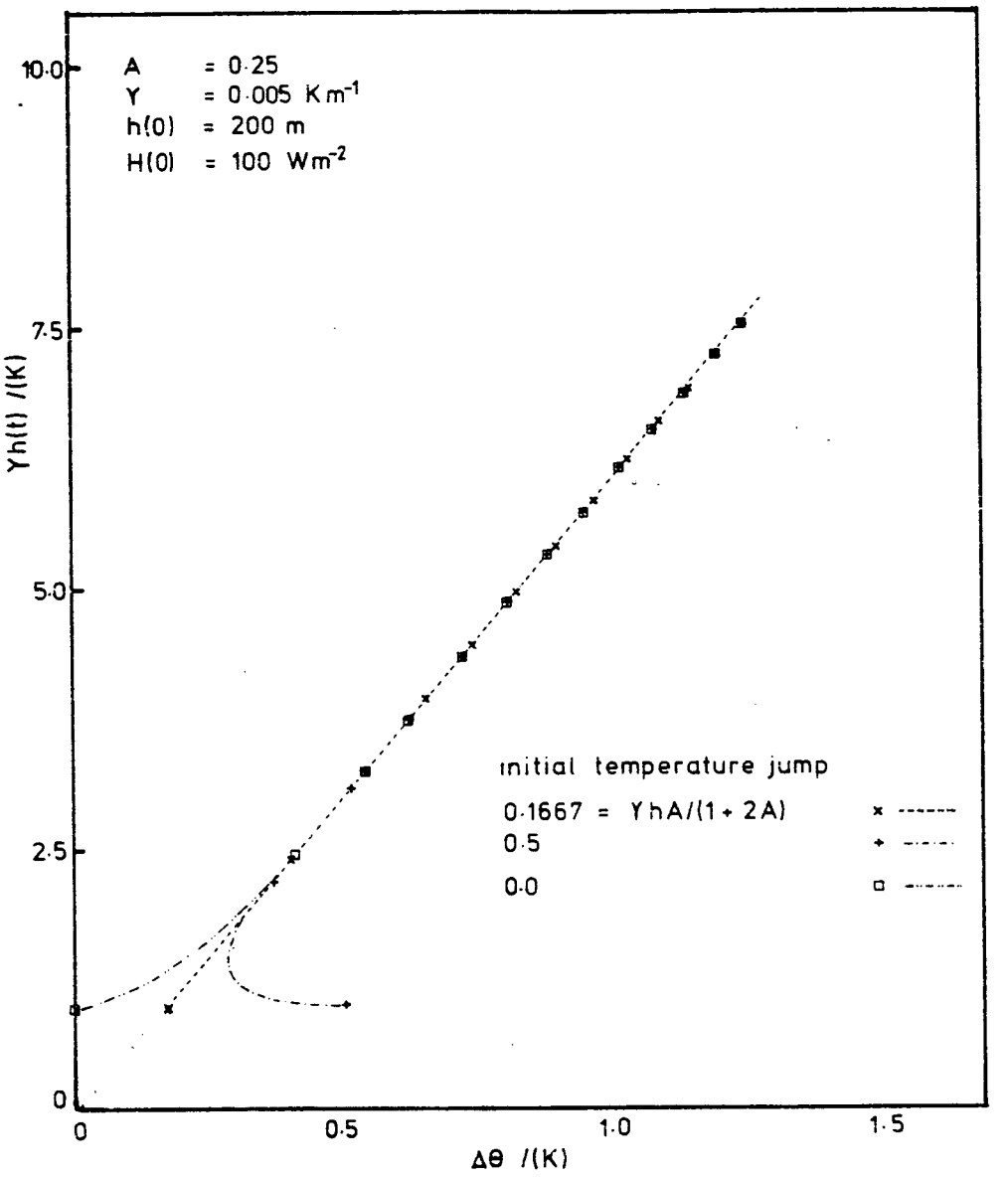

Figure 2.5 The Trajectory of the Solution in the $\Delta\theta$-γh Plane. Points are marked at hourly intervals.

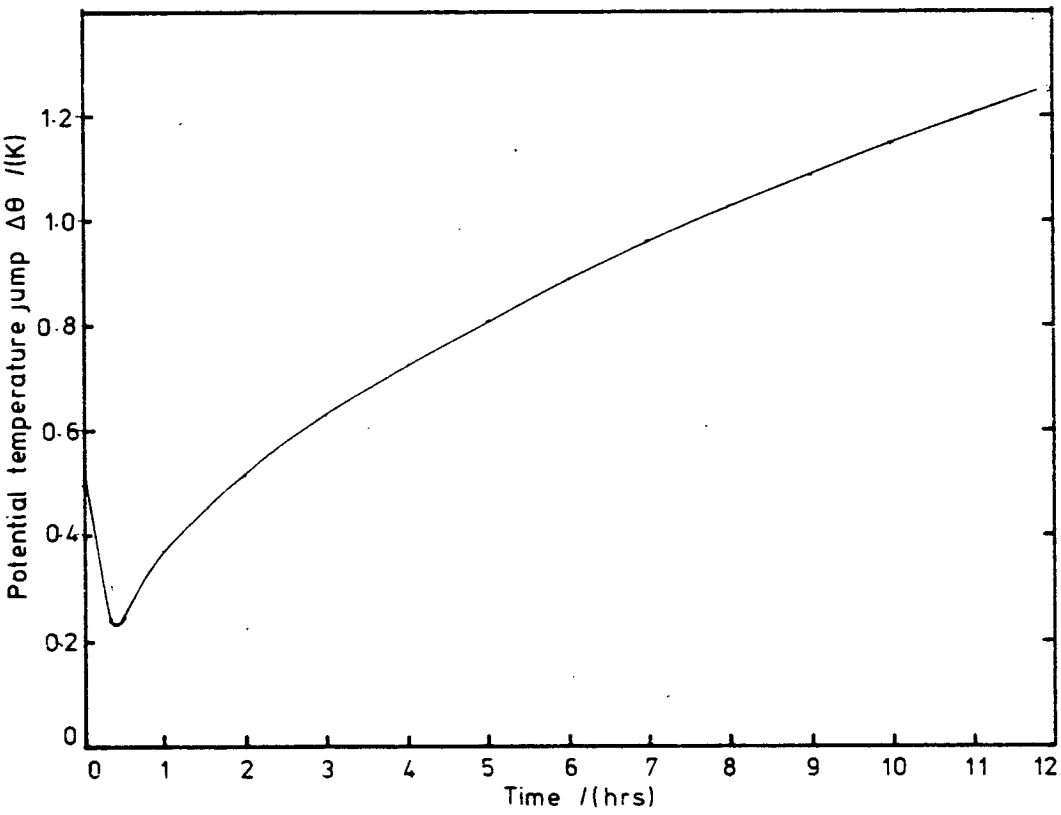

Figure 2.6 The Temperature Jump as a Function of Time

into thermal, potential and kinetic components. To obtain an idea of the sizes of these components and by how much they alter during the period when the surface heat flux is positive, consider a mixed layer 1 km deep with a potential temperature of 15 K, a mean wind speed of $10\ m\ s^{-1}$ and a water-vapour mixing ratio of $10\ g\ kg^{-1}$.

a) Enthalpy

In a dry atmosphere the enthalpy, E_r, is simply the total heat content of the layer which is, in general

$$E_T = \int_o^h \rho c_p\ \theta(z)\ dz$$

Ignoring the variation of the density of air in the vertical leads to a value of about 300 MJ m^{-2} for the layer described above. The latent heat contribution may be calculated from a similar expression, and for the values specified is about 25 MJ m^{-2}, approximately 10% of the contribution from the sensible heat of the layer.

The surface fluxes of sensible and latent heat at the surface balance the net radiation and heat flux into the soil. Typically, close to noon on cloud-free summer days over mid-latitude pasture land the energy available at the surface is about 400 Wm^{-2} (see, for example Monteith and Szeicz, 1961; Wood, 1977; Moores et al, 1979). This corresponds, assuming that the available energy is a sinusoidal function of time, to a mean value of 180 Wm^{-2} when averaged over the period from 0900 to 1500. During this time the energy input to the mixed layer amounts to 8 MJ m^{-2}. If this were added entirely as sensible heat it would result in an increase in the potential temperature of the layer of about 6 K.

b) Kinetic Energy

The total kinetic energy of the mean wind within the mixed layer is approximately 50 kJ m^{-2}. However of more importance in the present context is the kinetic energy of the turbulent eddies.

Figure 2.7, taken from the paper by Caughey and Palmer (1979) already referred to in chapter one, shows the non-dimensional vertical and horizontal velocity variances measured in convective conditions. The convective velocity scale w_*, defined in chapter one, is relatively insensitive to the surface heat flux and depth of the convective layer and is typically between 0.1 m s^{-1} and 1.0 m s^{-1}. The velocity variances can be seen to be almost independent of height throughout most of the mixed layer, each component being approximately 0.3 w_*^2. The resulting estimate of the eddy kinetic energy is, therefore, of the order of 1 kJ m^{-2}.

The time-scale on which the turbulent kinetic energy content of the mixed layer changes may be written in terms of the convective scaling speed w_* as

$$\left(\frac{1}{w_*^2} \frac{d}{dt} w_*^2 \right)^{-1} = \left(\frac{3}{2} \frac{1}{h} \frac{dh}{dt} + \frac{1}{H(o)} \frac{d}{dt} H(0) \right)^{-1}$$

Close to midday the turbulent heat flux at the surface changes only slowly and the rate of growth of the mixed layer is likely to attain its maximum value of, perhaps 0.05 m s^{-1} (see Cattle and Weston, 1975; Glazier et al, 1976; Lettau and Davidson, 1957; for boundary layer measurements). This gives a time-scale of about eight hours which suggests that Ball's assumption that the turbulent kinetic energy does not alter appreciably during the period in which the convective layer is growing is only valid as a first approximation. Over two

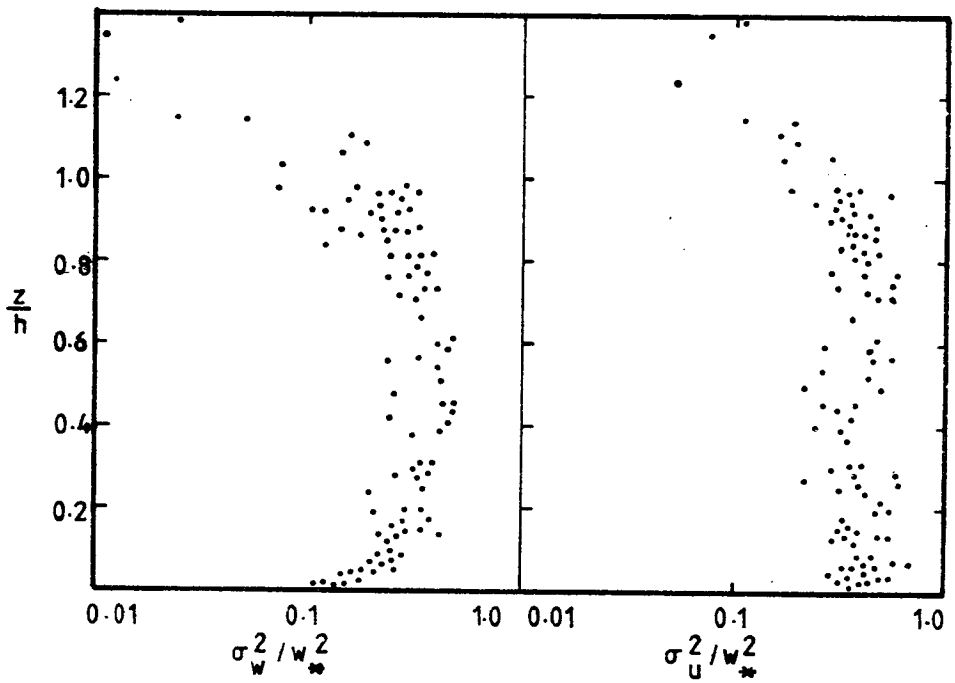

Figure 2.7 The Non-Dimensional Velocity Variances in the Convective Boundary Layer
(after Caughey and Palmer, 1979)

hours between 1100 local time and 1300 local time the turbulent kinetic energy content of the mixed layer would be expected to increase by 25%.

c) Potential Energy

In calculating the potential energy of the mixed layer the vertical variation of the density cannot be ignored. The appropriate quantity to examine is the change in potential energy arising from mixing a layer 1000 m deep, with a constant gradient of potential temperature adiabatically to a state of uniform potential temperature.

If the temperature within the layer is, initially, a linear function of height with gradient γ K m^{-1}, then the potential energy of the layer from the surface to a height h is equal to

$$PE = \int_o^h \frac{gP_o}{RT_o} \left(1 + \frac{\gamma z}{T_o} \right)^{-\frac{g}{R\gamma} - 1} z \, dz$$

Integrating this and expanding the result to third order in $\gamma h/T_o$ leads to

$$PE = \frac{1}{2} g \frac{P_o}{RT_o} h^2 \left[1 - \frac{2}{3} \left(1 + \frac{g}{R\gamma} \right) \frac{\gamma h}{T_o} \right]$$

P_o and T_o represent the pressure and temperature respectively, at the surface.

In mixing such a layer to an isentropic state the temperature at the base of the layer changes to $T_o + \frac{1}{2}(\gamma + \Gamma)h$, where Γ is the dry adiabatic lapse rate. If the initial gradient of temperature is 0.001 K m^{-1} then, ignoring the very small change in the depth of the layer caused by the mixing (which in this case amounts to less than 1 cm difference), the potential energy lost by the mixed layer is

approximately 5 kJ m^{-2}.

2.4 THE EFFECT OF THE RADIATIVE DIVERGENCE ON THE RATE OF ENTRAINMENT

The development of the convective layer over the course of a day is characterised by an increase in the potential temperature, the water-vapour mixing ratio and the inversion height. Given the turbulent sensible heat flux profile, H(z) Wm^{-2}, and the net downward irradiance, R(z) Wm^{-2}, throughout the mixed layer, the rate of change of the potential temperature at any height can be calculated from

$$\frac{\partial \theta}{\partial t} = - \frac{1}{\rho c_p} \frac{\partial}{\partial z} (H(z) - R(z))$$

Here H(z) is taken to be positive when directed upwards. Since, by assumption the potential temperature, θ_m K, within the mixed layer is independent of the vertical co-ordinate this equation can be integrated with respect to height to give an expression for the turbulent heat flux profile within the mixed layer

$$H(z) = H(0) - R(0) + R(z) - \rho c_p \dot{\theta}_m z \qquad \text{equation 2.7}$$

In convective conditions the turbulent heat flux at the surface is, by definition, positive and there is a downward entrained heat flux at the base of the inversion layer. Therefore there is at least one level, $z = z_*$, within the mixed layer at which the turbulent heat flux vanishes. If R(z) is a monotonic function of z then H(z) can have only one zero in the interval [0,h].

The net shortwave irradiance on a horizontal surface, S(z) Wm^{-2} directed downwards, is extinguished by absorption and scattering due to both molecules and aerosol particles. For the moment however

we shall ignore the scattering and assume that all absorption of the solar radiation is independent of wavelength. The absorbing material is assumed to be uniformly mixed throughout the convective layer. S(z) is, therefore, everywhere positive and is an increasing function of z.

The temperature in the mixed layer decreases with height so that the longwave irradiance, L(z) Wm^{-2}, is directed upwards and decreases, with height, at least in the lower part of the mixed layer. However, near to the temperature inversion the downward component of the infra-red radiation may be enhanced so that there may be a change of sign of $\frac{dL}{dz}$. The fact that the warmer air above the mixed layer is frequently much drier than that beneath lessens this enhancement of the downward longwave radiation. Even so, this means that R(z) need not be monotonic and that there may be more than one zero of H(z). However, the total cooling due to longwave divergence in a cloud-free convective boundary layer is very nearly balanced by the warming due to molecular absorption of the shortwave component (Glazier et al, 1976) and the warming due to absorption of the shortwave component by aerosol is much greater than either. It would not be justified to infer from this that the molecular absorption of the shortwave radiation balanced the longwave cooling everywhere within the mixed layer but, since the assumption that the layer remains well mixed has already been made neglect of both of these components should not seriously affect the results.

It is now possible to be certain that the height, z_* m, at which the turbulent heat flux vanishes is uniquely defined by

$$H(0) - S(0) + S(z_*) - \rho c_p \dot{\theta}_m z_* = 0 \qquad \text{equation 2.8}$$

where the shortwave irradiance is depleted only by aerosol absorption.

Since we are neglecting the effects of the longwave radiation equations 2.7 and 2.8 can now be combined to eliminate $\dot{\theta}_m$ and give an expression for the turbulent heat flux profile

$$H(z) = (H(0) - S(0))\left(1 - \frac{z}{z_*}\right) + S(z) - S(z_*)\frac{z}{z_*} \qquad \text{equation 2.9}$$

The entrained heat flux at the base of the inversion layer is parameterized in the same manner as Lilly (1968) by considering the turbulent kinetic energy equation (Ball, 1960).

Change in storage = advection + mechanical generation + buoyant generation - viscous dissipation + work done by entrainment

Since the mixed layer has already been assumed to be horizontally and vertically homogeneous the transport term is zero. The viscous dissipation is assumed to account for a constant fraction, 1-k, of the total buoyancy production of turbulent kinetic energy. The remaining fraction is assumed to be dissipated in entraining warm air downwards into the mixed layer and in maintaining the well mixed profiles. The reasoning used by Ball to justify his neglect of the storage term and mechanical generation term have been already outlined in chapter one.

The net rate of production of turbulent kinetic energy throughout the mixed layer may be written as

$$\int_0^h \frac{g}{\theta_m} \frac{H(z)}{c_p} \, dz$$

where, as before, g/θ_m is a buoyancy parameter and may be taken to be constant.

The turbulent kinetic energy equation can now be written as

$$0 = 0 + 0 + \int_0^{z_*} \frac{g}{\theta_m} \frac{H(z)}{c_p} dz - (1-k)\int_0^{z_*} \frac{g}{\theta_m} \frac{H(z)}{c_p} dz + \int_{z_*}^{h} \frac{g}{\theta_m} \frac{H(z)}{c_p} dz$$

which can simply be rearranged to

$$\int_0^{h} \frac{g}{\theta_m} \frac{H(z)}{c_p} dz = (1-k)\int_0^{z_*} \frac{g}{\theta_m} \frac{H(z)}{c_p} dz \qquad \text{equation 2.10}$$

Defining k in this fashion, as the fraction of the buoyancy-generated turbulent kinetic energy which is dissipated in entraining warm air into the mixed layer, means that if the sensible heat flux is linear in z then k is equal to the square of the entrainment ratio, A = -H(h)/H(0), defined in chapter one (see Deardorff, 1974).

The equation which is to be used to find z_* is derived by substituting the expression for the turbulent heat flux, equation 2.9, into equation 2.10. After performing the integrations this results in

$$[H(0) - S(0)][h - \frac{1}{2}\frac{h^2}{z_*} - \frac{1}{2}(1-k)z_*] + \int_0^{h} S(z)dz$$

$$- (1-k)\int_0^{z_*} S(z)dz - \frac{1}{2} S(z_*)[\frac{h^2}{z_*} - (1-k)z_*] \qquad \text{equation 2.11}$$

If the form of the function S(z) is known this equation can be solved for z_*. Equation 2.8 can subsequently be used to find $\dot{\theta}_m$ and H(h) can then be evaluated using equation 2.9. Once the entrained heat flux is known the rate at which the mixed layer deepens can be calculated and the evolution of the layer calculated numerically, solving equation 2.11 at each time step.

The numerical model which will be described in chapter three proceeds in this manner. However, if the shortwave irradiance at the

top of the mixed layer and the surface heat flux are held constant it is possible to produce a solution which is analagous to that derived for a non-absorbing mixed layer. In this modified solution the entrained flux ratio is no longer constant, but depends on the optical depth of the mixed layer, and on the relative size of the sensible heat flux and the shortwave irradiance at the surface.

There are two constraints on this model which need to be examined closely. The first is a physical limitation. The model is founded on the premise that the potential temperature beneath the inversion layer does not vary with height. Indeed this layer is assumed to be well mixed and, therefore, the components of the wind velocity and the concentrations of water-vapour and aerosol may also be taken to be independent of height. These conditions are observed when the turbulent kinetic energy density beneath an inversion is sufficiently large to smooth out vertical gradients of temperature, momentum or composition as they arise. This in turn depends on the buoyancy flux at the surface being large enough to maintain the turbulent kinetic energy within the layer at an adequate level.

If the opaque aerosol is evenly distributed throughout the mixed layer, then the absorption of shortwave radiation will tend to stabilise the layer. While the turbulent motions are vigorous enough this stabilising effect of the absorption will be overcome and the layer will remain well mixed, but as the optical depth of the layer increases, and the surface heat flux consequently decreases, a point will be reached where the turbulent vertical exchange is suppressed, initially at the top of the layer, and the model will cease to be appropriate.

The second constraint on the model is a mathematical one. The model specifies the turbulent heat flux profile which is required to

maintain a well mixed temperature profile and it is assumed that the flux profile changes sign precisely once between the surface and the base of the inversion layer. The existence of an even number of zeroes of the function which represents the vertical turbulent heat flux would be physically unrealistic as it would imply that the heat flux at the base of the inversion layer would be directed upwards.

The simplified, analytical model is identical to the numerical model to be described in chapter three except in the following two respects:

i) the shortwave radiation profile within the mixed layer is specified as

$$S(z) = S_i \left[\exp(-\tau(1-\zeta)) - r_s\exp(-\tau(1+\zeta))\right] \qquad \text{equation 2.12}$$

where τ represents the optical depth of the mixed layer, $\zeta = z/h$ is the height above the surface scaled with respect to the depth of the mixed layer, S_i is the downward directed shortwave irradiance just above the level of the inversion and r_s is the shortwave reflectivity of the earth's surface.

ii) all the boundary conditions are held constant. That is to to say, the optical depth of the mixed layer and all the energy fluxes, both at the earth's surface and at the top of the mixed layer are held constant.

By substituting the expression for the shortwave irradiance, equation 2.12, into equation 2.11, scaling all heights with respect to the inversion height and introducing the parameter $\psi = H(0)/((1-r_s)S_i e^{-\tau})$ an equation is derived which must be solved to give z_*, the

the height at which the heat flux changes sign.

$$(\exp(\tau\zeta_*)-1)\left(\tfrac{1}{2}(1-k)\zeta_*^2 - (1-k)\zeta_*/\tau - \tfrac{1}{2}\right)/(1-r_s)$$

$$-r_s(\exp(-\tau\zeta_*)-1)\left(\tfrac{1}{2}(1-k)\zeta_*^2 + (1-k)\zeta_*/\tau - \tfrac{1}{2}\right)/(1-r_s)$$

$$+ \zeta_*^2(1-k)\left(1 - \tfrac{1}{2}\psi\right) + \zeta_*(\psi-1+r_s(\exp(-\tau)-1))/(\tau(1-r_s)))$$

$$- \frac{1}{2}\psi = 0$$

where $\zeta_* = z_*/h$

This equation was solved numerically for various values of the parameters τ, ψ and r_s. Once z_* has been determined the entrainment flux ratio can be calculated from equation 2.9

$$A' = -\frac{H(h)}{H(0)} = -\frac{1}{4}\left[(\psi-1)(1-\zeta_*^{-1}) + \frac{\exp(\tau)-r_s\exp(-\tau)}{(1-r_s)} - \frac{(\exp(\tau\zeta_*)-r_s\exp(-\tau\zeta_*))}{\zeta_*(1-r_s)}\right]$$

The calculated values of this ratio are shown plotted in Figure 2.8. The calculations were carried out for surface albedoes of 0, 0.2 and 0.4 and for optical depths of 0.1, 0.25 and 0.5. From this diagram it is apparent that the absorption of shortwave radiation reduces the entrainment ratio and the reduction is greater for greater optical depths. When the surface heat flux is only a small fraction of solar radiation absorbed at the earth's surface the entrainment ratio is more sensitive to the optical depth of the mixed layer. Increases in the surface albedo tend to decrease the entrainment ratio but the effect is small except for the more turbid layers.

The ratio ψ parameterizes the surface energy balance and if the net radiation at the surface is denoted by R_N, and G represents the

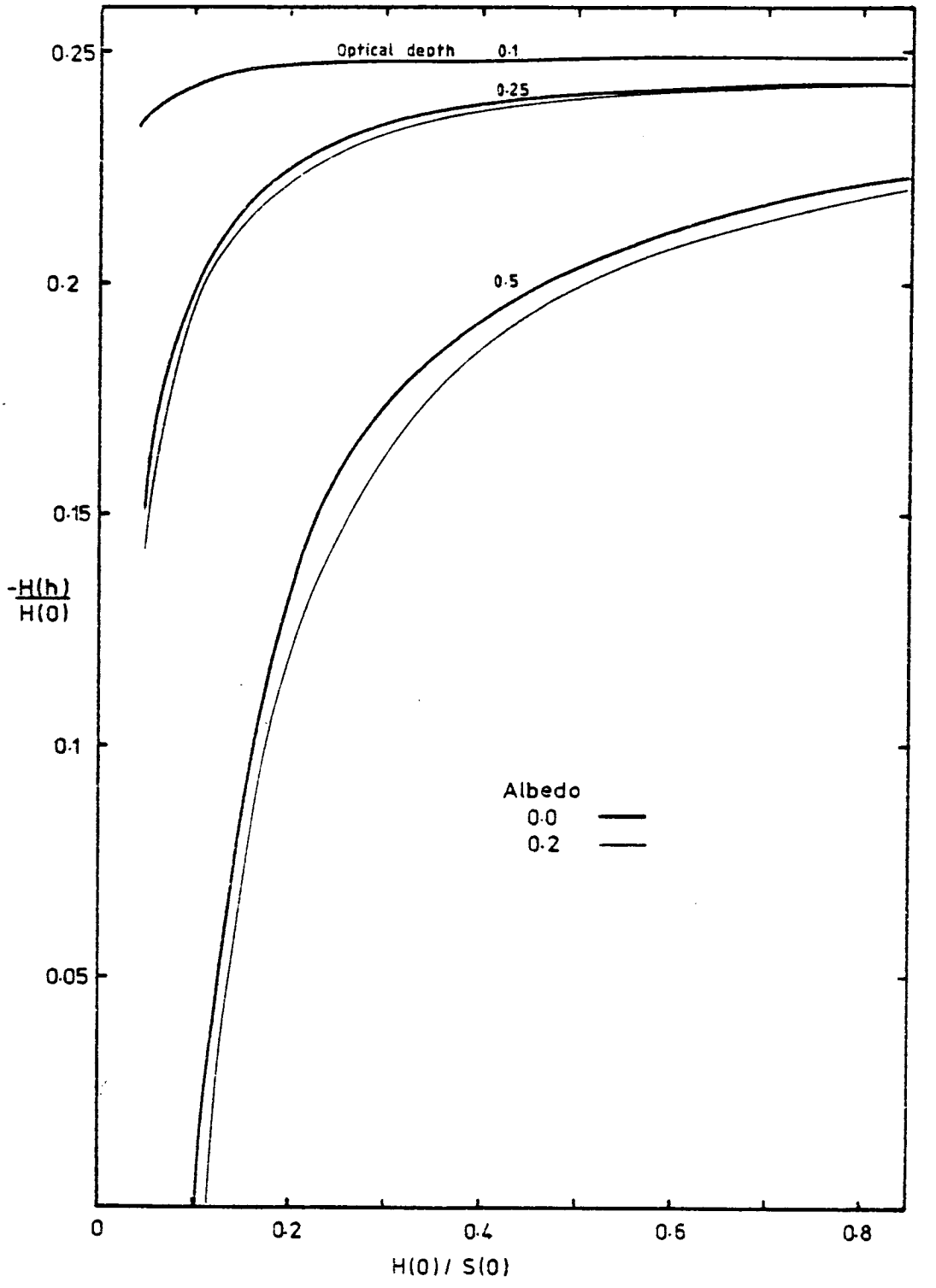

Figure 2.8 The Variation of the Entrainment Flux Ratio with ψ. Calculated for mixed layers of optical depths 0.1, 0.25 and 0.5

heat flux into the soil, then ψ may be expressed as

$$\psi = \frac{H(0)}{S(0)} = \left(\frac{\beta}{1+\beta}\right)\left(\frac{R_N-G}{S(0)}\right)$$

where β is the Bowen ratio. In attempting to determine the likely range of the value of ψ it should be remembered that each of these quantities varies, at an individual site, over the course of a day, apart from varying from place to place and from day to day. Therefore we shall look at conditions over mid-latitude grassland within two hours of local noon on a cloud-free summer day. Typical values of the various components of the surface energy budget for such a location and time are shown in Table 2.2

The Bowen ratio may be as small as 0.1 over a very moist surface, or as large as 10 over a very dry one. This range of the Bowen ratio results in values of the first factor in the expression for ψ of between 0.09 and 0.91.

The numerator of the second factor, (R_N-G), is the energy available at the surface to be transferred into the atmosphere. Typically this quantity varies between about 300 Wm^{-2} in October to 500 Wm^{-2} in June (Wood, 1977).

The longwave radiative loss from the earth's surface will be close to 100 Wm^{-2} (Monteith, 1974). The soil heat flux might attain a maximum value of perhaps 50 Wm^{-2} to 100 Wm^{-2}. These figures, taken together, imply that the downwelling solar irradiance at the earth's surface should be between 550 Wm^{-2} and 900 Wm^{-2}, assuming that the albedo of the surface is 0.2, values which are entirely in accord with published measurements of solar radiation at the earth's surface (see, for example, Deacon 1969).

	Net Downward Radiation Wm^{-2}	Sensible Heat Flux Wm^{-2}	Latent Heat Flux Wm^{-2}	Soil Heat Flux Wm^{-2}
0435	-49	- 8	-20	-49
0635	-31	- 5	- 1	-43
0835	193	186	60	58
1035	440	334	91	138
1235	524	461	76	148
1435	427	356	24	105
1635	161	118	26	25
1835	-65	-18	- 6	-31
2035	-77	-27	- 8	-34
2235	-67	-20	- 2	-38
0035	-64	-21	+ 5	-39
0235	-60	-18	+15	-39

Table 2.2a) The Surface Energy Budget During the Day. Data from the O'Neill Experiment for 7 September 1953 (Lettau and Davidson 1957)

Date	Time (GMT)	Sensible Heat Flux Wm^{-2}	Latent Heat Flux Wm^{-2}
19 Aug. 74	1118 - 1559	70 ± 60	210 ± 40
20 Aug. 74	0910 - 1300	140 ± 70	230 ± 40
	1300 - 1510	80 ± 60	170 ± 40
21 Aug. 74	1057 - 1555	60 ± 60	220 ± 40

Table 2.2b) Turbulent Fluxes at the Surface (from Moores et al, 1980)

Using the figures quoted here the second factor in this expression should lie between 0.6 and 0.8. This represents a maximum value which will be attained close to midday, the energy available at the surface, and hence this second factor, having risen from a value of zero shortly after sunrise when convection from the surface begins. A realistic range for the parameter ψ is, therefore, from 0 to 0.7.

Measurements made during the O'Neill experiment (Lettau and Davidson, 1957) show that between 0835 local time and 1635 ψ varies from 0.3 to a maximum of 0.6 or so close to noon and back to about 0.3.

2.5 A POTENTIAL ENERGY CONSTRAINT

The model described in the previous section is, as has already been stated, only valid if the turbulent kinetic energy generated within mixed layer is sufficient to maintain the well mixed profiles. In the absence of any turbulent mixing the absorption of solar radiation by aerosol, which is assumed to be distributed uniformly, tends to increase the stability of the layer. The layer will remain well mixed as long as the rate at which turbulent kinetic energy is generated is greater than the rate at which the absorption decreases the potential energy of the layer.

The rate at which turbulent kinetic energy is generated by buoyancy forces in the well mixed layer is

$$\int_o^h \frac{g}{\theta_m} \frac{H(z)}{c_p} \, dz$$

The turbulent heat flux can be expressed in terms of the turbulent and radiative fluxes at the upper and lower boundaries of the mixed layer.

By substituting the general expression for the heat flux, equation 2.9, and eliminating the quantity $S(z_*)$ by again using equation 2.9 this time evaluated at the top of the mixed layer, the rate at which turbulent kinetic energy is generated becomes

$$\frac{d}{dt}\,TKE = \frac{g}{c_p\theta_m}\left[\frac{h}{2}(H(0)+H(h)-S(0)-S(h))) + \int_o^h S(z)dz\right] \qquad \text{equation 2.13}$$

It should be remembered that this expression represents the net rate of production of turbulent kinetic energy by buoyancy. If the assumption that a fraction (1-k) of the buoyancy generated TKE is dissipated by viscosity, is still valid in a turbid convective layer then only the remainder, a fraction k of that generated, is available for maintaining the mixed profiles and for the entrainment at the top of the mixed layer. This available turbulent kinetic energy may be calculated by multiplying the right-hand side of equation 2.11 by the factor $k/(1-k)$.

The instantaneous rate of change of the available potential energy induced by the absorption of solar radiation may be written as

$$\int_o^h gz\,\frac{d\rho}{dt}\,dz - \frac{\partial}{\partial\theta_m}\left(\int_o^h gz\rho dz\right)\frac{d\theta_m}{dt} \qquad \text{equation 2.14}$$

The second term of this expression accounts for the change in the potential energy of the layer brought about by altering the potential temperature of the layer without altering the stability.

By differentiating the perfect gas law and expressing the result in terms of potential temperature the rate of change of the density of air can be expressed in terms of the shortwave divergence

$$\frac{d\rho}{dt} = -\frac{\rho}{\theta}\frac{d\theta}{dt} = -\frac{1}{c_p\theta}\frac{dS}{dz}$$

This makes the evaluation of the first term in the expression for the rate of change of the potential energy of the layer easy.

The mixed layer is of uniform potential temperature so that the density can be written as

$$\rho = \rho_o \left(1 - \frac{\Gamma z}{\theta_m}\right)^{c_p/R-1}$$

where ρ_o represents the air density at the earth's surface where the atmospheric pressure is assumed to be 1000 mb. R is the gas constant for dry air. The potential energy of the mixed layer, found by integrating this expression over the depth of the mixed layer, is equal to

$$\frac{1}{2} g\rho_o h^2 \left[1 - \frac{2}{3}\left(\frac{c_p}{R} - 1\right)\frac{\Gamma h}{\theta_m} + 0\left(\left(\frac{\Gamma h}{\theta_m}\right)^2\right)\right]$$

The first order term in $\frac{\Gamma h}{\theta_m}$ is, typically, about 0.05. Neglecting it and the higher order terms, differentiating with respect to potentially the mixed layer temperature and substituting into equation 2.14, the rate of change of the mixed layer potential energy is

$$-\frac{g}{c_p\theta_m}\left(hS(h) - \int_o^h S(z)dz\right) + \frac{1}{2}\frac{g\rho_o h^2}{\theta_m}\cdot\frac{1}{\rho_o c_p}\frac{(S(h)-S(0))}{h}$$

which on rearranging may be written as

$$-\frac{g}{c_p\theta_m}\left(\frac{1}{2}h(S(h) + S(0)) - \int_o^h S(z)dz\right)$$

Now the condition for the layer to remain well mixed is that the sum of the rates of change of the turbulent kinetic energy and the potential energy must be greater than zero.

$$\frac{g}{c_p\theta_m}\left[\frac{k}{(1-k)}\left\{\frac{1}{2}h(H(0)+H(h)-S(0)-S(h)) + \int_o^h S(z)dz\right\}\right.$$
$$\left. - \frac{1}{2}h(S(0)+S(h)) + \int_o^h S(z)dz\right] > 0$$

which on simplifying becomes

$$\frac{1}{2}k(H(0)+H(h)) - \frac{1}{2}(S(0)+S(h)) + \frac{1}{h}\int_o^h S(z)dz > 0$$

When the radiative flux within the mixed layer is of the exponential form described earlier, equation 2.12, this condition is easily expressed in terms of the entrainment ratio A' and the ratio, ψ, of the sensible heat flux at the surface and the shortwave irradiance at the surface.

$$1 - \frac{1}{k(1-r_s)\psi}\left(e^{\tau}+1-r_s(e^{-\tau}+1) - \frac{2}{\tau}(e^{\tau}-1) - \frac{2r_s}{\tau}(e^{-\tau}-1)\right) > A'$$

For small optical depths this constraint can be simplified by expanding the exponential functions. The constant and first order terms in τ vanish and retaining only the first two non-zero terms of the resulting series leads to

$$1 - \frac{\tau^2}{k(1-r_s)}\left[\frac{(1-r_s)}{3!} + \frac{2(1+r_s)}{4!}\tau\right] > A'$$

The ranges of values of ψ and A' for which the model fulfils the potential energy constraint can be calculated from this inequality. This has been done for the results shown in Figure 2.9. When the surface albedo is zero the energy condition is satisfied in the upper part of the diagram, above the line AA. As the albedo of the surface is increased the corresponding boundary of the region in which the constraint is satisfied moves upwards, thus further restricting the

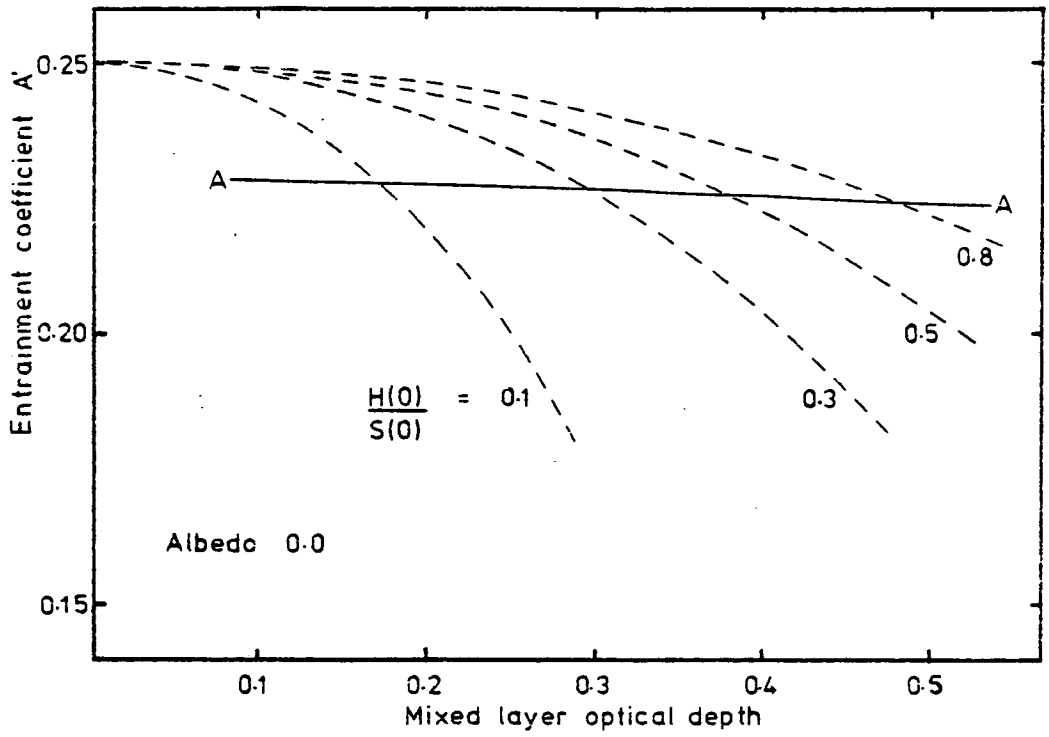

Figure 2.9 The Potential Energy Constraint

possible range of variation of the entrainment ratio.

It will be noticed that if the optical depth of the mixed layer is greater than 0.48 it is not possible to satisfy the condition. In other words even if the sensible heat flux accounts for 80% of the solar radiation absorbed at the surface, a large fraction in practice, convection will not be vigorous enough to maintain the well mixed profiles. If the surface albedo is set to a more realistic value of 0.2 then the mixed layer cannot be maintained for optical depths greater than 0.41.

2.6 THE DEVELOPMENT OF A TURBID MIXED LAYER

Having determined how absorption of radiation within the mixed layer alters the entrained heat flux ratio it is possible to use a slightly modified form of equation 2.4 to describe the development of a turbid convective layer. The modifications necessary are

i) to use the modified entrainment flux ratio, A', in place of the constant A. This does not alter the form of the equation at all

ii) to include the effect of the direct heating of the air due to the absorption. This may be expressed as a fraction ε of the surface heat flux, H(0), which results in an extra factor, $(1+\varepsilon)$, appearing in the right-hand side of the expression of the conservation of enthalpy.

The modified form of equation 2.4 is

$$Z^{(1+\varepsilon)/A}\left[Z^2(1+\varepsilon) + (1+\varepsilon+2A')\left(\frac{2\Delta\theta(t_1)}{\gamma h(t_1)} - 1 - \frac{2}{\gamma h^2(t_1)}\int_{t_1}^{t}(1+\varepsilon)\frac{H(0)}{\rho c_p}dt\right)\right]$$
$$+ (1+\varepsilon+2A')\left[\frac{2A'}{1+\varepsilon+2A'} - \frac{2\Delta\theta(t_1)}{\gamma h(t_1)}\right] = 0$$

As before, if the initial conditions are such that the second term on the left-hand side of this equation is zero then the solutions for $h(t)$ and $\Delta\theta(t)$ have particularly simple forms.

$$h(t) = \sqrt{h^2(t_1) + \frac{2(1+\varepsilon+2A')}{\gamma}\int_{t_1}^{t}\frac{H(0)}{\rho c_p}\,dt}$$

$$\Delta\theta(t) = \left(\frac{A'}{1+\varepsilon+2A'}\right)\gamma h(t)$$

and in cases in which the initial conditions are not constrained in this way the solutions tend to this simple form as the layer deepens.

It is immediately apparent that, if the gradient of the original potential temperature profile remains unchanged, a turbid layer will deepen more quickly than a clear one if

$$(1+\varepsilon+2A')\,\psi S_i\,(1-r_s)e^{-\tau} > (1+2A)\,\psi S_i\,(1-r_s)$$

For realistic values of the model parameters this condition is normally fulfilled, and the more turbid layers deepen more quickly. If the surface albedo is set to zero then the surface heat flux must be greater than 50% of the shortwave energy absorbed at the surface, before the more turbid layers deepen more slowly. As the surface albedo is increased so this condition is satisfied for greater values of ψ. Figure 2.10 shows the locus of this condition for various values of r_s and ψ.

It is equally obvious from these simple solutions that, as a

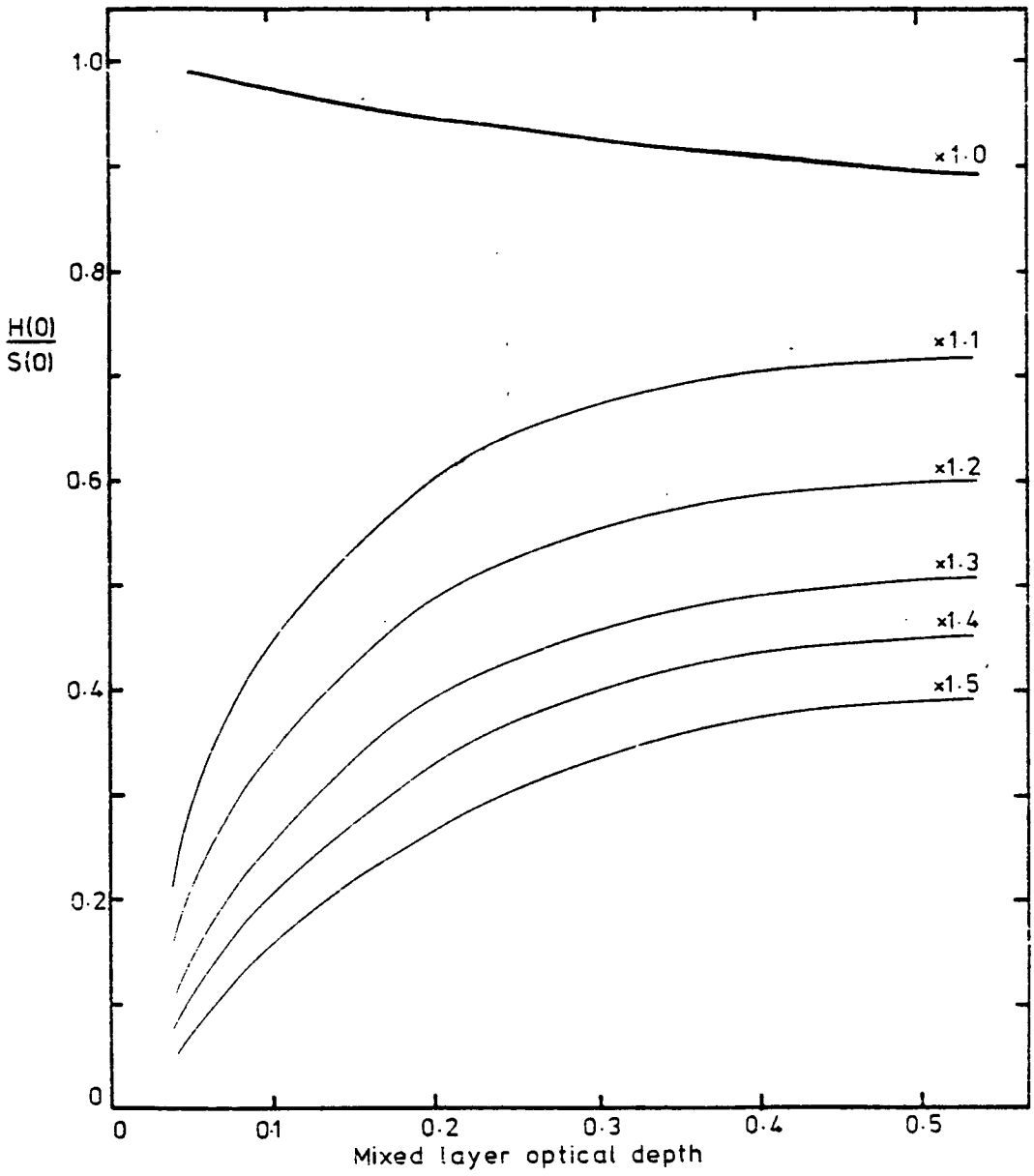

Figure 2.10 Contours of the Rate of Growth of Turbid Mixed Layers Compared to that of a Transparent One

turbid mixed layer deepens the temperature jump at the top of the layer will be smaller than that at the top of a comparable mixed layer of greater transparency. The more turbid mixed layers, as might be expected, will be warmer.

Changes in the values of the albedo, r_s, or ψ alter both the slope of the trajectories plotted in Figure 2.11 and the rate at which these trajectories are traversed. The slope is decreased and the rate at which the trajectories traversed is increased by either decreasing the surface albedo or by increasing the parameter ψ.

These properties of the model, and indeed of the atmospheric convective layer, may be understood by some general considerations. Shortwave radiative energy enters the mixed layer by one of two routes, directly, as a result of absorption before or after reflection at the surface, or indirectly, being absorbed at the surface and transferred to the mixed layer by turbulent exchange. Since the energy which is absorbed at the earth's surface is partitioned into four separate components, of which only one leads to a warming of the mixed layer, direct absorption of incoming solar radiation results in a greater energy input to the mixed layer than would otherwise occur. At the same time by reducing the surface turbulent heat flux, absorption of solar radiation within the mixed layer reduces the entrained heat flux at the base of the inversion as well as reducing the entrainment flux ratio.

The enhanced growth rates of turbid mixed layers predicted by the modified versions of equations 2.5 and 2.6 occur because the increased heating of the mixed layer, due to radiation absorption, decreases the size of the temperature jump at the top of the mixed layer. The entrained heat flux is determined by the entrainment flux

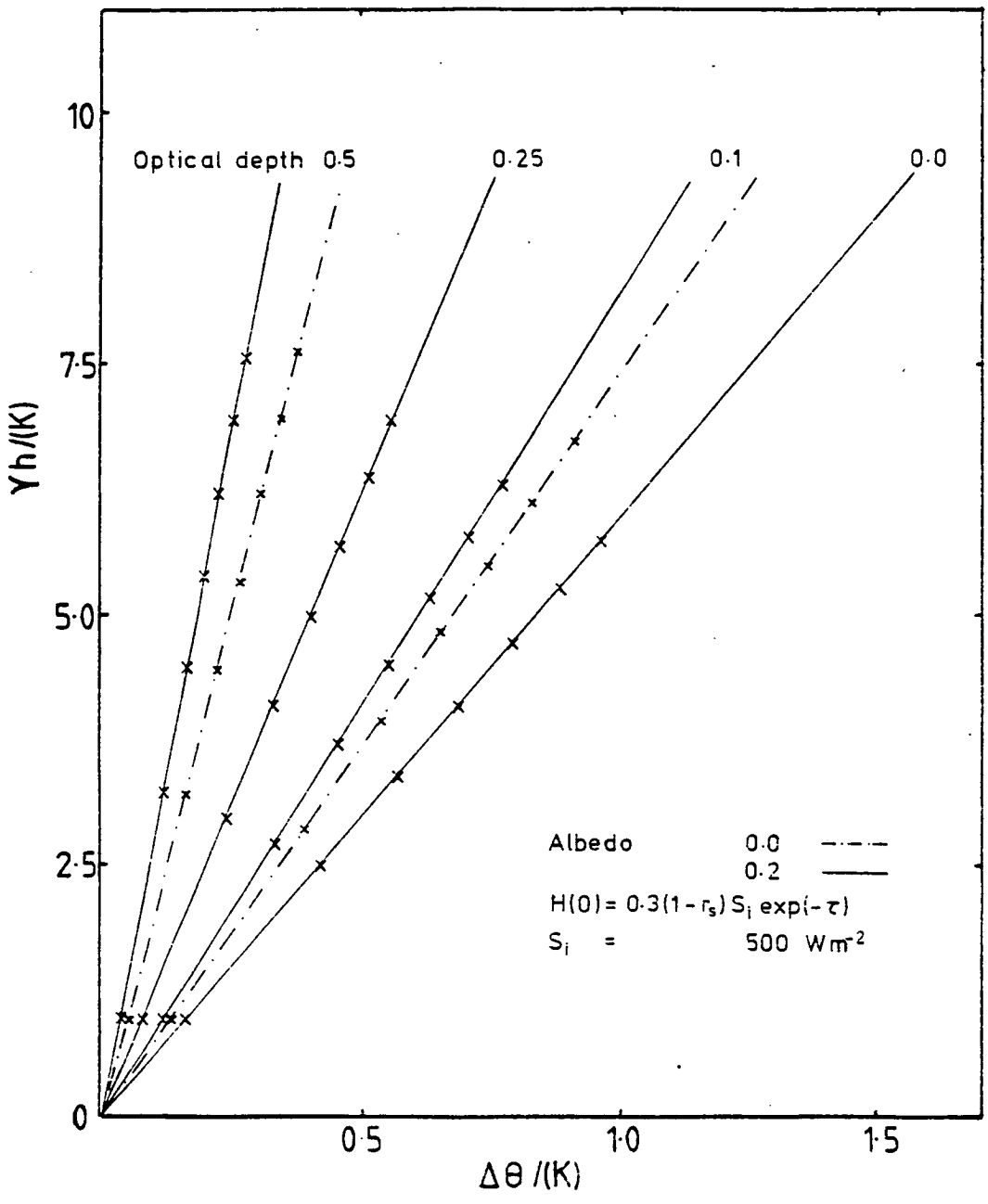

Figure 2.11 Trajectories of the Analytic Solution for a Turbid Mixed Layer

ratio A' and the surface heat flux and as the size of the temperature jump decreases the rate of entrainment, or rate of growth of the mixed layer, must increase correspondingly. When these simple solutions are appropriate the decrease in the size of the temperature jump, brought about by the absorption is obviously more than sufficient to compensate for the reduction in both A' and the surface heat flux.

The solutions derived from arbitrary initial conditions rapidly converge to the simple solutions. However although the adjustment is rapid the initial period of adjustment, when the mixed layer deepens only slowly, results in the subsequent development of the layer lagging behind the comparable simple solution. This is of particular importance, for, in practice all of the model parameters, with the possible exception of the surface albedo, are functions of the sun's elevation and therefore change quite considerably over the hours of daylight. Hence it is unlikely that the simple solutions will provide a good description of the development of a real turbid mixed layer except, possibly, close to midday when the solar elevation changes relatively slowly.

2.7 SUMMARY OF RESULTS AND LIMITATIONS OF THE ANALYTIC MODEL

The most important results derived from this analytic model in this chapter are:

i) Absorption of radiative energy within the mixed layer reduces the entrainment flux ratio by an amount which depends on the magnitude and distribution of the absorption within the layer, and on the conditions at the earth's surface, in so far as they affect the radiative and turbulent flux profiles within the mixed layer.

For values of the model parameters which are representative of conditions over vegetated land surfaces in mid-latitudes on cloud-free summer days the entrainment ratio may be reduced by up to 40% of its value for a non-turbid mixed layer.

ii) Absorption of the downwelling shortwave radiation stream tends to stabilise the mixed layer temperature profile. An additional constraint must be imposed on the model, that the turbulent kinetic energy generated by buoyancy within the mixed layer must balance both the viscous dissipation of TKE and the work done in maintaining the well mixed temperature profile. This additional constraint severely restricts the conditions under which the well mixed profiles can be maintained and the model remain valid. The effect of this to reduce the possible range of variation of the entrainment flux ratio to about 10% of its value for a non-turbid mixed layer.

iii) The solutions of the mixed layer equations derived here by assuming that the external parameters are constant, converge to solutions which do not depend on the initial conditions. These solutions predict that the direct heating within the mixed layer due to absorption of shortwave radiation by aerosol causes the mixed layer to deepen and warm up more quickly than a comparable transparent layer.

It would not seem to be justified to extend this conclusion to include cases in which the external parameters are time dependent, particularly in view of the time taken for the general solutions to converge to the asymptote, and that while the adjustment is taking place the mixed layer grows very much more slowly than it does afterwards.

These results have been derived at a cost of making a number of

approximations. The most important of these, in the light of the third conclusion above, is the assumption that the external parameters of the model, the solar irradiance above the mixed layer, the optical depth of the layer and the surface energy budget parameter ψ, are each independent of time. In reality the solar irradiance at the top of the mixed layer and the path length through the mixed layer of the direct solar beam each depend on the elevation of the sun. These time dependencies will be included in the numerical model.

The aerosol loading is, in general, also time dependent. Particles are removed from the atmosphere by dry deposition, wet deposition and rain-out process, although only the first of these is important within the present context. Sources of dry aerosol, especially anthropomorphic sources, exhibit marked diurnal variation in the rates at which they supply material to the atmosphere. It is likely, therefore that, under the conditions assumed here, the aerosol loading of a turbid mixed layer, and therefore its turbidity, will gradually increase during the day time.

The specification of the shortwave irradiance within the mixed layer takes no account of scattering by either aerosol particles or gaseous molecules. As a result of this the energy input to the combined boundary layer-soil layer remains constant. The interaction of aerosol and radiation within the mixed layer simply alters the proportion of the energy input to the two components of the system. Atmospheric aerosol scatters as well as absorbs solar radiation. As a result increased aerosol concentrations in the atmosphere alter the overall energy input to the boundary layer-soil layer system.

Because of the importance of the condition of the earth's surface and upper layer in determining the partition of energy at the

surface, and since the details of that partition are likely to depend on the turbidity of the mixed layer the parameterization of the surface turbulent heat flux as a constant fraction of the energy available is felt to be inadequate.

The numerical model to be described next is intended to provide a closer approximation to reality than the analytic model particularly in the three respects outlined here.

CHAPTER 3

THE NUMERICAL MODEL

3.1 INTRODUCTION

The numerical model to be described now is based on the analytic model described in chapter two but the manner in which the radiative fluxes are specified and the means by which the turbulent fluxes at the earth's surface are calculated differ from the very simple parameterizations which were used to facilitate obtaining an analytic solution.

The intentions, in developing this more complex model are:

i) to include the diurnal variation of the shortwave irradiance throughout the mixed layer and at the earth's surface, and therefore those of the turbulent fluxes of heat and moisture, brought about by the apparent motion of the sun across the sky.

ii) to include the effect of scattering of radiation by aerosol within the mixed layer as well as that of absorption, and

iii) to improve the specification of the sensible heat flux at the surface.

The shortwave fluxes within the boundary layer will be calculated by a two-stream method, which takes account of scattering by aerosol, given the downward solar irradiance at the top of the mixed layer, the albedo of the surface and two parameters which describe the optical properties of the absorbing material within the mixed layer.

The solar irradiance at the top of the mixed layer, both direct and diffuse components, is found by computing the effects of molecular scattering and of absorption by water vapour and ozone. Absorption by aerosol in the air above the mixed layer is not included mainly because of the complexity of the calculation and the relative lack of data on the concentrations and optical properties of the material. However the effect of aerosol absorption and scattering may be parameterized by comparing the calculated irradiance at the earth's surface beneath an atmosphere devoid of aerosol with actual observations. The radiation scheme might then be legitimately tuned by the introduction of a factor, derived from the comparison, which represents the mean transmittance of the aerosol over the solar spectrum.

The improvement in the specification of the sensible heat flux at the surface is achieved by introducing a surface energy balance to relate the turbulent fluxes to the net incoming radiation at the surface and the heat flux into the soil. Calculation of the soil heat flux, and of the surface temperature, necessitates the inclusion of a model of the soil to a depth of about one metre, at which depth the temperature may be considered constant over periods of a few days.

The introduction of the surface energy balance requires that the downward infra-red irradiance at the surface is known. Since the lower atmosphere is relatively opaque to radiation of wavelengths greater than three microns, the infra-red irradiance at the surface is determined largely by the temperature and moisture structure in the atmosphere's lowest kilometre or so.

The infra-red irradiance is specified at the top of the mixed layer, the value being that appropriate for one of the two atmospheric

profiles which are used in determining the extinction of shortwave radiation by water vapour and ozone in the atmosphere above the mixed layer.

3.2 CALCULATION OF THE SHORTWAVE IRRADIANCE ABOVE THE MIXED LAYER

In order to provide realistic energy inputs at the ground over the course of a day the time-dependent solar irradiance has to be calculated. A basic assumption of the model is that the aerosol present within the mixed layer is modifying the solar beam. The method used to calculate the attenuation by the aerosol within the mixed layer is described in section 3.3. However the irradiance of the direct solar beam and the downward diffuse irradiance at the top of the layer are required for this calculation and must be determined by other means.

The solar beam is scattered and absorbed by a variety of chemical species in the atmosphere. The most important of these are ozone, carbon dioxide and water-vapour. In addition, atmospheric aerosol above the mixed layer depletes the shortwave irradiance. The transmittance of any atmospheric layer depends on the amount of each of these optically active species present and on the temperature and pressure of the layer. Furthermore, the transmittance is a strongly varying function of wavelength. An accurate solution of the radiative transfer equation requires detailed knowledge of the temperature profile, the mixing ratios of each of the optically active constituents and of the absorption coefficients of each species across the whole of the solar spectrum.

The results from an accurate numerical calculation of the

absorption by ozone and by water-vapour have been parameterized by Lacis and Hansen (1974) in terms of the path-lengths of each of the absorbers. The parameterization of the water-vapour absorption is closer to the accurate values if the path-length is scaled to try to take account of the pressure and temperature dependence of the absorption. These two parameterizations are used to calculate the depletion of the direct solar beam.

The diffuse radiation arises from molecular scattering of energy out of the direct beam and also from scattering by larger aerosol particles. The molecular scattering may be calculated using Rayleigh theory, valid when the scattering particles are much smaller than the wavelength of the incident radiation. Since the concentrations and optical properties of aerosol in the stratosphere and upper troposphere are not well known their effect has not been calculated. Furthermore, since the aerosol particles are of a size of the same order as the wavelength of the radiation, Rayleigh theory would be invalid and more comlex Mie theory would have to be used instead.

Ignoring the contribution of aerosol to the scattering and absorption means that the calculated direct irradiance is likely to be too large and the diffuse component correspondingly too small. As the solar zenith angle is increased the discrepancies would be expected to increase.

a) Absorption of Shortwave Radiation in the Upper Atmosphere

The absorption of shortwave radiation by water-vapour and ozone has been computed by means of a parameterization due to Lacis and Hansen (1974). The fractional depletion of the direct solar beam by ozone, a_{oz}, is given by

$$a_{oz} = \frac{0.2118x}{1+0.042+0.000323x^2} + \frac{1.082x}{(1+138.6x)^{0.205}} + \frac{0.0658x}{1+(103.6x)^3}$$

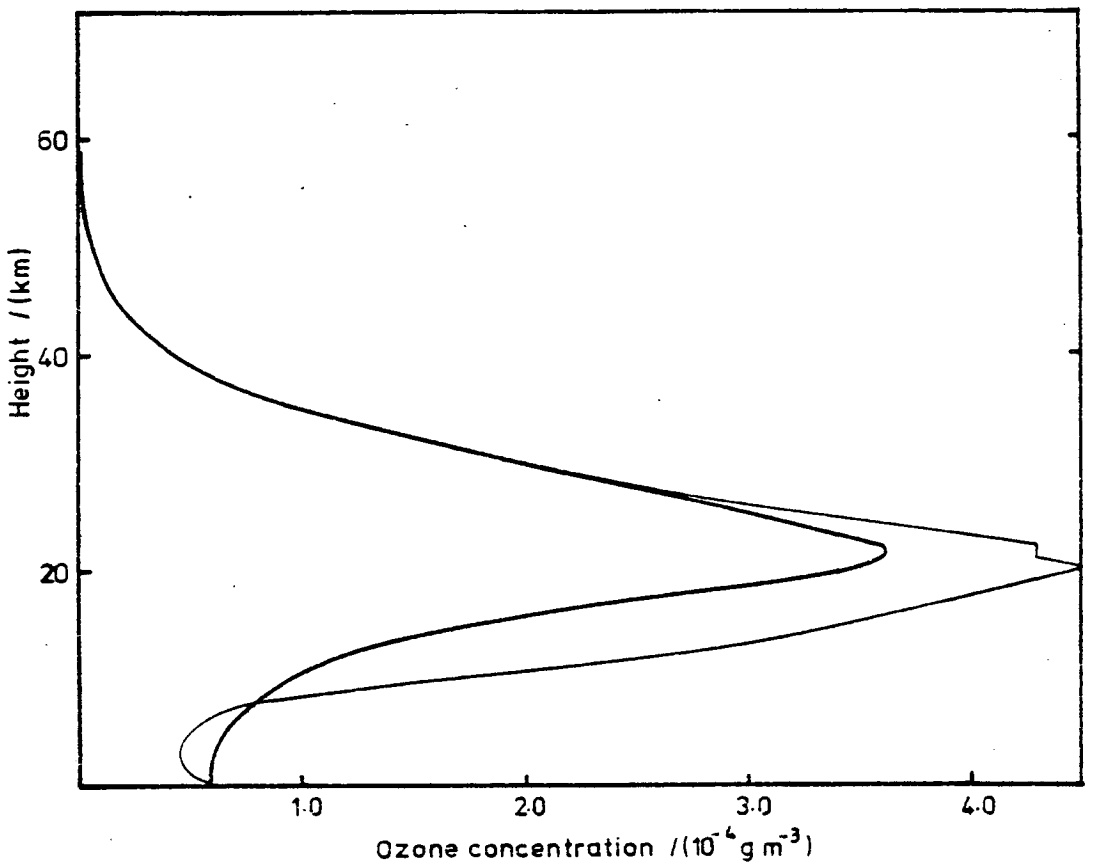

Figure 3.1 The Concentration of Ozone in the Atmosphere. Data taken from the COESA mid-latitude winter (—) and summer (–) profiles

where x is the ozone path length in centimetres. The first term represents the absorption in the ultra-violet Hartley bands, the second and third terms that due to the Chappuis band in the visible part of the spectrum. This expression is said to be accurate to better than 0.5% for 10^{-4} cm < x < 1.0 cm.

The relative air mass used in calculating the ozone path-length has to take account of the earth's curvature since most of the ozone is found at heights of about 20 km. Following Rodgers (1967), the relative air mass m is taken to be

$$m = \frac{35}{\sqrt{(1224.0\ \mu^2 + 1)}}$$

where μ is the cosine of the solar zenith angle.

Since this study is concerned only with the lowest layers of the atmosphere, it is not necessary to consider the absorption of upwelling shortwave radiation reflected from the earth's surface.

In a similar way Lacis and Hansen parameterize absorption by water-vapour. The formula they give is

$$a_{wv} = \frac{2.9y}{(1 + 141.5y)^{0.635} + 5.925y}$$

where y represents the scaled water-vapour path-length, in centimetres, which is defined below. This expression is accurate to within 1% for scaled water-vapour path-lengths within the range from 0.01 cm to 10 cm.

Unlike ozone, the water-vapour is predominantly in the lowest 10 to 15 kilometres of the atmosphere, beneath the tropopause, so that it is acceptable to approximate the relative air-mass by the reciprocal of the cosine of the solar zenith angle.

As a first step toward accounting for the pressure broadening

of the absorption lines in the water-vapour spectrum, it is customary to scale the geometric path-length in a pressure and temperature dependent way. Then the scaled water-vapour path-length from the surface to a height z is

$$y = \frac{1}{g} \int_{o}^{p(z)} q(z) \left[\frac{p(z)}{p(o)}\right]^{\frac{1}{2}} \left[\frac{T(o)}{T(z)}\right]^{\frac{1}{2}} dp$$

The shortcomings of the temperature dependence employed in this type of scaling have been pointed out by Chou and Arking (1980). Line by line calculations of the water-vapour absorption show that it increases as temperature increases. The scaling used by Lacis and Hansen was originally suggested by Elsasser and was derived by ignoring the temperature dependence of the intensity of water-vapour absorption lines which, in fact, dominates the temperature dependence of the line half-width. Chou and Arking also criticised the use of the temperature at the bottom of the atmosphere as the reference temperature as it introduces large errors in the middle and upper troposphere. However, since the parameterization was derived using this scaling, no greater accuracy is likely to be achieved by altering the temperature dependence without reformulating the expression used to calculate the fractional absorption.

The distributions of ozone, water-vapour and temperature from the top of the atmosphere down to the top of the convective layer are needed to be able to evaluate the solar irradiance at the top of the mixed layer. The COESA supplementary atmospheres for mid-latitudes (45°) for winter and summer have been used to give total ozone paths and scaled water-vapour path-lengths. The ozone profiles are shown in Figure 3.1 and the water-vapour path-lengths in Figure 3.2.

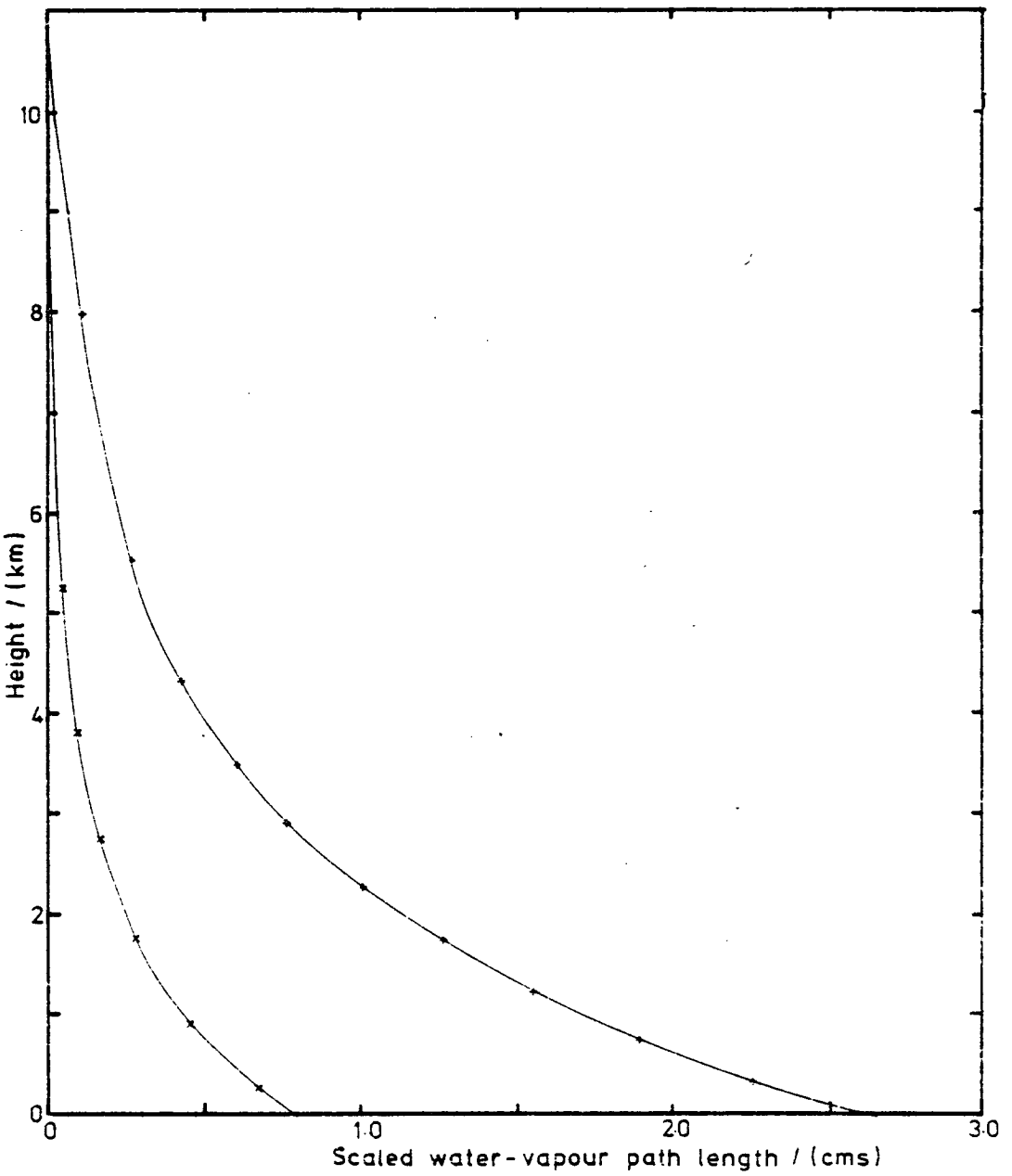

Figure 3.2 The Scaled Water Vapour Path-Length in the Atmosphere based on the COESA mid-latitude winter (×) and summer (+) profiles

The use of such climatological data may be objected to on the grounds that the temperature and humidity profiles may not be typical of the conditions being modelled. For example, the climatological profiles show no sign of a convective layer or capping inversion layer. Systematic departures from the climatic profiles in the upper atmosphere might be associated with the presence of convective boundary layers of the type being studied here.

However, the irradiance at the top of the mixed layer is relatively insensitive to changes in conditions in the upper atmosphere. The fractional absorption due to ozone varies from 0.023, calculated for the summer COESA profile, to 0.025 for the winter profile. The effect of water-vapour on both the longwave and shortwave radiation streams is greatest in the lowest parts of the atmosphere where most of the water vapour is.

b) Rayleigh Scattering above the Mixed Layer

In order to calculate the molecular scattering of radiation out of the direct solar beam and into the diffuse component a method devised by Chandrasekhar has been used which is described by Diermendjian and Sekara (1954).

The monochromatic global irradiance, $G(\tau,\mu)$ Wm^{-2}, within a plane parallel atmosphere of infinite extent, in which there is no absorption and in which the only scattering particles are small enough for Rayleigh scattering theory to be an accurate approximation, is given, in Chandrasekhars solution of the radiative transfer equation, in terms of the monochromatic irradiance at the top of the atmosphere, $I_o(\lambda)$ Wm^{-2}, and two functions $Z(\tau,\mu)$ and $S(\tau)$, values of which are

tabulated by Diermendjian and Sekara.

$$G(\tau,\mu) = \mu Io \left[Z(\tau,\mu) \frac{(1-r_s(S(\tau_o)-S(\tau)))}{1-r_s S(\tau_o)} + \exp\left(-\frac{\tau}{\mu}\right) \right]$$

The albedo of the underlying surface is represented by r_s and τ_o is the optical depth of the entire atmosphere. The first term in this expression represents the diffuse irradiance and the second represents the contribution from the direct beam.

A sixth order polynomial in τ was fitted to the tabulated values of $S(\tau)$. The results are accurate to within 1% of the tabulated values except at very small optical depths. Attempts to fit two-dimensional Tchebyshev polynomials to $Z(\tau,\mu)$ became unwieldy and it was found to be simpler, and more accurate, to employ a look-up table of 180 elements, the value of the function being obtained from a linear interpolation between the four nearest entries in the table.

Details of both the coefficients of the polynomial function and the entries in the look-up table are contained in the appendix.

The optical depth at any level within a clean dry atmosphere has been parameterized by Magraaf and Griggs (1969). Only molecular, Rayleigh scattering is included in the parameterization. The optical depth, τ_R, between the top of the atmosphere and a height z is strongly dependent on the wavelength of the radiation considered and is given by

$$\tau_R(\lambda,z) = \frac{0.0088\lambda^{(0.2\lambda-4.15)}}{\exp(0.118z+0.00116z^2)}$$

where λ, the wavelength, is measured in micrometres and z in kilometres.

At the short end of the solar spectrum the Rayleigh optical

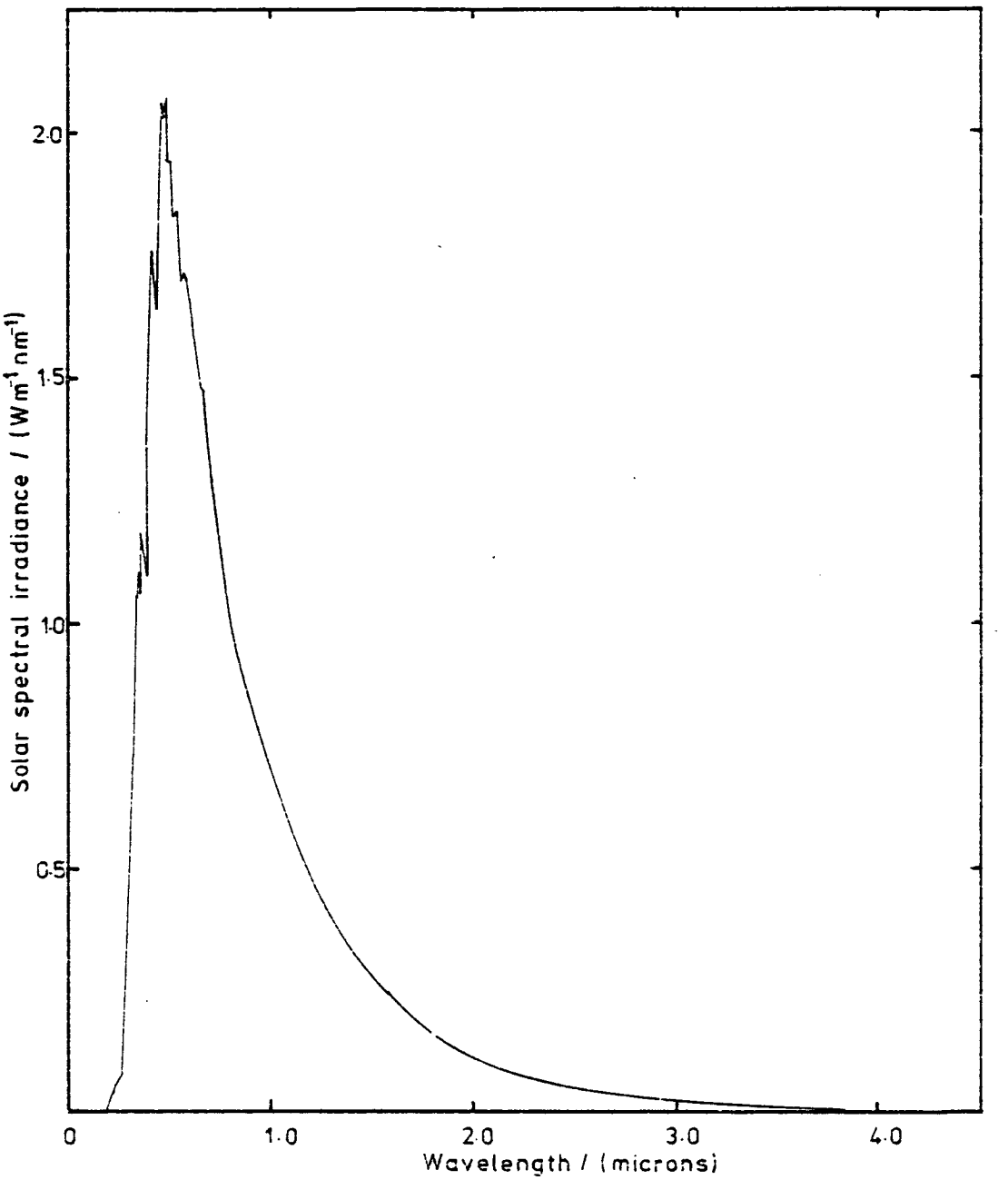

Figure 3.3 The Spectral Distribution of the Solar Irradiance, Normal to the Beam, at the Top of the Earth's Atmosphere
(data from Thekaekara and Drummond, 1971)

depth at the surface given by this expression is approximately unity. The rate of decrease of the optical depth with wavelength is, however, rapid and the calculated optical depth of the atmosphere at wavelengths of 1 μm is only 0.01.

Data on the specific solar irradiance at the top of the earth's atmosphere at 73 points in the wavelength range between 0.16 μm and 10.0 μm were taken from that published by Thekaekara and Drummond (1971). The irradiance at intermediate wavelengths is found by linear interpolation.

The downward direct and diffuse irradiances at any level within a dry, clean, Rayleigh atmosphere could now be calculated by numerically evaluating the expressions

$$\int_{0.0}^{10.0} \mu I_o(\lambda) Z(\tau_R(\lambda,z),\mu) \frac{(1-r_s(S(\tau_R(\lambda,o))-S(\tau_R(\lambda,z))))}{1-r_s S(\tau_R(\lambda,o))} d\lambda$$

for the diffuse component and

$$\int_{0.0}^{10.0} \mu I_o(\lambda) \exp(-\tau_R(\lambda,z)/\mu) d\lambda$$

for the direct beam.

c) Combination of the Effects of Rayleigh Scattering and Absorption by Water-Vapour and Ozone

In general in radiative transfer problems it is not possible to add together the calculated effects of two different processes and expect the result to bear much relation to the observations. Therefore, although the parameterized absorptances for water-vapour and ozone and the calculated effect of Rayleigh scattering are all, separately, accurate it is not at all obvious how, or indeed whether,

their combined effect can be found simply from these individual calculations.

Fortunately the three processes being considered here happen to be independent in a sense which does permit a relatively simple combination to be justified. First of all, since the atmospheric ozone distribution has a large maximum at a height of about 25 km most of the absorption due to ozone takes place above the troposphere, where most of the water-vapour is located, and where most of the molecular scattering takes place. Ozone absorption is restricted to wavelengths less than 0.4 μm. Water-vapour absorption on the other hand is only important at wavelengths greater than 0.7 μm. The Rayleigh scattering cross-section is inversely proportional to the fourth power of the wavelength, so that only the short wavelength end of the spectrum is affected.

Because these three processes take place at different heights or affect different regions of the spectrum, the individual computations may be combined as if the ozone absorption occurs first, depleting only the direct beam, which is subsequently scattered in passing through the troposphere. Since it is predominantly blue light which is scattered, the water-vapour absorption may be thought of as depleting the direct beam only. Then the irradiance of the direct beam, F_r Wm^{-2}, and the diffuse beam, F_f Wm^{-2}, are written in terms of the solar irradiance at the top of the atmosphere I_o Wm^{-2} and the cosine of the solar zenith angle

$$F_r(\lambda) = (1-a_{oz})\mu I_o(\lambda)(\exp(-\tau_R(\lambda,z)/\mu)-a_{wv}) \qquad \text{equation 3.1}$$

$$F_f(\lambda) = (1-a_{oz})(G(\tau_R(\lambda,z),\mu)-\mu I_o \exp(-\tau_R(\lambda,z)/\mu)) \qquad \text{equation 3.2}$$

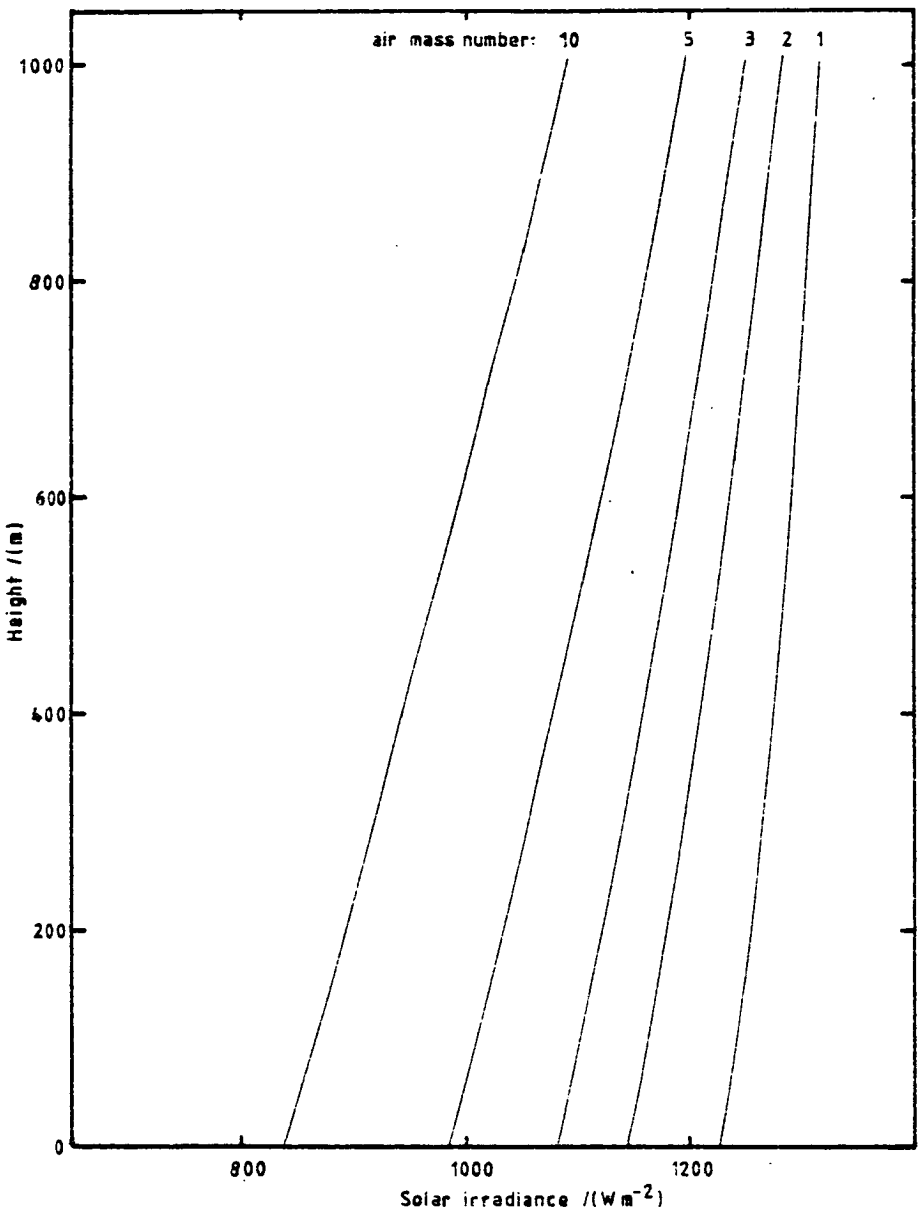

Figure 3.4 The Irradiance of the Direct Solar Beam on a Surface Normal to the Direction of Propagation in a Rayleigh Atmosphere

where $\exp(-\tau_R/\mu)$ represents the extinction of the direct beam by Rayleigh scattering. The integration of these expressions over the solar spectrum is carried out numerically.

Paltridge and Platt (1976) give details of a series of measurements of the downwelling direct and diffuse solar irradiances on a horizontal plane at the earth's surface in cloudless conditions over a period of several years. The measurements are highly correlated with the solar elevation, θ. The scatter that does occur is held to be due to varying aerosol and water-vapour loadings during the period when the measurements were made. The lines of best-fit are given by the expressions.

$$F_r = 1000(1-\exp(-0.06\theta))\ \sin\theta$$

$$F_f = 5 + 96(1-\exp(-0.05\theta))$$

Paltridge and Platt suggest that for many applications these expressions would be sufficiently accurate, the alternative being to develop a complete radiative transfer scheme.

The requirement in the present investigation is to obtain values of the downward direct and diffuse solar irradiances at the top of the mixed layer. It is not obvious, a priori, by how much these two quantities will vary over the lowest two or three kilometres of the atmosphere. However the scattering and absorption extinctions are likely to be greatest lower down in the atmosphere as the greatest molecular densities occur there.

Figure 3.4 shows the irradiance of the direct beam in a clean dry atmosphere in which the only depletion is due to Rayleigh scattering. The calculations were made using Magraaf and Grigg's expression

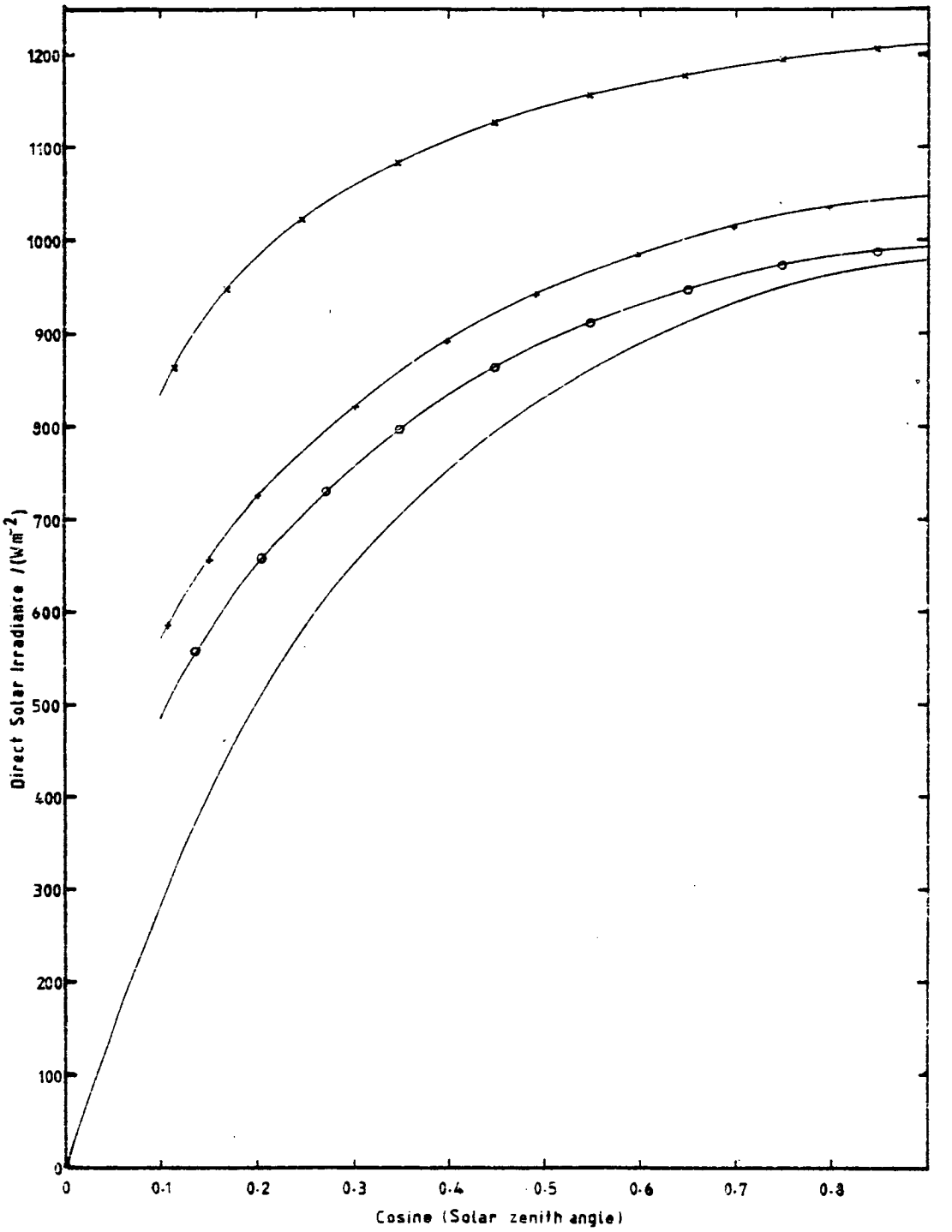

Figure 3.5 The Irradiance of the Direct Solar Component on a Horizontal Plane at the Surface

Mean Aspendale values: ——
Summer profiles: o——o
Winter profiles: +——+
No absorption: ×——×

for the optical depth as a function of height in a Rayleigh atmosphere. The calculated differences between the direct irradiance at the surface and that at a height of three kilometres vary with the assumed solar zenith angle. However at an air-mass number of five, which corresponds to a solar zenith angle of nearly 80°, the direct irradiance at a height of three kilometres is approximately 7% greater than that at the surface. Had extinction by water-vapour and aerosol been included the difference between the direct irradiance at these heights would have been larger. Therefore, except as a very rough first approximation the Aspendale expressions would not be suitable for calculating the shortwave irradiances at the top of the mixed layer.

Figures 3.5 and 3.6 show the direct irradiance of the solar beam and the diffuse irradiance at the earth's surface calculated from equations 3.1 and 3.2. The calculations were performed using both the summer and winter profiles of water-vapour and ozone described earlier. The appropriate Aspendale means are also plotted for comparison.

The direct irradiance is greater for the winter profile than for the summer one. This would be expected as the winter profile contains less water-vapour. More significantly the irradiances calculated using either summer or winter profiles overestimate the direct irradiance at the surface when compared to the Aspendale figures. The Aspendale direct irradiance varies from 69% to 97% of the calculated values, depending on the particular profile used and the solar zenith angle. At large air-mass numbers the difference between the observed values and those calculated is greatest.

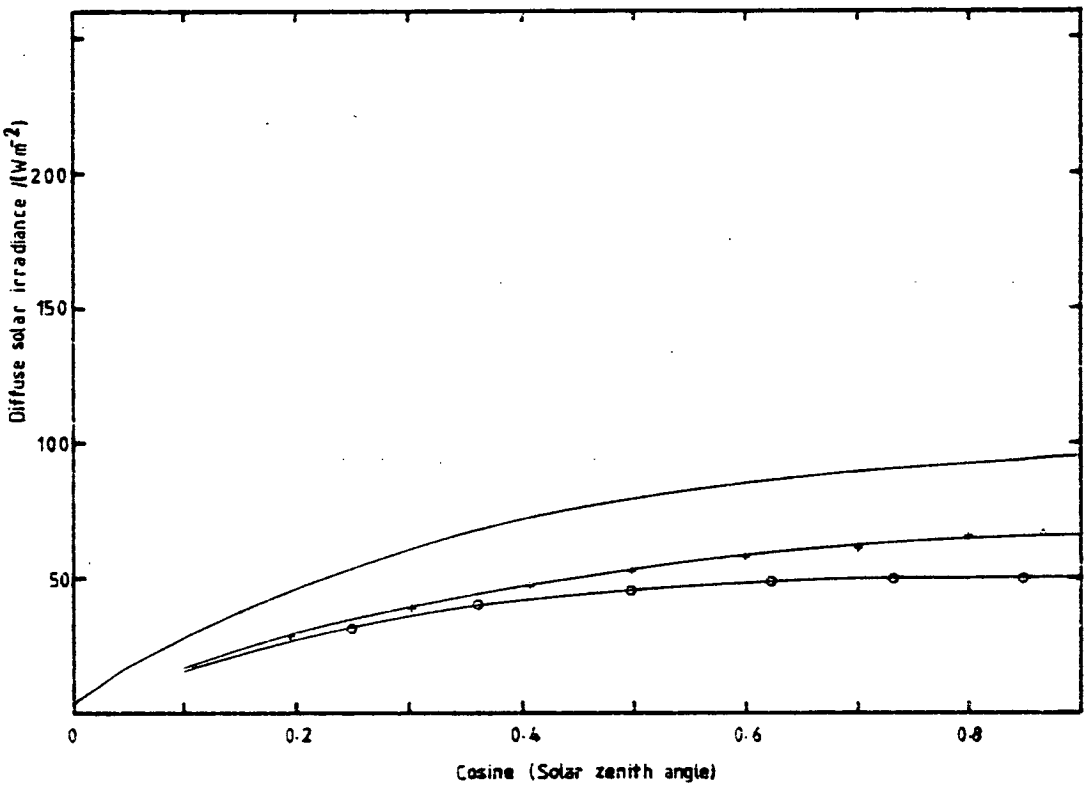

Figure 3.6 The Irradiance of the Diffuse Solar Component at the Surface. The symbols are the same as for Figure 3.5

These discrepancies are consistent with the omission of the effects of atmospheric aerosol in making the calculations. Eltermann and Toolin (1965) calculated the effect that a typical atmospheric aerosol distribution has on the calculated irradiance of the solar beam at the bottom of the atmosphere. The aerosol concentration profile they used is shown in Figure 3.7 and their results are contained in Table 3.1. The vertical transmittance of the aerosol, according to Eltermann and Toolin, is about 0.8. Because this is a value averaged over the whole solar spectrum and since extinction by aerosol varies with the wavelength of the radiation, the transmittances at larger zenith angles are somewhat larger than would be found were we considering monochromatic radiation.

The calculated direct irradiance could be brought into closer agreement with the Aspendale values by assuming the optical depth of a vertical column of the atmosphere due to aerosol extinction is approximately 0.2 and by including an appropriate transmittance in equation 3.1.

The calculated diffuse irradiances at the ground are consistently smaller than the mean Aspendale values. The magnitude of the diffuse component is relatively insensitive to the ozone and water-vapour profiles but does depend on the surface albedo.

For a surface albedo of 0.3, the calculated diffuse irradiance is about 70% of the Aspendale value and the ratio of the two is almost independent of the solar zenith angle. The calculated dependence of this ratio on solar zenith angle is greater for smaller surface albedoes.

It is more difficult to bring the calculated diffuse irradiance into agreement with the Aspendale values without introducing an

Relative Air-Mass Number	Ratio of Solar Irradiance at the Surface Beneath Atmosphere with Aerosol to that Beneath Atmosphere Without	
	Standard Aerosol Loading	Half Standard Aerosol Loading
1.0	0.81	0.92
3.0	0.52	0.75
5.0	0.41	0.63

Table 3.1 The Solar Irradiance at the Surface Calculated for Two Aerosol Loadings. The 'Standard' Aerosol Concentration Profile is Illustrated in Figure 3.7. (Eltermann and Toolin, 1965)

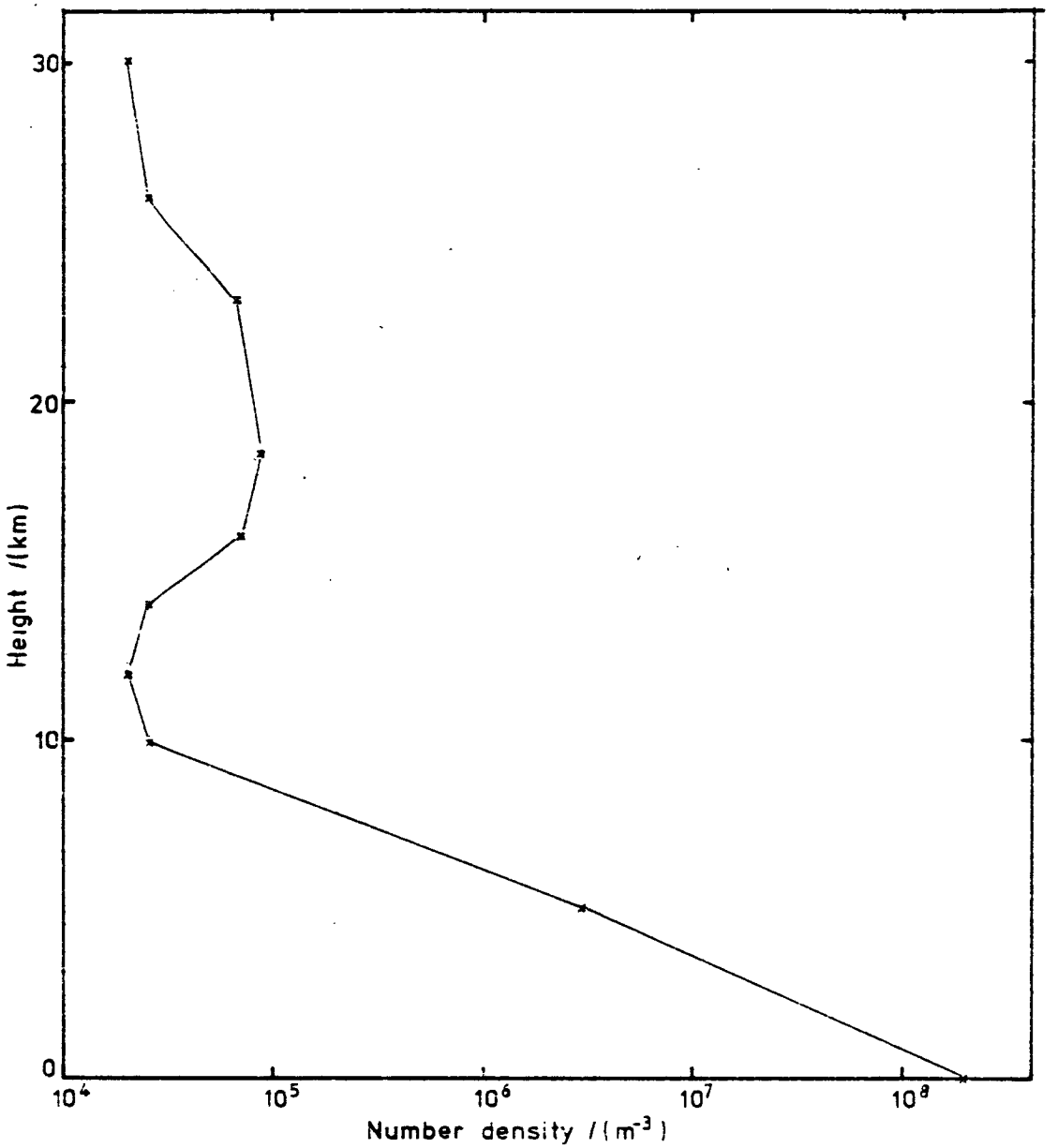

Figure 3.7 'Standard' Distribution of Aerosol
(from Eltermann and Toolin, 1965)

unacceptable number of ad hoc factors. Atmospheric aerosol depletes the direct solar beam by absorption and scattering. The latter increases the diffuse component which is itself depleted by aerosol absorption. An overall 'aerosol transmittance' is, therefore, of less use in calculating the diffuse component than in calculating the direct irradiance.

Since, in what follows, the intention is to compare the results of computations of the boundary layer model one with another rather than with experimental data the 'aerosol transmittances' have not been included in the radiation calculations unless specifically stated.

3.3 SHORTWAVE RADIATION WITHIN THE MIXED LAYER

The computation of the shortwave irradiance within the convective layer is carried out using a 'two-stream' approximation. A number of different forms of this type of radiation model have been described in the literature. The diffuse radiance, $I(\tau,\mu,\phi)$ Wm^{-2} $ster^{-1}$, is in general a function of the optical depth, τ, between the top of the atmosphere and the level being considered, the zenith angle, θ, of the sun or, as it is more convenient, the cosine of the zenith angle, μ, is used, and the azimuth angle of the sun, ϕ. The two-stream approximations result in equations which describe the radiation field in terms of two functions $I^{+}(\tau)$ and $I^{-}(\tau)$ which represent the radiance integrated over the upward and downward looking hemispheres respectively. The detailed angular distribution of the radiance is not specified. This is of no consequence since many applications require only the radiative divergence within an absorbing layer.

Detailed derivations of the two-stream equations have been given by many authors in a variety of contexts. However, Meador and Weaver (1980) present a unified account and comparison of most of the commonly used variations.

Meador and Weaver begin with the general radiative transfer equation.

$$\mu \frac{\partial I}{\partial \tau}(\tau,\mu,\phi) = I(\tau,\mu,\phi) - \frac{1}{4\pi}\int_{-1}^{1}\int_{0}^{2\pi} p(\mu,\phi;\mu',\phi')I(\tau,\mu',\phi')d\phi' d\mu'$$

$$- \frac{1}{4} F\, p(\mu,\phi;-\mu_o,\phi_o)\exp(-\tau/\mu_o)$$

This expresses the fact that the change in the diffuse radiance from a particular direction depends on the incident diffuse radiance from that direction, the energy scattered from other directions and the energy which is scattered into the diffuse component from the direct solar beam. The direct beam is treated separately from the diffuse component. The quantity πF Wm^{-2} represents the irradiance of the collinated solar beam at the top of the atmosphere normal to the direction defined by $(-\mu_o, -\phi_o)$. The scattering phase function $p(\mu,\phi;\mu',\phi')$ represents the fraction of the radiant energy incident on a single particle from direction (μ',ϕ') which is scattered into direction (μ,ϕ).

The radiative transfer equation can be integrated over all azimuth angles to give

$$\mu \frac{\partial I}{\partial \tau}(\tau,\mu) = I(\tau,\mu) - \frac{1}{2}\int_{-1}^{1} p(\mu;\mu')\, I(\tau,\mu')d\mu' - \frac{\pi}{2} F\, p(\mu;-\mu_o)\exp(-\tau/\mu_o)$$

equation 3.3

where the functions

$$I(\tau,\mu) = \int_0^{2\pi} I(\tau,\mu,\phi)d\phi \quad \text{and} \quad p(\mu;\mu') = \int_0^{2\pi} p(\mu,\phi;\mu'\phi') \frac{d\phi}{2\pi}$$

are to be distinguished from the respective integrands.

The integrated phase function $p(\mu;\mu')$ is independent of ϕ' if the phase function itself, $p(\mu,\phi;\mu',\phi)$, depends only on the cosine of the scattering angle. In fact in this case $p(\mu;\mu')$ can be expressed in terms of a series of products of Legendre polynomials with arguments μ and μ'.

The final two-stream equations are obtained by integrating equation 3.3 over all zenith angles and expressing the resulting equation first in terms of $I^+(\tau)$ and then in terms of $I^-(\tau)$. The two resulting equations may be written as

$$\frac{d}{dt} I^{\pm}(\tau) = \pm \int_0^1 I(\tau,\pm\mu)d\mu \mp \frac{1}{2} \int_0^1 \int_{-1}^1 p(\pm\mu,\mu')I(\tau,\mu')d\mu'd\mu$$
$$\mp \frac{1}{2} \pi F \exp(-\tau/\mu_o) \int_0^1 p(\pm\mu,-\mu_o)d\mu$$

In order to proceed further, it is necessary to approximate the quantity $I(\tau,\mu)$, in such a way as to be able to express the integrals which occur in the first two terms on the right hand side of this equation as functions of the hemispheric irradiances. The many different forms of two-stream methods which have been described arise from the various approximations which have been used at this stage.

Meador and Weaver describe a number of different approximations and compare the accuracy with which they calculate the reflectance and transmittance of an atmosphere of arbitrary optical depth overlying a mass-reflecting surface using results from an accurate discrete-ordinate calculation as a comparison. They conclude that the familiar

two-stream approximations ("Eddington", "delta function" and "quadrature" method for example) generally perform less well than a "hybrid" approximation they describe. Nevertheless the quadrature approximation is used here because it is easier to implement and for small optical depths and solar zenith angles less than 60° gives results which agree with those from the more accurate method to within 10%. Details are contained in the appendix.

After making the necessary approximations the final two-stream equations are

$$\frac{dI^+}{d\tau} = \gamma_1 I^+ - \gamma_2 I^- - \pi F w_o \gamma_3 e^{-\tau/\mu_o}$$

$$\frac{dI^-}{d\tau} = \gamma_2 I^+ - \gamma_1 I^- + \pi F w_o \gamma_4 e^{-\tau/\mu_o}$$

where w_o is the single scattering albedo. The coefficients γ_i are independent of τ but depend on the approximation assumed for the dependence of the integrated radiance $I(\tau,\mu)$ on solar zenith angle prior to performing the integration over the two hemispheres.

The general solution of these coupled ordinary differential equations is fairly easy to obtain

$$I^+(\tau) = A_1 \exp(\alpha\tau) + A_2 \exp(-\alpha\tau) + B_1 \exp(-\tau/\mu_o) \qquad \text{equation 3.4}$$

$$I^-(\tau) = \alpha_1 A_1 \exp(\alpha\tau) + \alpha_2 A_2 \exp(-\alpha\tau) + B_2 \exp(-\tau/\mu_o) \qquad \text{equation 3.5}$$

The other constants are detailed in the appendix.

Two boundary conditions are required to determine A_1 and A_2. They are provided by specifying the diffuse irradiance at the top of the model to be equal to the downward stream $I^-(o)$, and by assuming that the earth's surface is a diffuse reflector with albedo r_s, so that the upward stream just above the surface is given by

$$I^+(\tau) = r_s(I^-(\tau) + \pi F\mu_o \exp(-\tau/\mu_o))$$

Then substituting these expressions into equations 3.4 and 3.5 leads

to $A_1 = (F_f - \alpha_2 - A_2 - B_2)/\alpha$

and $$A_2 = \frac{[(1-r_s\alpha_1)(F_f-B_2)\exp(\alpha\tau)+\alpha_1(B_1-r_s(B_2+\mu_o\pi F))\exp(-\tau/\mu_o)]}{(1-\gamma\alpha_1)(\alpha_2-\alpha_1)}$$

Now, having determined the γ_i which depend only on the single scattering albedo, w_o, and the asymmetry factor g, no matter which approximation is used, $I^+(\tau)$ and $I^-(\tau)$ can be calculated at any level within the layer. The total upward solar irradiance at the surface is then given by

$$\int_{-1}^{1} I(\tau,\mu)d\mu \quad - \mu_o\pi F e^{-\tau/\mu_o}$$

and the integral is expressed in terms of $I^+(\tau)$ and $I^-(\tau)$.

3.4 CALCULATION OF THE LONGWAVE IRRADIANCE

The infra-red component of the downward radiation at the surface is emitted largely from atmospheric water-vapour in the lowest few kilometres of the atmosphere. Although ozone and carbon-dioxide are important longwave emitters, their contribution in the lowest layers is small compared to that of water-vapour.

A very simple means of calculating the downward longwave

irradiance at the surface is used. The downward longwave irradiance at a height of three kilometres was calculated, using an Elsasser chart from the temperature and water-vapour profiles defined by the COESA standard atmospheres, which were also used in calculating the absorption of shortwave radiation.

The total divergence of longwave radiation across the mixed layer is calculated from a formula given by Kondratyev (1969), so that the longwave irradiance at the surface, L(o) Wm^{-2}, is calculated from

$$L(o) = L(h)t(\ell) + \sigma\theta_m (1-t(\ell))$$

The function $t(\ell)$, which represents the longwave transmittance of a column which has a water-vapour path-length ℓ cm, is calculated from an expression given by Kondratyev

$$t(\ell) = \frac{1}{4} \sum_{j=1}^{4} \exp(-k_j \ell)$$

where the constants k_j have the following values:

$$k_1 = 0.10 \text{ cm}^{-1}; \quad k_2 = 4.96 \text{ cm}^{-1}; \quad k_3 = 19.6 \text{ cm}^{-1}; \quad k_4 = 114.0 \text{ cm}^{-1}$$

3.5 THE SOIL SCHEME

The heat-flux into the soil is one of the terms of the surface energy balance which plays a part in determining the surface temperature. The heat-flux into and within the soil will be determined by the temperature structure within the soil and its thermal properties.

Estimates of the ratio of the surface soil heat flux to the sensible heat-flux into the atmosphere, averaged over that part of

the day when the atmospheric heat-flux is directed away from the surface, were made by Sellers (1965) for a range of values of the surface roughness length and friction velocity. The heat stored in the soil over the period varied from about a half to about twice the total sensible heat transfer into the atmosphere.

Monteith (1973) quotes Sellers' results and compares the heat-flux into the soil with the net radiation at the surface. The soil-flux being from 30% to about 60% of the net radiation over a dry unvegetated surface.

The presence of vegetation will tend to reduce the soil-flux to 5%-10% of the net radiation, at least during the daytime, although at night, when the turbulent fluxes all but disappear and the net radiation is negative, the soil-flux more or less balances the latter, there being no other flux of heat directed away from the surface. Table 3.2 summarises these estimates.

Measurements made by Pasquill (1949) (see Table 3.3) over pasture land show the ratio of the soil heat flux to the net radiation to be as much as 50%, while measurements made at O'Neill as part of the Great Plains experiment (Lettau and Davison, 1957) give soil heat fluxes rising to about 20% of the net radiation during the daytime. Similar results are reported in Smith and Hunt (1978), the ratio $G:R_N$ measured in the early afternoon over grass with scattered broken cloud or clear sky being 20%-40%.

The transfer of heat within the soil takes place mainly by conduction. The soil itself is not an homogenous continuum, it is made up of particles of quartz, clay and organic matter in various proportions. In addition, the spaces between the individual particles

$u_*/(m\ s^{-1})$	$z_o/(cm)$		
	0.1	1.0	10.0
0.2	1.89	1.55	1.21
0.4	1.00	0.83	0.66
0.6	0.68	0.57	0.46

Table 3.2 Ratio of Heat Stored in Soil to Heat Transferred to Atmosphere While Latter is Directed Upwards (Sellers, 1965)

	Time GMT				
	10.33	12.30	15.30	17.30	19.30
G/R	0.56	0.48	-0.04	0.8	0.63
G/H	0.25	0.49	-4.25	0.65	0.91
β	1.87	1.71	-0.041	-2.6	-3
$T_s/(K)$	16.3	17.9	13.4	7.3	5.7

Table 3.3 Ratio of Soil Flux, G, to Net-Radiation, R and to Sensible Heat Flux, H. Bowen ratio β and Surface Temperature, T_s, From Measurements Made Through the Day. (Pasquill, 1949)

may be partly or entirely filled with water, unless of course the soil dries out completely. In a moist soil heat may be transferred across the pore spaces by evaporation and subsequent condensation of water-vapour.

The thermal conductivity and the specific heat of the soil both alter with the proportion of each soil component and with the moisture content of the soil. It would be extremely unlikely that the thermal diffusivity was found to be uniform either horizontally or vertically. The soil temperature measurements made at O'Neill (Lettau and Davison, 1957) illustrate this very well. The variation in the overall thermal diffusivity caused by varying moisture content is greatest for very dry soils, as the soil becomes moister it also becomes less sensitive to changes in its moisture content.

a) Solution of the Thermal Diffusion Equation

The model of the soil is, of necessity, greatly simplified. Measurements of the soil composition and moisture content made at the same time as detailed boundary layer measurements are, if made at all, not very detailed. The model should reproduce the behaviour of a soil-like stratum. To this end all inhomogeneities in composition and any variation in moisture content are ignored. The thermal properties are specified directly, the soil diffusivity, κ (m^2s^{-1}), and the thermal conductivity, k ($Wm^{-1}°C^{-1}$), are taken to be 0.5×10^{-6} m^2s^{-1} and 1.5 $Wm^{-1}°C^{-1}$ respectively, values which are typically of a moist clay soil.

The soil scheme is required to calculate the heat-flux across the air-soil interface over a small time interval given an estimate

of the surface temperature and the temperature profile in the soil at the beginning of the time interval. Since the soil is by assumption uniform and the temperature varies only vertically the one-dimensional conduction equation describes the evolution of the soil temperature with time and the solution to this equation can be manipulated to find the heat-flux profile and in particular the heat-flux at the surface.

The temperature profile at the current time step provides the necessary initial condition. The boundary condition at the air-soil interface is defined by the current value of the surface temperature, T_s, and the estimated surface temperature at the forward time-step. It is then assumed that over the intervening time, Δt, the surface temperature changes linearly. The fact that this boundary condition is a function of time introduces an extra complication into the solution of the equation.

It is a familiar observation that the amplitude of the diurnal temperature wave in the soil decreases rapidly with depth and is no longer apparent at greater depths than about 50 cms. Figure 3.8 shows measurements taken at O'Neill (Lettau and Davison 1957). At a depth of 40 cms the daily temperature variation was about 0.7 K, while at 80 cm it was about 0.3 K. This type of behaviour is consistent with that of the solutions to the conduction equation with a sinusoidal heat-flux imposed at one boundary. The solution decays exponentially with a 'damping depth' D given by $D = (\frac{2k}{w})^{\frac{1}{2}}$, where w is the angular frequency of the imposed heat-flux. For a thermal diffusivity of $0.5 \times 10^{-6} ms^{-2}$ and a twenty-four hour period the damping depth is approximately 10 cms, at which depth the temperature variation

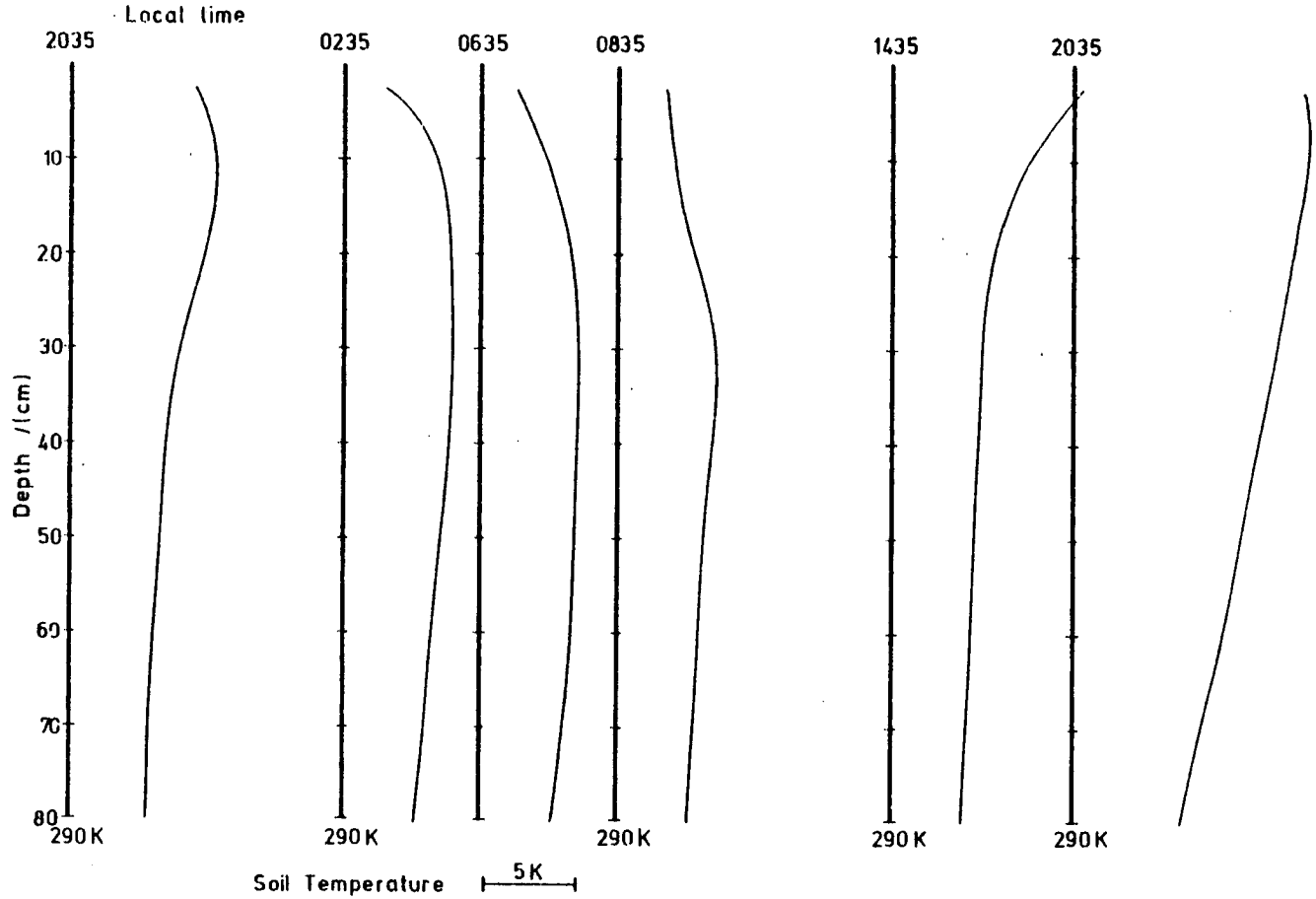

Figure 3.8 The Soil Temperature Profiles Measured During the O'Neill Experiment Between 8-Aug-53 and 9-Aug-53
(data from Lettau and Davidson, 1957)

should be 1/e of that at the surface.

The second boundary condition is taken to be that, at a depth z_d m, the temperature is constant. The complete description of the soil temperature is

$$\frac{\partial T}{\partial t}(z,t) = \kappa \frac{\partial^2 T}{\partial z^2}(z,t)$$

$$T(z_d,t) = T_d = \text{const}$$

$$T(o,t) = T(o,t_o) + \frac{t-t_o}{\Delta t}\{T(o,t_o+\Delta t) - T(o,t_o)\}$$

$$T(z,t_o) = J(z)$$

Here $J(z)$ represents the known temperature profile at the initial instant t_o. The solution is to be found for $t_o \leq t \leq t_o + \Delta t$.

The solution to such a system can be written down in terms of the solutions to simpler systems involving boundary conditions which are not time-dependent (see Sneddon, 1957). In this case, since there are no internal sources, the solution requires two functions $\phi_1(z,t)$ and $\phi_2(z,t,t')$. The first of these satisfies the time-independent diffusion equation

$$0 = \kappa \frac{\partial^2 \phi_1}{\partial z}$$

with boundary conditions

$$\phi_1(0,t) = T(0,t_o) + \frac{(t-t_o)}{\Delta t}(T(0,t_o+\Delta t)-T(0,t_o))$$

and $\phi_1(z_d,t) = T_d$

so that

$$\phi_1(z,t) = az + b$$

with $a = [Td - T(0,t_o) - \frac{(t-t_o)}{\Delta t} (T(0,t_o+\Delta t - T(0,t_o)] \frac{1}{z_d}$

and $b = T(0,t_o) + \frac{t-t_o}{\Delta t} (T(0,t_o+\Delta t) - T(0,t_o))$

The second function $\phi_2(z,t,t')$ satisfies the full diffusion equation with an initial condition which is a function of the parameter t' and z. The boundary conditions on ϕ_2 are that it is zero on both boundaries. The initial condition is

$$\phi_2(z,t_o,t') = J(z) - \phi_1(z,t') \qquad \text{equation 3.6}$$

The boundary conditions are satisfied if

$$\phi_2(z,t,t') = \sum_{m=1}^{\infty} C_m \sin(k_m z)\exp(-\kappa k_m(t-t_o)) \qquad \text{equation 3.7}$$

where $k_m = \frac{m\pi}{z_d}$ and the C_m may be functions only of t'.

The initial condition on T(z,t) can be written

$$T(z,t_o) = T(0,t_o)(1-z/z_d) + T_d\, z/z_d + \sum_{j=1}^{\infty} \alpha_j \sin(k_j z) \qquad \text{equation 3.8}$$

and the coefficients C_m can be evaluated by substitution of 3.7 and 3.8 into equation 3.6; multiplying the result by $\sin(k_i z)$ and integrating with respect to z over the interval $[0,z_d]$ then leads to

$$C_m = \alpha_m - \frac{2}{z_d} \frac{(t'-t_o)}{\Delta t} (T(0,t_o+\Delta t)-T(0,t_o)) \int_o^{z_d} (1-z/z_d)\sin(k_m z)dz$$

$$= \alpha_m - \frac{2}{k_m z_d} \frac{(t'-t_o)}{\Delta t} (T(0,t_o+\Delta t)-T(0,t_o))$$

The solution of the original boundary value problem can now be written in terms of ϕ_1 and ϕ_2

$$T(z,t) = \phi_1(z,t) + \frac{\partial}{\partial t} \int_o^t \phi_2(z,t-t',t')\, dt'$$

which becomes

$$T(z,t) = T_d \, {}^{z}/_{z_d} + (T(0,t_o) + \frac{\Delta T(t-t_o)}{\kappa \, k_m^3 \, z_d \, \Delta t} +$$

$$\sum_{m=0}^{\infty} \{\alpha_m \exp(-\kappa k_m^2 (t-t_o)) - \frac{2\Delta T}{\kappa k_m^3 z_d \Delta t}(1-\exp(-\kappa k_m^3 (t-t_o))\sin(k_m z))\}$$

where $\Delta T = T(0,t_o+\Delta t) - T_o(0,t_o)$.

The coefficients α_m are defined by the initial temperature profile. By suitably redefining the α_m at every time-step, the form of the solution remains as equation 3.10. Then the coefficients, α'_m, to be used for the succeeding time-step have the form

$$\alpha'_m = \alpha_m \exp(-\kappa \, k_m^2 \, \Delta t) - \frac{2\Delta T}{\kappa k_m^3 z_d \Delta t} (1-\exp(-\kappa \, k_m^2 \, \Delta t))$$

3.6 CALCULATION OF THE TURBULENT FLUXES

The preceding sections of this chapter have described the methods by which the radiative fluxes at the earth's surface and the heat flux into the soil are to be calculated. The remaining components of the surface energy balance are the turbulent fluxes of heat and moisture into the air. These may be calculated, by means of surface layer similarity theory, in terms of the temperature, water-vapour mixing ratio and wind speed at two levels both within the surface layer. The 'surface layer' refers to that part of the atmosphere, nearest to the surface, where the turbulent fluxes are approximately constant with height. This layer is, in general, of the order of 100 metres deep.

Perhaps because the surface layer is easily accessible from the ground there have been a number of experimental investigations of the

structure of turbulence and turbulent transfer within the surface layer (see, for example, Lettau and Davidson, 1957; Clarke et al, 1971; Swinbank, 1964; Businger et al, 1971). By contrast, analogous measurements of the rest of the convective boundary layer are less numerous (Caughey and Palmer, 1979; Lenschow and Johnson, 1968; Nicholls, 1977) and the theoretical framework is less firmly established. Nevertheless some means is required of relating the model's mixed layer parameters to the surface layer variables. A convenient relation which serves this purpose is provided by Deardorff (1972) on the basis of boundary layer simulations performed using his three dimensional numerical model.

A similar link is needed between the temperature and moisture at the earth's surface and the corresponding quantities at the lower level within the surface layer. In a paper previously referred to, Deardorff (1974) devised a means of achieving this based on theoretical considerations and laboratory measurements described by Zilitinkevich (1970).

The theory to be described now will be used to calculate the turbulent fluxes of heat and water-vapour at the surface from values of the mixed layer potential temperature and water-vapour mixing ratio and the temperature of the earth's surface.

a) Surface Layer Similarity Theory

The fundamental assumption of the similarity theory as it was formulated by Monin and Obukhov is that "all dimensionless single point statistical parameters obtained when speeds are measured with scale u_* and lengths with scale L will be universal functions of the dimensionless

ratio z/L" (Zilitinkevich, 1970).

The scaling quantities u_* and L, the Monin-Obukhov length and a temperature scale θ_* are defined by

$$u_*^2 = \frac{\tau(o)}{\rho} \quad , \quad \theta_* = \frac{H(o)}{\rho c_p u_*}$$

$$L = -u_*^3/(\kappa(g/\bar{\theta})(H(o)/\rho c_p))$$

$\tau(o)$ represents the tangential stress at the earth's surface and κ is Von-Karman's constant.

Much effort has been expended in determining the form of the universal functions. Various expressions are given in the literature which seem to fit the available data equally well. Choice of which form to use may well rest on which expression is easiest or most convenient to manipulate mathematically.

Businger (1971) gives one particular set of empirical expressions for the non-dimensional gradients of momentum, $\phi_m(z/L)$, potential temperature, $\phi_\theta(z/L)$ and water-vapour mixing ratio, which has the same form as that for potential temperature

$$\frac{\kappa z}{u_*}\frac{\partial u}{\partial z} = \phi_u\left(\frac{z}{L}\right) = \begin{cases} 1 + \beta\frac{z}{L} & \frac{z}{L} > 0 \\ (1 - \gamma_u\frac{z}{L})^{-\frac{1}{4}} & \frac{z}{L} < 0 \end{cases} \qquad \text{equation 3.9}$$

$$\kappa z\, u_*\frac{\rho c_p}{H(0)}\frac{\partial\theta}{\partial z} = \phi_\theta\left(\frac{z}{L}\right) = \begin{cases} R + \beta\frac{z}{L} & \frac{z}{L} > 0 \\ R(1 - \gamma_\theta\frac{z}{L})^{-\frac{1}{2}} & \frac{z}{L} < 0 \end{cases} \qquad \text{equation 3.10}$$

where $R = 0.74$, $\beta = 4.7$, $\gamma_u = 15$ and $\gamma_\theta = 9$.

There is not general agreement about the correct values of these

four constants. In reducing his experimental data Businger assigned a value of 0.35 to the von Karman constant instead of the more usual value of 0.41. Evidence to support the larger value comes mainly from wind tunnel measurements and Businger has suggested that the difference between the two values arises from the much larger Reynolds number which is appropriate in the atmosphere.

It is usually assumed that in conditions of neutral stability the non-dimensional profiles of momentum and heat are equal. However, Dyer (1974), in reviewing flux-profile relationships in the surface layer points out that there is experimental evidence that this assumption is not justified and that as neutral conditions are approached $\phi_u/\phi_\theta \rightarrow 1.35$. It is for this reason that Businger assigns a value of 0.74 to R. Even so, in his review Dyer concludes that the most convincing relationships are those published by Dyer and Hicks (1970) which specify

$$\kappa = 0.41 \qquad R = 1.0 \qquad \beta = 5 \qquad \gamma_u = \gamma_\theta = 16$$

The difference between the two profiles is small, except in conditions near to neutral stability, but since use is made later on of two parameterizations which were derived using Businger's profile that form was used to describe the surface layer profiles.

The surface layer theory is used to calculate the turbulent fluxes of heat and moisture at the surface given the potential temperature, water-vapour mixing ratio and wind speed at two levels within the surface layer. The profile functions are defined in terms of the Monin-Obukhov length scale which is, itself, a function of the surface heat flux. The form of the profiles can be derived from the expressions

describing the non-dimensional gradients by integrating equations 3.9 and 3.10 from a height z_o, the roughness length, to an arbitrary height, z, within the surface layer. By adapting a method described by Paulson (1970) the profiles are described by

$$u(z) = u(z) - u(z_o) = \frac{u*}{\kappa} [\ln (z/z_o) - \psi_u(z/L)]$$

$$\theta(z) - \theta(z_o) = \frac{\theta*}{\kappa} [R\ln (z/z_o) - \psi_\theta(z/L)]$$

The profile functions are defined in terms of the non-dimensional gradients as

$$\psi_u(z/L) = \int_o^{z/L} \frac{1-\phi_u(z'/L)}{(z'/L)} d(z'/L)$$

and

$$\psi_\theta(z/L) = \int_o^{z/L} \frac{R-\phi_\theta(z'/L)}{(z'/L)} d(z'/L)$$

and the forms appropriate for the Businger stability functions are

$$\psi_u(z/L) = \begin{cases} \beta\frac{z}{L} & \frac{z}{L} > 0 \\ -\ln[\frac{1}{8}(1+\varepsilon^2)(1+\varepsilon)^2]+2\tan^{-1}(\varepsilon)-\frac{\pi}{2} & \frac{z}{L} < 0 \end{cases} \quad \text{equation 3.11}$$

where $\varepsilon = (1-\gamma_u \frac{z}{L})^{\frac{1}{4}}$

and

$$\psi_\theta(z/L) = \begin{cases} \beta\frac{z}{L} & \frac{z}{L} > 0 \\ -2R\ln[\frac{1}{2}(1+\eta)] & \frac{z}{L} < 0 \end{cases} \quad \text{equation 3.12}$$

where $\eta = (1-\gamma_\theta \frac{z}{L})^{\frac{1}{2}}$

We have now to invert these relationships to express the Monin

Obukhov (M-O) length in terms of the surface layer temperature and wind speed. Because of the form of the profile functions this is not entirely straightforward and we follow Barker and Baxter (1975).

Substituting for the scales u_* and θ_* in the definition of the M-O length leads to an expression for the non-dimensional stability parameter z/L as a bulk Richardson number, R_i, multiplied by a combination of the profile functions, $\psi_u(z/L)$ and $\psi_\theta(z/L)$.

$$\frac{z}{L} = \left(\frac{g}{\theta} z \frac{(\theta(z)-\theta(z_o))}{u^2(z)}\right) \frac{(\ln(z/z_o) - \psi_u(z/L))^2}{(R\ln(z/z_o) - \psi_u(z/L))} \qquad \text{equation 3.13}$$

Now by inverting the expressions for $\psi_u(z/L)$ and $\psi_\theta(z/L)$ from equations 3.11 and 3.12 it would be possible, in principle, to solve for L. For stable conditions the equation that results is quadratic in z/L and

$$\frac{z}{L} = \left(\frac{(R_i - \frac{R}{2\beta}) + (\frac{(1-R)R_i}{\beta} + \frac{R^2}{4\beta^2})^{\frac{1}{2}}}{(1-\beta R_i)}\right) \ln(\frac{z}{z_o})$$

The particular root is chosen to ensure that $z/L \to 0$ as the Richardson number $R_i \to 0$.

In unstable conditions the equation for z/L is transcendental and can only be solved numerically. Barker and Baxter have calculated the Richardson number over a range of values of z/L from equation 3.13 and parameterized the results. For values of $z/L \lesssim -0.05$ they conclude that

$$\frac{z}{L} = R_i \left(\frac{0.471}{\kappa} \ln(\frac{z}{z_o}) - 1.045\right)$$

as long as $\frac{1}{\kappa}\ln(\frac{z}{z_o}) \gtrsim 10$. If the Von Karman constant has a value of

0.35 this restricts the upper level to heights greater than $30 z_o$. If the Von Karman constant has a value of 0.41 the limit is at a height of $60\ z_o$.

In slightly unstable conditions, when $0 > {}^{z}/_{L} > -0.05$ a closer approximation to the solution can be obtained by using the solution to the quadratic.

By using these equations the stability parameter ${}^{z}/_{L}$ can be calculated and then the temperature and velocity scales, u_* and θ_* can be found. The product $\rho c_p u_* \theta_*$ is equal to the surface heat flux. By an entirely analagous procedure the surface latent heat flux can also be calculated.

b) Link With The Mixed Layer Variables

The surface layer similarity theory described previously is used to calculate the surface fluxes from the profiles of wind speed, potential temperature and water-vapour mixing ratio at two lengths both within the surface layer. The boundary layer model itself provides the values of these variables within the mixed layer and some means of relating the mixed layer values to those at the upper level in the surface layer is required. This is provided by Deardorff (1972) in a manner which is consistent with the formalism used by Paulson and Barker and Baxter.

Deardorff assumed that the profiles above the surface layer can be described as universal dimensionless functions of a single dimensionless argument by analogy with standard surface layer theory. The dimensionless argument used is h/L, the depth of the mixed layer scaled by the Monin Obukhov length scale.

Using results from numerical simulations of a convective boundary layer, Deardorff proposed that the differences between the wind speed and temperature in the mixed layer u_m and θ_m, and those at the upper level in the layer, u_a and θ_a were best described by

$$\left.\begin{aligned} u_m - u_a &= 8.4u_*(1 - 50h/L)^{-0.16} \\ \theta_m - \theta_a &= 7.3\theta_*(1 - 5.8h/L)^{-0.47} \end{aligned}\right\} \quad h/L < 0$$

$$\left.\begin{aligned} u_m - u_a &= u_*(8.4 + 0.6h/L) \\ \theta_m - \theta_a &= \theta_*(7.3 + 0.6\ h/L) \end{aligned}\right\} \quad h/L > 0$$

The height of the upper level within the surface layer is taken to be 0.025 h.

By combining these expressions with the equations for the appropriate profiles within the surface layer, the wind speed and potential temperature at the upper level of the surface layer, u_a and θ_a, can be eliminated and the profiles expressed as functions of two dimensionless parameters, h/z_o and h/L. By adopting a strategy similar to that used by Barker and Baxter, which was described earlier, Deardorff was able to obtain an expression for the bulk Richardson number, R'_{iB} of the layer extending from the lowest level of the surface layer to the top of the mixed layer.

As before, the Monin-Obukhov length scale, L, is unknown and awkward to determine. The bulk Richardson number, an alternative stability parameter to z/L, is easily calculated from the large-scale variables, θ_m, u_m, h and $\theta(z_o)$. The relationship expressing the Richardson number in terms of non-dimensional parameter z/L, is transcendental and so cannot be inverted to give the latter in terms of

the Richardson number. However the relationship can be used to calculate the Richardson number over a range of values of z/L and an empirical interpolation function found which will enable the Monin-Obukhov length to be easily evaluated.

In fact Deardorff derived empirical functions for the drag coefficient $C_u = u*/u_m$ and the heat transfer coefficient $C_\theta = \theta*/(\theta_m - \theta(z_o))$ in terms of the mixed layer bulk Richardson number. In condition of neutral stability these coefficients are given by

$$C_{uN}^{-1} = \ln(0.025h/z_o)/\kappa + 8.4$$

$$C_{\theta N}^{-1} = R\ln(0.025h/z_o)\kappa + 7.3$$

In unstable conditions, when $R_{iB}' < 0$

$$C_u^{-1} = C_{uN}^{-1} - 25 \exp(0.26\zeta - 0.03\zeta^2)$$

$$C_\theta^{-1} = C_{\theta N}^{-1} + C_{uN}^{-1} - C_{uN}^{-1}$$

where $\zeta = \log(-R_{iB}') - 3.5$

and in stable conditions, when Ri_B' is positive

$$C_u = C_{uN}(1 - R_{iB}'/3.05)$$

$$C_\theta = C_{\theta N}(1 - R_{iB}'/3.05)$$

From these relationships, once the Richardson number is known, the velocity and temperature scales, u_* and θ_* can be found, and from them the surface heat flux calculated.

c) Link with the Surface Variables

The gradients of potential temperature, water-vapour mixing ratio and wind speed are likely to attain their greatest values close to the earth's surface. Since the surface temperature enters the surface energy balance raised to the fourth power, in the emitted longwave radiation term, any underestimate of the surface temperature will result in an overestimate of the net radiation which will be reflected in the estimates of the turbulent fluxes. These, of course, depend on the temperature at the lower level, z_o, of the surface layer. Often this is taken to be equal to the surface temperature. However such an approximation will result in overlarge estimates of the surface heat flux, especially in very unstable conditions when the difference between the temperature at the surface and that at z_o will be greatest.

Zilitinkevich (1970) extended surface layer similarity theory to the region between the surface and the base of the surface layer. In this region, since molecular diffusion is the most important mechanism for transfer of heat, the Monin-Obukhov length can no longer be a relevant length scale. Instead the shape of the temperature profile is determined by the Reynolds number, Re, and the Prandtl number, Pr. By direct analogy with surface layer theory, and using an identical temperature scale, $\theta*$, the temperature difference between the surface and the base of the surface layer is

$$\theta(z_o) - \theta(0) = - \theta* P_\theta(Re, Pr)$$

In the atmosphere the Prandtl number is constant and has a value of about 0.7 and from a number of laboratory experiments Zilitinkevich

deduced the form of the temperature profile on the Reynolds number to be

$$P\ (Re,\ Pr) \quad = \quad 0.9 \left(\frac{u_* z_o}{\nu}\right)^{0.45}$$

where ν is the kinematic viscosity of air and has a value of 1.5×10^{-5} $m^2\ s^{-1}$ at a temperature of 293 K. The slow variation of ν with temperature has been neglected.

This relationship was used by Deardorff (1974) in his three-dimensional numerical model, but in applying it to atmospheric conditions he proposed that the constant of proportionality be 0.28 and this smaller value has been used. An analogous equation describes the humidity profile between the surface and the level $z = z_o$.

d) The Latent Heat Flux at the Surface

The turbulent flux of latent energy from the surface can be calculated in the same way as the sensible heat flux was found once the water-vapour mixing ratio at the surface is known. This could be achieved by extending the model of the soil layer to calculate the soil moisture explicitly. However a simpler means is available. Myrup (1969), in modelling the development of an urban heat island, fixed the water-vapour mixing ratio at the surface to be a predetermined fraction of the saturation mixing ratio calculated at the surface temperature. Deardorff (1974) used a similar idea but instead fixed the latent energy flux to be a fraction, M (which he referred to as the Halstead parameter) of that which would result if the surface were saturated at the surface temperature. This latter parameterization has been used. The Halstead parameter is treated as a

constant although for his numerical simulation of Day 33 of the Wangara data, Deardorff used an empirical time-dependent form to account for the relatively small change that occurred over the twenty four hours of the simulation.

In practice these surface flux calculations were carried out in terms of the virtual potential temperature rather than in terms of the potential temperature; this is both more accurate, when the water-vapour concentration is large, and more convenient.

3.7 IMPLEMENTATION

This final section of chapter three consists of a general description of the way in which the numerical calculations are organised. Because the profiles of potential temperature, water-vapour mixing ratio and aerosol concentration are all assumed to be independent of height the equations describing the evolution of these variables have a simple form. The rate of change of each of these quantities is equal to the mean gradient of the appropriate flux across the mixed layer. By defining the entrainment velocity, w_e, in terms of the rate at which the mixed layer deepens and the vertical velocity of the air at the top of the layer, induced by large scale subsidence, w

$$w_e = \frac{dh}{dt} - w$$

the fluxes at the top of the mixed layer can be expressed as the product of w_e and the difference between the appropriate quantity above and beneath the top of the mixed layer. Of course, the potential temperature equation has an extra term to account for the

radiative heating.

The equations for the rates of change of the mixed layer potential temperature and humidity or aerosol concentration are

$$\frac{d\theta_m}{dt} = (H(0) - H(h) + S(h) - S(0))/\rho c_p h$$

$$\frac{dq_m}{dt} = (E(0) + \rho(q(h) - q_m)w_e)/\rho h$$

where, as before, $H(z)$, $S(z)$ and $\lambda E(z)$, represent the fluxes of sensible heat, shortwave radiation and latent heat respectively and $q(z)$ is the water-vapour mixing ratio. The corresponding equation for aerosol concentration is identical to that for water-vapour.

The equations for the components of the wind velocity, within the layer are easily derived from the general Navier-Stokes equation by assuming that above the mixed layer the wind is geostrophic and directed along the x-axis with speed G ms^{-1} (Carson and Smith, 1974)

$$\frac{du}{dt} = fv + (-u_*^2\cos\alpha + (G-u)w_e)/h$$

$$\frac{dv}{dt} = -f(u-G) + (-u_*^2\sin\alpha - vw_e)/h$$

The wind within the mixed layer is directed at an angle α across the isobars.

In implementing the numerical model these equations are integrated in time by a simple Euler-forward scheme. The greater part of the computation necessary arises in calculating the radiative and turbulent heat fluxes. Although the Euler integration scheme demands a much smaller time step than other more sophisticated methods, in order to ensure that the numerical solution is stable and compatible

with the analytic solution, it is extremely simple to use and the extra time taken is small compared to that taken in calculating the fluxes.

Once the initial conditions have been specified the calculation proceeds as represented in Figure 3.9. The solar declination appropriate for the specified date is calculated and used each time the radiative fluxes are evaluated to calculate the solar zenith angle for the given latitude and local time.

The water-vapour and ozone profiles in the upper atmosphere are specified as those appropriate for one of the COESA atmospheres described earlier in section 3.2(a). The ozone path length low down in the troposphere is assumed to be independent of height but the scaled water-vapour path length is calculated as an exponential function of the height of the mixed layer. The irradiances of the direct and diffuse components of the shortwave radiation stream on a horizontal surface at the top of the mixed layer can then be calculated using the scheme detailed in section 3.2. This provides all the necessary input parameters for the two-stream radiation scheme (section 3.3). The constant factors in equations 3.4 and 3.5 are calculated at this stage and retained for use later in calculating the shortwave irradiances at various heights between the earth's surface and the base of the inversion.

It should be pointed out that, strictly speaking, the downward diffuse irradiance at the top of the mixed layer, indeed at any level within the atmosphere, depends on the properties of the atmosphere beneath, and the underlying surface. A fraction of the radiation back scattered or reflected upwards from the mixed layer will be back scattered once again by the atmosphere above thus augmenting

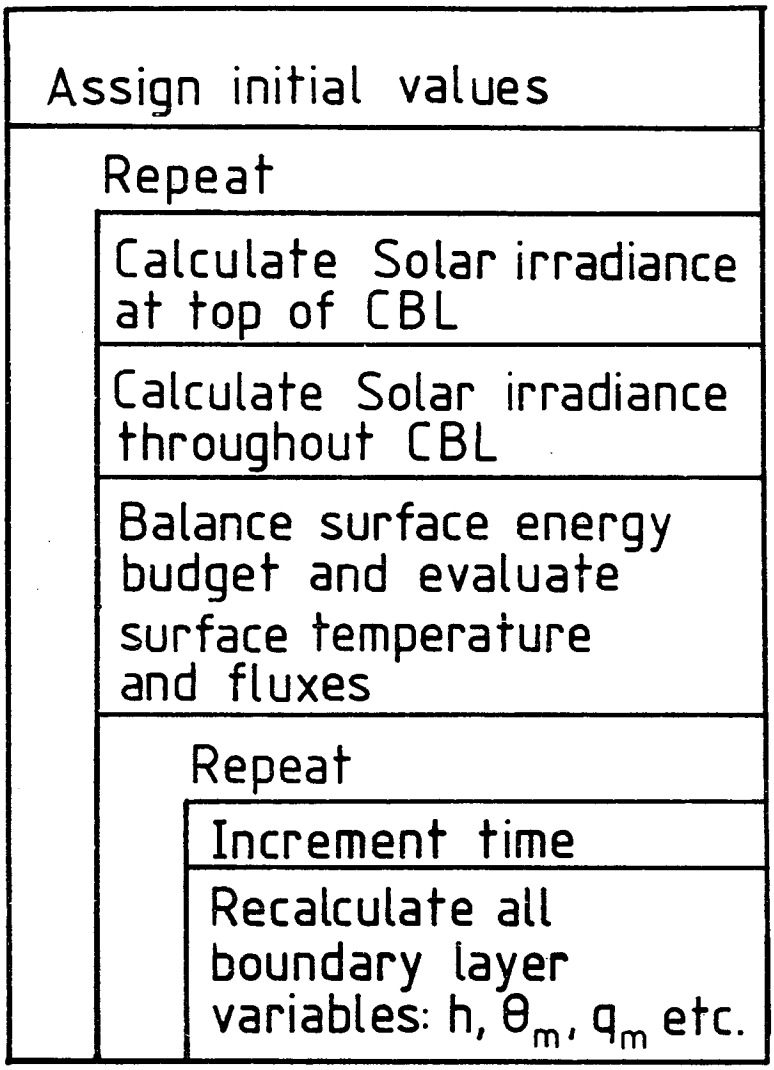

Figure 3.9 The Organisation of the Calculations

the downward diffuse component at the top of the mixed layer. However, in practice, since the atmosphere is optically thin and the back scattering ratio for both molecules and aerosol particles is small, this component is likely to be small compared with the unscattered incoming radiation and consequently it is neglected.

The COESA temperature and water-vapour profiles were used to calculate the downward longwave irradiance at a height of three kilometres. The calculated values are 288 Wm^{-2} for the summer profile and 161 Wm^{-2} for the winter profile. Using the appropriate value, the water-vapour content of the mixed layer and the temperature calculated at the middle of the layer, the longwave irradiance at the surface of the earth is calculated using Kondratyev's parameterization which was described in section 3.4.

The surface energy budget is then balanced, and, in the process, the surface temperature, the soil heat flux and the surface turbulent fluxes are evaluated. The surface energy budget is balanced by numerically finding the zero of the function

$$f(T_s) = S(0) + L(0) - \sigma T_s^4 - H(0) - \lambda E(0) - G(0)$$

In fact the temperature at the lower level of the surface layer, approximated by $\theta(z_o)$, is used as the independent variable instead of the surface temperature. This makes the calculations easier to organise without affecting the result. Given an assumed value of $\theta(z_o)$ the turbulent fluxes are calculated using the equations described in section 3.6(b). Once the scaling temperature is known the results of section 3.6(c) are used to find the temperature at the surface itself.

The zero of the function $f(T_s)$ is found using a standard routine from the Numerical Algorithms Group (NAG) library. The routine chosen (C05ACF) locates the zero of the function by repeatedly evaluating the function at the mid-point of an interval known to contain the zero. On the basis of the sign of the function at the end-points and mid-point of the interval the half interval which contains the zero can be identified to provide the starting point for the next iteration.

In evaluating the function $f(T_s)$ the soil heat flux is computed in the manner described in section 3.5. When the surface energy budget has been balanced the Fourier coefficients which describe the soil temperature profile are updated.

The manner in which the initial value of the surface temperature is determined should be mentioned. The initial conditions specify the soil temperature at eight levels beneath the surface. The boundary layer parameters are specified and the time of day - thus enabling the radiative fluxes to be calculated. In calculating the soil heat flux initially it is assumed that the surface temperature was constant during the preceding time step.

The turbulent fluxes at the surface and the shortwave radiation profile within the mixed layer are now known. The boundary layer equations can now be integrated forwards in time. The time step used is independent of the time interval between successive determinations of the fluxes.

Because the shortwave radiation profile is not necessarily a simple exponential function of height the solution to the boundary layer equations which was obtained in chapter two cannot be used

directly. Instead the height at which the turbulent heat flux disappears is determined numerically by using the NAG routine (C05ACF) mentioned previously to find the zero of the function

$$g(z) = (H(0)-S(0))(h-\tfrac{1}{2}h^2/z - \tfrac{1}{2}(1-k)z) - \tfrac{1}{2}S(z)(h^2/z-(1-k)z)+\int_0^z S(z')dz' - (1-k)\int_0^h S(z')dz'$$

in the interval [0,h]. Once this height has been determined the entrained heat flux can be calculated, the entrainment velocity found and the mixed layer variables incremented.

CHAPTER 4

THE RESULTS FROM THE NUMERICAL MODEL

4.1 INTRODUCTION

The theoretical framework behind the detailed numerical model has been described in chapter 3 and some features of the evolution of a daytime convective boundary layer, in which aerosol absorbs part of the shortwave radiation, have been explored using the simple model of chapter 2. In this chapter the results obtained from the more detailed numerical model will be described. However, before presenting the computed simulations of the convective layer, the behaviour of the soil scheme is examined and the turbulent fluxes and surface temperatures predicted by the surface energy balance are compared with measurements made during the O'Neill experiment (Lettau and Davidson, 1957) in an effort to generate some confidence in the results obtained.

In the following section the numerical stability of the model is discussed. The time-scales of the physical processes included in the model provide upper bounds to the time-step used. A theoretical stability analysis of the model was not attempted. Instead, to ensure that the time integration was stable the model was run several times with various time-steps and the results compared. As a result of these integrations the time-step was set at 36 seconds for all the subsequent integrations. In order to reduce the computing time the radiation subroutines were not called at every time-step but, without apparently affecting the results, only once every twenty-five time-steps, corresponding to once every fifteen minutes.

Finally the results obtained from the model are presented and discussed. First, by varying the aerosol loading within the mixed layer the effect of shortwave absorption on the growth of the mixed layer and the increase in the temperature of both the mixed layer and the soil is examined. The total energy input into the boundary layer and soil layer and its distribution are examined as functions of the optical depth of the mixed layer.

The effect of the variation of the entrained flux ratio over the course of twelve hours is examined by comparing the results obtained from the model described previously with those obtained by keeping the entrained flux ratio constant, ignoring the effects of the aerosol absorption on the stability of the mixed layer and the consequent effect on the turbulent kinetic energy budget of the mixed layer.

4.2 THE SOIL SCHEME

The temperature profile within the soil is specified by the first twenty terms of a Fourier sine series, the coefficients of which alter each time the soil temperatures are updated. It is important to note that, although the initial temperature profile may be specified by a few, low frequency components, those coefficients of the series which are initially set to zero may become non-zero at the second and subsequent time-steps. The theoretical derivation presented in section 3.5 gives no guide to how many terms of the series are required to calculate the surface temperature and surface heat flux to an acceptable degree of accuracy.

In order to estimate the error involved in truncating the

Fourier series the values of the first forty coefficients, a_m, were calculated at intervals of two hours over a period of sixty hours, having assumed a sinusoidal surface temperature, with a twenty-four hour period, and an initially linear temperature profile within the soil. The amplitudes of each Fourier component were calculated using the final equation of section 3.5(a). Table 4.1 shows the calculated amplitudes of five of the Fourier components over the second complete cycle.

Time (hours)	Fourier Amplitudes/(10^{-4})				
	a_1	a_5	a_{15}	a_{20}	a_{40}
24	-2911.0	-74.79	-2.780	-1.173	-0.3475
26	-4709.0	-67.02	-2.418	-1.1019	-0.3015
28	-5234.0	-41.30	-1.409	-0.5916	-0.1747
30	-4349.0	- 4.507	-0.0221	-0.0060	-0.0011
32	-2292.0	+33.49	-1.371	+0.5811	+0.1727
33	- 989.0	49.70	1.950	0.825	0.2449
34	+ 382.0	62.51	2.396	1.013	0.3003
36	2957.0	74.79	2.780	1.173	0.3475
38	4742.0	67.02	2.418	1.019	0.3015
40	5257.0	41.30	1.409	0.5916	0.1747
42	4365.0	4.507	0.0221	0.0060	0.0011
44	2303.0	-33.49	-1.371	-0.5811	-0.1727
45	998.5	-49.70	-1.950	-0.825	-0.2449
46	- 374.4	-62.51	-2.396	-1.013	-0.3003
48	-2952.0	-74.79	-2.780	-1.173	-0.3475

Table 4.1 Fourier Coefficients of the Soil Temperature Profile Calculated for a Sinusoidal Surface Temperature Wave of Unit Amplitude and Twenty-Four Hour Period

The effect of the initial temperature profile is only apparent in the first coefficient, the others display an entirely periodic

variation with time. The maximum amplitude attained by each component decreases very rapidly with increasing wavenumber. The maximum amplitude attained by the 20th component is only 0.06% of that of the first.

However, since the coefficients do not vary in phase with one another there are occasions when only the lower wavenumber terms vanish or become small. During such periods truncation of the series at a particular wavenumber is likely to lead to a greater relative error than might be expected from an examination of the relative sizes of the maximum amplitude of each component.

When this scheme is used in the numerical model the gradient of the temperature profile will be calculated, in order to evaluate the soil heat flux at the surface. The temperature gradient is evaluated by the summation of the series of terms of the form 'ma_m', which, obviously, does not decrease as quickly as the series $\{a_m\}$. Thus, although the amplitude of the twentieth coefficient, a_{20}, is only 0.2% of that of the coefficient a_1, after thirty-four hours, when a_1 is close to zero, the contribution of the higher wavenumber component to the temperature gradient is approximately 5% that of the first component.

Some of the partial sums of the series $\{ma_m\}$ are shown in Table 4.2. For most of the time, truncating the summation of this series at the twentieth term yields results which differ very little from those obtained by continuing the summation to the fortieth term.

Time (hours)	$S_n = \sum_{o}^{n} ma_m$			
	S_5	S_{15}	S_{20}	S_{40}
24	-0.6945	-0.8040	-0.8188	-0.8414
26	-0.8707	-0.9669	-0.9797	-0.9993
28	-0.8124	-0.8696	-0.8770	-0.8884
30	-0.5357	-0.5384	-0.5385	-0.5386
32	-0.1150	-0.0624	-0.0551	-0.0439
33	+0.1151	+0.1906	+0.2010	+0.2169
34	0.3372	0.4307	0.4434	0.4630
36	0.6992	0.8087	0.8234	0.8460
38	0.8739	0.9702	0.9830	1.0026
40	0.8147	0.8718	0.8793	0.8907
42	0.5372	0.5400	0.5401	0.5402
44	0.1159	0.0635	0.0562	0.0450
45	-0.1142	-0.1897	-0.2000	-0.2159
46	-0.3364	-0.4299	-0.4426	-0.4622
48	-0.6898	-0.8081	-0.8289	-0.8455

Table 4.2 Partial Sums of the Fourier Series of the Soil Temperature Gradient

The integrations to be described later were all carried out using twenty Fourier coefficients. To test the effect of truncating the series one integration was repeated using only fifteen components. The initial conditions and the various constants were assigned the same values as in the integrations to be described later in section 4.5. The greatest difference between the surface temperatures calculated in the two integrations is less than 0.6 K. However the mixed layer potential temperatures agree to within 0.02 K and the calculated depths of the mixed layer to within 6 metres. The largest discrepancy between the two calculated values of the surface temperature

occurs, as expected, at the time when the low wavenumber coefficients vanish. This happens in the late afternoon when convection has ceased and so does not affect the mixed layer development at all.

4.3 THE SURFACE ENERGY BALANCE

A comparison was made between the surface temperature and surface turbulent heat fluxes predicted by the surface energy balance scheme, which was described in sections 3.6 and 3.7, with data from the O'Neill experiment for 0835 and 1235 local time on the 7th September 1953 (Lettau and Davidson, 1957).

The values of the surface albedo and roughness length were estimated for the O'Neill site by the investigators and their estimates of 0.34 and 0.0044 m were used in these calculations. The mixed layer potential temperature, mixing ratio and wind speed were taken to be the mean values in the layer beneath the capping inversion, which, in both profiles was easily identified. The downwelling short-wave and infra-red fluxes were calculated from the radiation measurements. The turbulent fluxes and the soil heat flux at the surface were not measured directly but were calculated by Lettau from the profile data. The surface temperature was estimated from the radiation data and the Halstead parameter calculated from the formula

$$M = \frac{c_p}{\lambda} \frac{\lambda E(o)}{H(o)} \frac{(\theta_m - T_s)}{(q_m - q_{sat}(T_s))}$$

The surface energy budget was calculated for a range of values of the Halstead parameter and the resulting surface temperatures and turbulent fluxes compared with Lettau's values. The results are plotted in Figure 4.1 from which it is evident that the calculated results do not seem to be capable of reproducing the O'Neill fluxes. However examination of Lettau's results for 1235, shown in Table 4.3, reveal that the surface fluxes he derived do not balance, and therefore agreement between the two sets of results in all respects

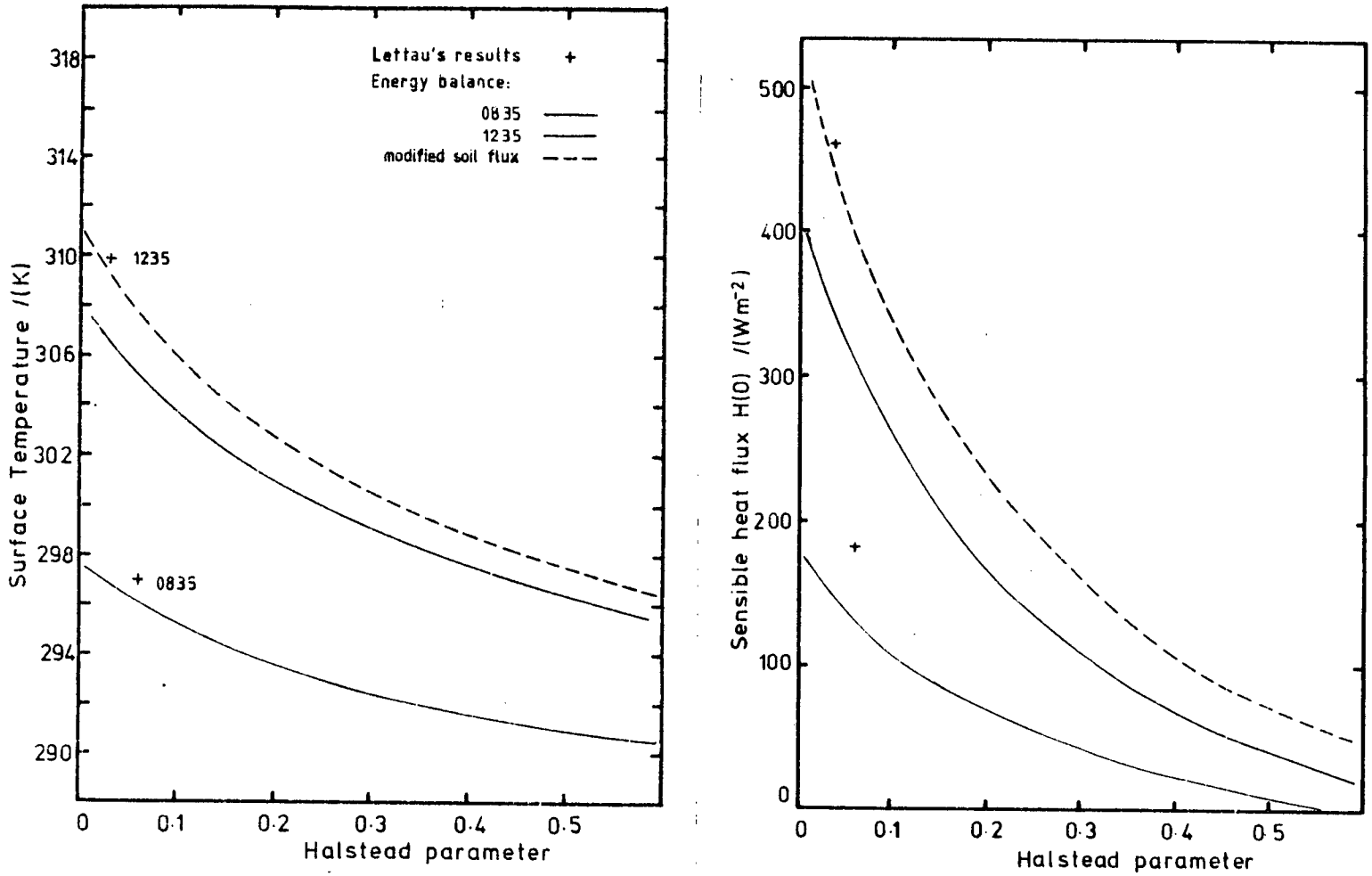

Figure 4.1 Surface Temperature and Sensible Heat Flux Predicted by the Surface Energy Balance as Functions of the Halstead Parameter.

cannot be expected.

The calculated results included in Table 4.3 are judged to be the nearest to the O'Neill fluxes that can be achieved. The final column of the table contains the surface temperature and turbulent fluxes calculated by the surface energy balance using the O'Neill data for 1235 but with the soil heat flux reduced to balance the energy budget. The agreement between the two sets of results is much improved.

		0835 LT		1235 LT		
		(1)	(2)	(1)	(2)	(3)
Net shortwave irradiance	Wm^{-2}	295	295	598	598	598
Downwelling IR irradiance	Wm^{-2}	342	342	452	452	452
Soil heat flux	Wm^{-2}	60	60	148	148	12
Mixed layer potential temperature	K	291.7	291.7	295.2	295.2	295.2
Mixing ratio	$g\ kg^{-1}$	7.7	7.7	8.4	8.4	8.4
Wind speed	ms^{-1}	13	13	13	13	13
Halstead parameter		0.06	0.025	0.03	0.025	0.025
Surface temperature	K	297.2	297.7	309.9	306.7	309.6
Sensible heat flux	Wm^{-2}	186	161	460	366	471
Latent heat flux	Wm^{-2}	60	23	76	58	69

Table 4.3 The Surface Energy Budget According to Lettau (1); Calculated Results (2) and Results Using a Modified Soil Flux (3)

4.4 NUMERICAL STABILITY

The choice of the model time-step and of the time-interval between successive evaluations of the energy fluxes is limited by the natural time scales associated with the processes included in the model. In the present instance it is the rates at which the energy fluxes at the surface vary which is important. The shortwave radiation flux at the surface depends on the solar zenith angle and the rate at which the flux varies obviously depends on geographical position and time of day. The rate at which the soil heat flux varies depends on the composition of the soil layer. The remaining fluxes depend on the temperature and humidity of the mixed layer and that of the surface. We will examine each of these, briefly, in turn.

The solar zenith angle varies most quickly when the sun is low in the sky; towards midday the zenith angle is very nearly constant. Convection does not begin until an hour or two after sunrise; this is illustrated by the boundary layer profiles from Wangara in Figure 1.1 and the flux data from O'Neill plotted in Figure 4.2. The maximum rate of change of the solar zenith angle occurs close to sunrise or sunset at latitudes in which the ecliptic passes through the zenith. When, in such conditions, the sun reaches an elevation of 30° above the horizon it takes approximately fifteen minutes for the solar irradiance of a horizontal surface to increase by 10% of its current value. This estimate does not include the effects of increased absorption at large zenith angles. Thus, it should not be necessary to re-calculate the solar flux more frequently than once every five or ten minutes.

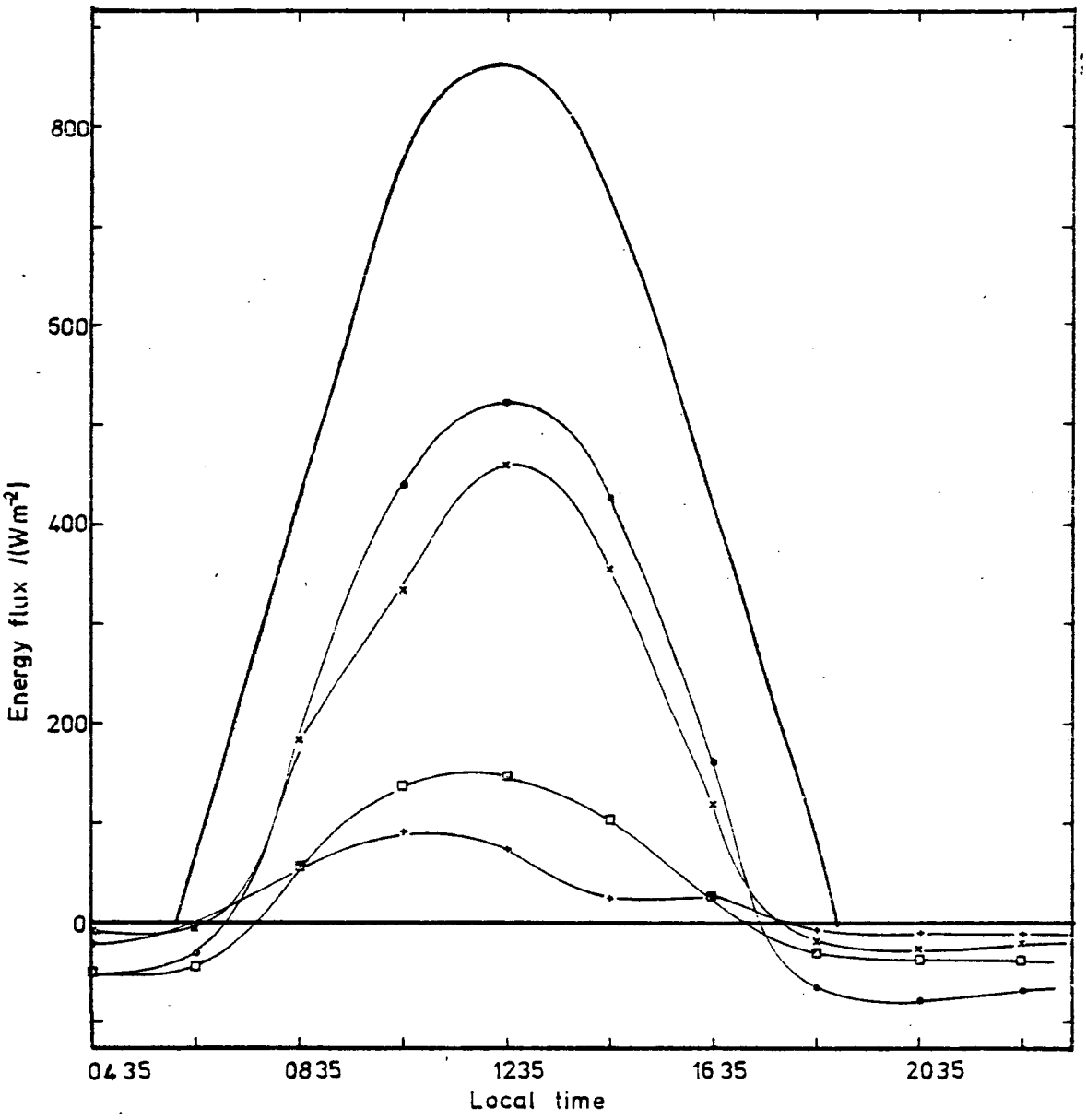

Figure 4.2 The Energy Fluxes at the Surface at O'Neill
7 September 1953

Downward short wave irradiance.
Net radiation flux.
Sensible heat flux.
Latent heat flux.
Heat flux into the soil.

The turbulent fluxes of sensible and latent heat, and the heat flux into the soil vary as the temperature and humidity structure of the mixed layer and soil layer vary. During the period when the surface heat flux is directed away from the surface the turbulent fluxes and soil flux are approximately sinusoidal functions of time with periods, judged from the length of time during which the fluxes are positive, which are from eighteen to twenty-two hours. Arguments similar to those advanced with respect to the solar irradiance can be applied to the surface fluxes to suggest that they need not be re-calculated more frequently than once every five or ten minutes.

It would be sensible to enquire whether the results of the numerical model are compatible with those of the analytic model. To this end the numerical model was run with the mixed layer water-vapour mixing ratio and that for the atmosphere above the inversion and the Halstead parameter all set to zero. This is necessary to avoid difficulties with latent energy fluxes which cannot be included in the analytic model as it stands. The sensible heat flux generated by the numerical model can be approximated by a sinusoidal function of time with a period of 17.14 hours and a maximum value of 275.5 Wm^{-2}. The fluxes are shown in Figure 4.3 and the calculated depth of the mixed layer and mixed layer potential temperature are shown in Figure 4.4.

The agreement between the two sets of results is encouraging. The sinusoidal function overestimates the sensible heat flux calculated by the numerical model and, although the differences between the mixed layer temperatures are no greater than 0.2 K, the analytic solution predicts a mixed layer some 60 m deeper than the numerical calculation after six hours.

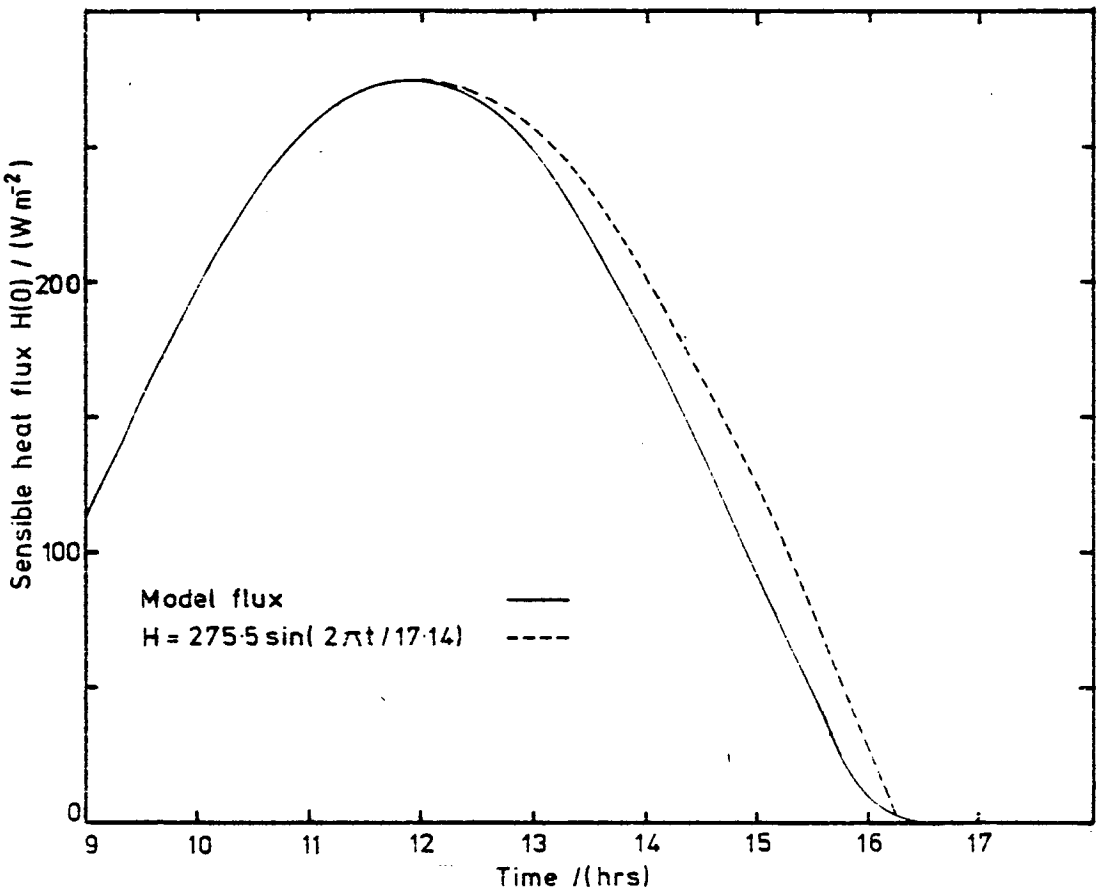

Figure 4.3 The Sensible Heat Flux at the Surface Calculated by the Numerical Model and the Sinusoidal Function Used to Approximate it

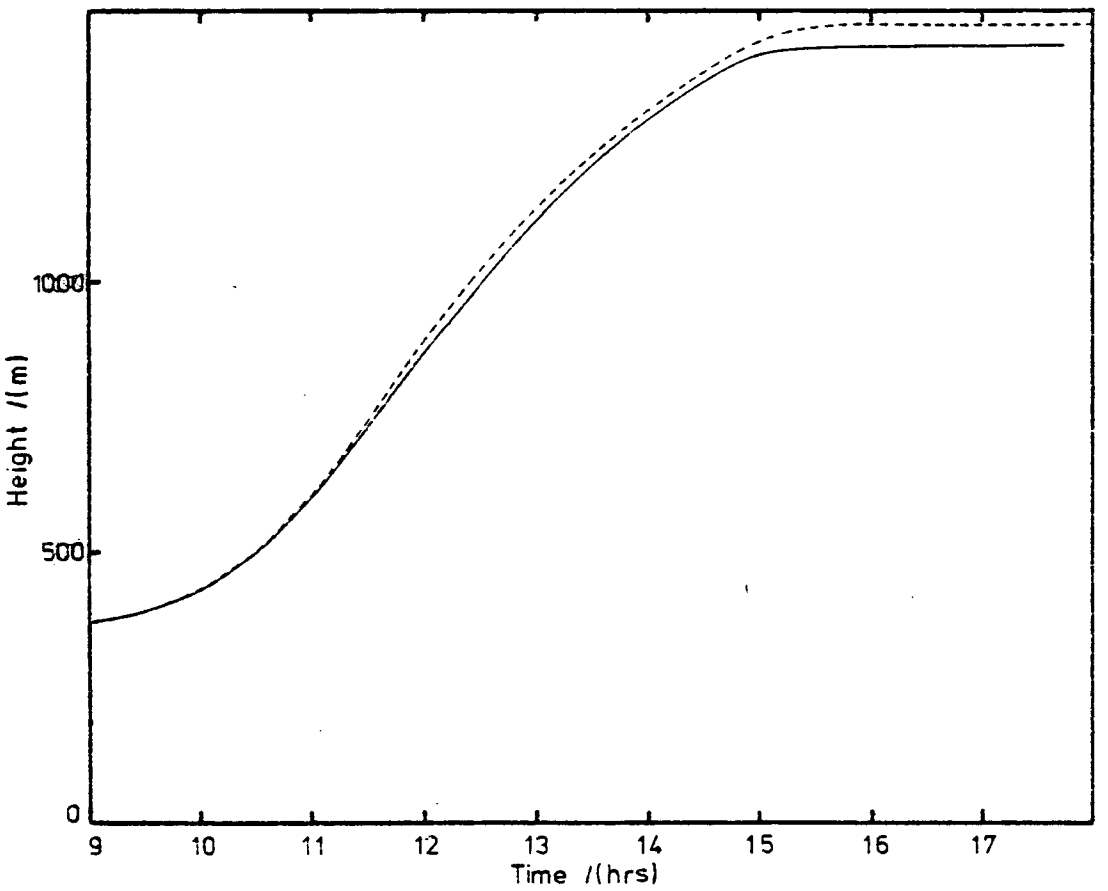

Figure 4.4 a) The Mixed Layer Depth Calculated by the Numerical Model (——) and by the Analytic Model (---)

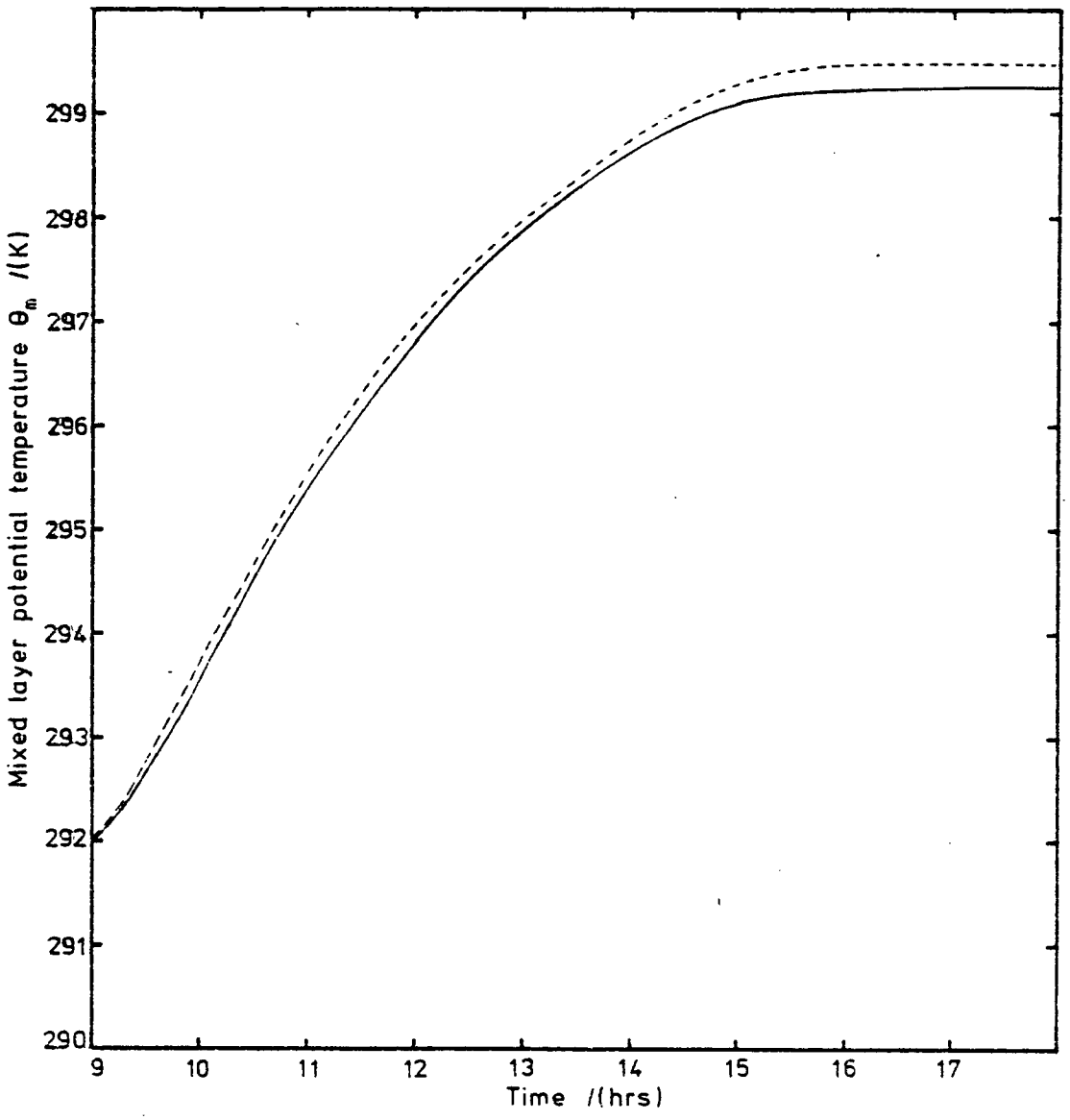

Figure 4.4 b) The Mixed Layer Potential Temperature Calculated by the Numerical Model (——) and by the Analytic Model (---)

To ensure that the time-step chosen was not too large the model was run four times, using identical initial conditions but with different time-steps and different intervals between the calculation of the energy fluxes at the surface. The time-steps used are shown in Table 4.4 and the initial conditions are as shown in Table 4.5. The relative time taken for each integration over six hours of model time shows that it is the evaluation of the surface fluxes which largely determines the speed with which the calculation proceeds. Even though limited computing time did not prove to be a serious constraint, this is, after all a one dimensional model, it would be sensible to reduce the computation time as much as possible without introducing unacceptable inaccuracies.

The calculated development of the mixed layer in all four integrations agree very well. The greatest differences are found between the results of run 1 and run 4 and the results of run 2 and run 3 differ least. In what follows only the results from runs 1 and 4 are considered. The mixed layer potential temperatures agree to within 0.05 K, the discrepancy between the two sets of results increasing throughout the integration. The depth of the mixed layer shows a similar behaviour; the difference between the two sets of results increases to 2 m after six hours, which is less than 1% of the total change in the depth of the layer over the period.

The calculated surface sensible heat flux and the surface temperature are more sensitive. However, care must be exercised in comparing the calculated values of these variables directly. The surface temperature, and therefore the turbulent fluxes and soil heat flux, is calculated by balancing the energy transport across

Run No.	Time-Step secs	Time Between Flux Evaluation secs	Relative Time Taken
1	18	180	14
2	36	360	7
3	360	360	7
4	900	900	1

Table 4.4 Time-Steps Used for Investigating the Numerical Stability of the Model

Latitude		50.0 N
Date		21 September
Roughness length	z_o	0.01
Albedo	r_s	0.2
Halstead parameter	M	0.0001
Soil diffusivity	κ	0.23×10^{-6} m^2 s^{-1}
Soil conductivity	k	0.359 Wm^{-1} K^{-1}
Soil depth	z_d	0.8 m

Initial Soil Temperature Profile

z (m)	0.1	0.2	0.3	0.4	0.5	0.6	0.7	0.8
T (K)	290.1	292.2	293.2	293.4	293.35	293.3	293.25	293.2

Atmospheric profiles above CBL

$\theta(z) = 293.15 + 0.0051z$ (K)

$q(z) = 0.1$ (g/kg)

geostrophic wind speed 13 ms^{-1}

Aerosol

Single scattering albedo	w_o	0.8
Backscattering ratio	b	0.1
Extinction coefficient		5.0

Mixed layer initial conditions

Depth	h	370 m
Potential temperature	θ_m	292 K
Mixing ratio	q_m	0.1 g/kg
Aerosol concentration		0.5µg m^{-3}
Optical depth		0.0009

Table 4.5 Initial Conditions Used for Stability Investigation

the air-soil interface over the period between one evaluation of the surface fluxes and the next, and therefore values calculated using different temporal resolutions should not be expected to be identical. The surface temperature calculated in run 4, with the largest interval between successive calculations, is 0.5 K higher, initially, than that calculated in run 1. The difference between the two decreases during the integration, changing sign shortly after midday. This type of behaviour is consistent with the temperature being an average over two intervals of different lengths. After six hours the difference between the two surface temperatures is 0.25 K, the result from run 1 being larger.

The surface sensible heat flux behaves, as might be expected, in a similar fashion to the surface temperature. Initially the two calculations differ by about 15 Wm^{-2} which is about 6% of the smaller of the two values, that calculated with the finer resolution. Close to midday the two calculations agree to within 0.5 Wm^{-2}.

In the light of these results the time-step used in all the other integrations of the model was set at 36 seconds and the radiative and turbulent fluxes at the surface and the soil flux were calculated once every 900 seconds.

4.5 DISCUSSION OF THE RESULTS

To assess the effect that various aerosol loadings have on the development of the model three sets of results will be presented. Each of the three integrations ran from 0900 local time to 1800. The initial conditions were identical in each case, except for the aerosol concentrations in the mixed layer. The remaining initial conditions were as shown in Table 4.6. The aerosol concentrations were specified as: 1) 0.054 $\mu g\ m^{-3}$ and 2) 162.2 $\mu g\ m^{-3}$. The resulting optical depths of the mixed layer were 0.0001 and 0.3 respectively. The first set of results are applicable to an almost non-turbid mixed layer and the second set to a light polluted layer.

It is not straightforward to interpret the assumed turbidity of a layer in terms of visibility, for example, without also specifying the size distribution of the aerosol. Glazier et al (1976) measured the turbidity, which is equal to the component of the optical depth of the layer due to aerosol alone. The range of their values is from 0.2 to 0.4. They suggest that the shortwave convergence due to atmospheric gases is approximately a third of that due to aerosol, which would suggest that in the absence of aerosol the atmospheric convective boundary layer would best be represented by the second of the three integrations.

Welch and Zdunkowski (1976) calculate that a loading of 700 $\mu g\ m^{-3}$ of typical aerosol particles, whose sizes follow a Junge distribution, results in a visual range of about 2.6 km if the relative humidity is 80%. This corresponds to heavy industrial pollution and to achieve similar absorption rates within the mixed layer the optical depth used in the present model would have to be set as high as 1.2.

Latitude		42.5 N
Date		7 September
Roughness length	z_o	0.005 m
Albedo	r_s	0.2
Halstead parameter	M	0.01
Soil diffusivity	κ	0.25×10^{-6} m^2 s^{-1}
Soil conductivity	k	0.359 Wm^{-1} K^{-1}
Soil depth	z_d	0.8 m

Initial Soil Temperature Profile

z (m)	0.1	0.2	0.3	0.4	0.5	0.6	0.7	0.8
T (K)	290.1	292.2	293.2	293.4	293.35	293.3	293.25	293.2

Atmospheric profiles above CBL

$$\theta(z) = 290.43 + 0.0051z \text{ (K)}$$

$$q(z) = 7.97 - 0.001z \text{ (g/kg)}$$

Aerosol

Single scattering albedo	w_o	0.8
Back-scattering ratio	b	0.1
Extinction coefficient		5.0 m^2 kg^{-1}

Table 4.6 Model Parameters for the Integrations

The surface fluxes generated by these three integrations behave very much as might be expected in the light of the lessons drawn from the analytic model of chapter two. Increasing the optical depth of the mixed layer reduces the shortwave energy which reaches the surface. As a direct result the turbulent fluxes and the soil heat flux are reduced. The downward longwave irradiance at the surface has been parameterized in terms of the mixed layer temperature and moisture and is relatively insensitive to the changes in the optical depth of the layer. The infra-red radiation emitted from the surface is, of course, strongly dependent on the temperature of the surface. Addition of aerosol results in lower surface temperatures and hence, the longwave radiation from the surface is lessened. However whereas the shortwave energy absorbed at the surface at noon is reduced by 31% in increasing the optical depth of the mixed layer from 0.0001 to 0.3, the longwave emission from the surface is reduced by only 18%. The turbulent heat flux is reduced from 358 Wm^{-2} by 41% to 210 Wm^{-2} and changes sign about thirty-five minutes earlier in the more turbid example. The latent heat flux is a small fraction of the sensible heat flux because of the very small value assigned to the Halstead parameter, and when the optical depth of the layer is increased the latent heat flux is reduced from 27 Wm^{-2} to 17 Wm^{-2}. The radiative fluxes and the turbulent heat flux over the nine hours of the integration are shown in Figures 4.5 and 4.6.

However, the effect of aerosol absorption on the development of the mixed layer predicted by the numerical model is qualitatively different from that predicted by the analytic model. Recall that the latter predicted that, for realistic values of the surface albedo,

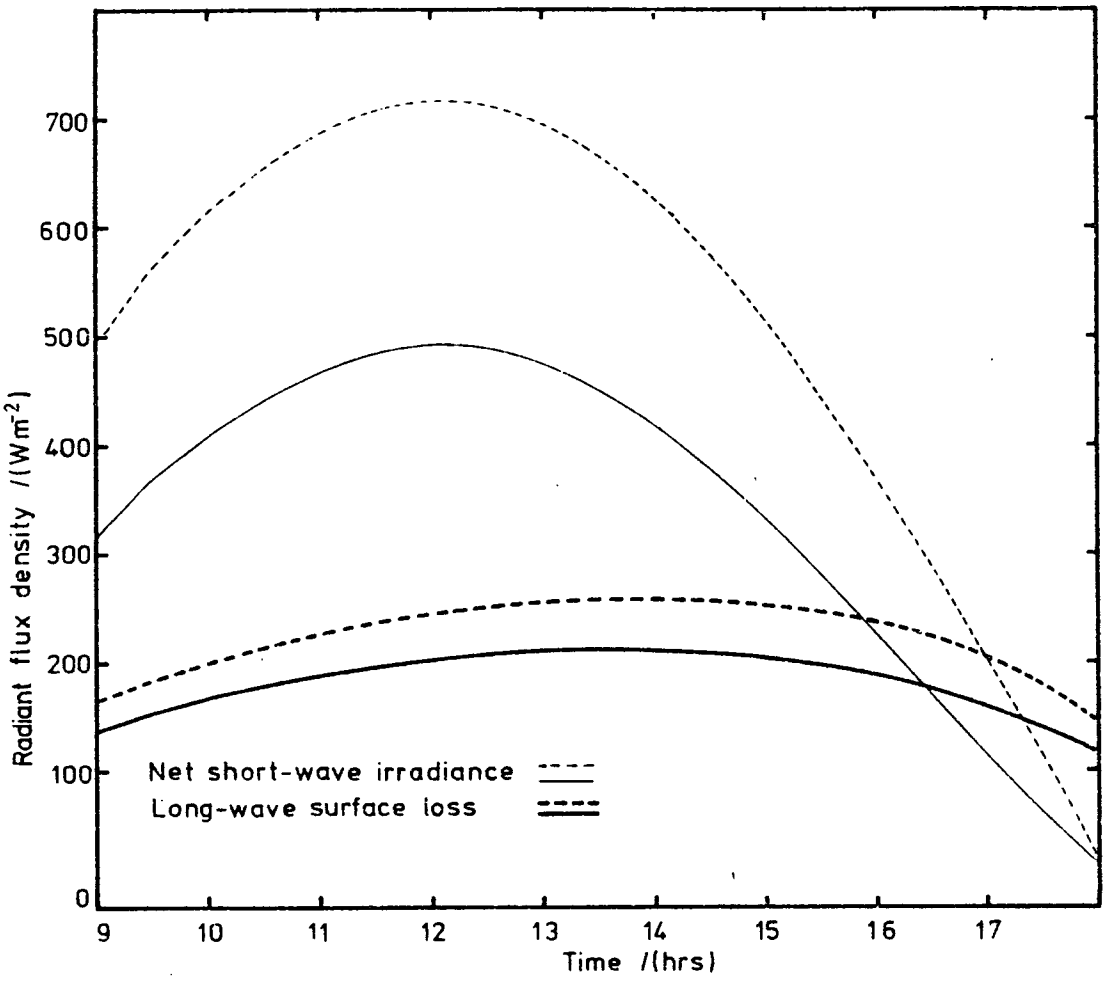

Figure 4.5 The Net Radiation Fluxes Calculated by the Numerical Model at the Surface for Mixed Layer Optical Depths of 0.0001 (---) and 0.3 (——)

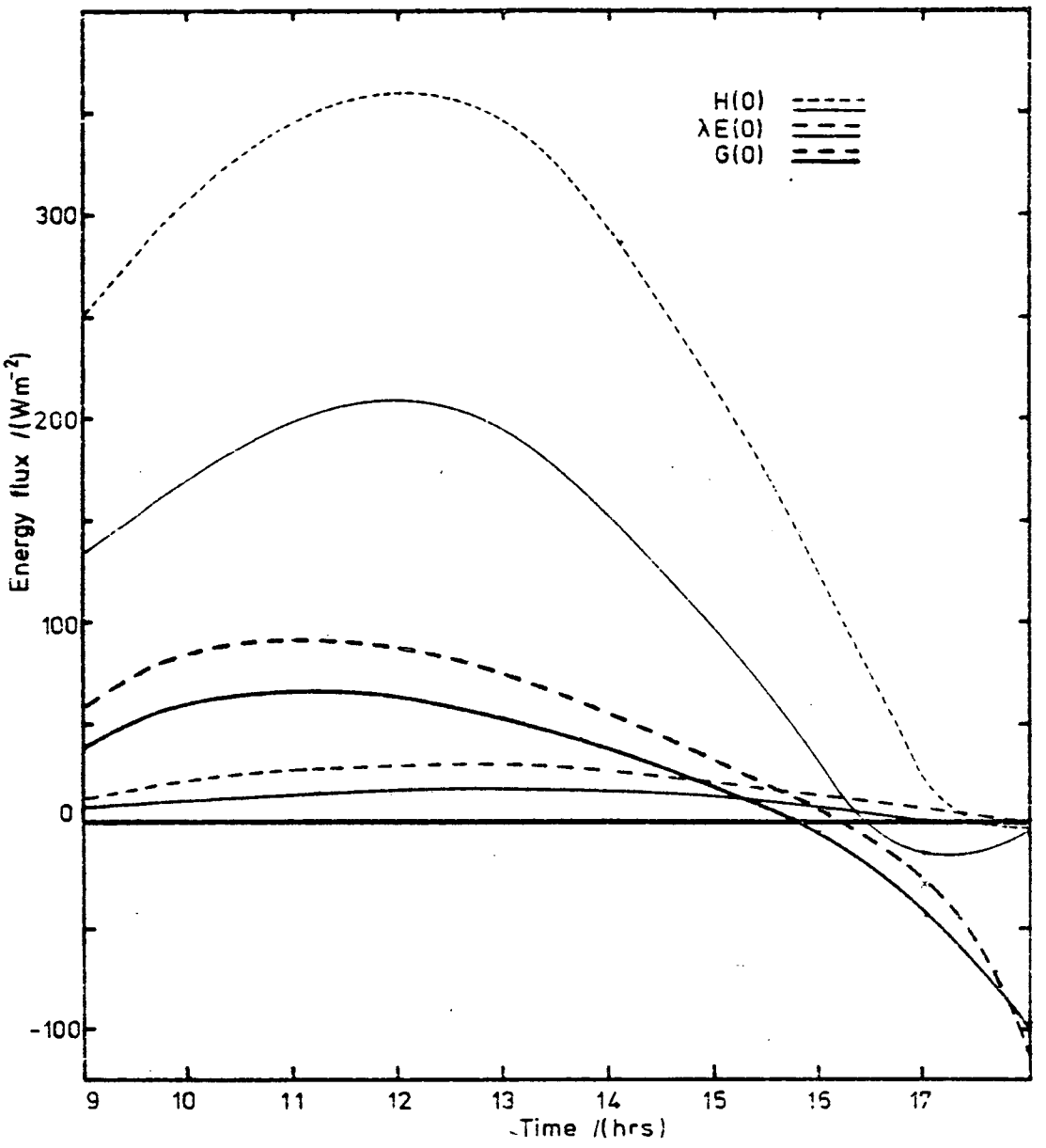

Figure 4.6 The Turbulent Fluxes and Soil Heat Flux Calculated by the Numerical Model for Mixed Layer Optical Depths of 0.0001 (---) and 0.3 (——)

the mixed layer would deepen more quickly and its temperature rise more quickly as a result of the addition of aerosol to the layer. Figures 4.7 and 4.8 show the values of the mixed layer depth and mixed layer potential temperature calculated by the numerical model for mixed layer optical depths of 0.0001 and 0.3. The development of the more turbid layer is retarded; it deepens more slowly and is cooler than the less turbid example.

Figure 4.9 shows the trajectories of these solutions in the $\Delta\theta$-γh plane. The first solution, for a very small optical depth, follows a straight line through the origin which corresponds to a value of $\Delta\theta/\gamma h$ of $\frac{1}{5}$. This is just as would be expected from the results of chapter 2. The initial temperature jump was chosen to ensure that the initial point lies on the straight line, thus avoiding a period of reduced growth of the mixed layer while the temperature jump adjusts to a size appropriate to the entrainment ratio and the potential temperature gradient above the mixed layer.

The effect of the direct heating induced by the aerosol absorption is apparent in the trajectory calculated for a mixed layer optical depth of 0.3. The temperature jump adjusts between 0900 and 1000. Thereafter, until about 1500, the solution follows a nearly straight path with a slope which differs from that for the nearly non-turbid solution because of the effect of the direct heating. The variation of the entrainment ratio throughout this period is small - it would manifest itself as a change in the slope of the trajectory. Such a change does not become apparent until after 1500.

The primary aim of this study is to investigate the effect that absorption of radiation by aerosol within the convective boundary

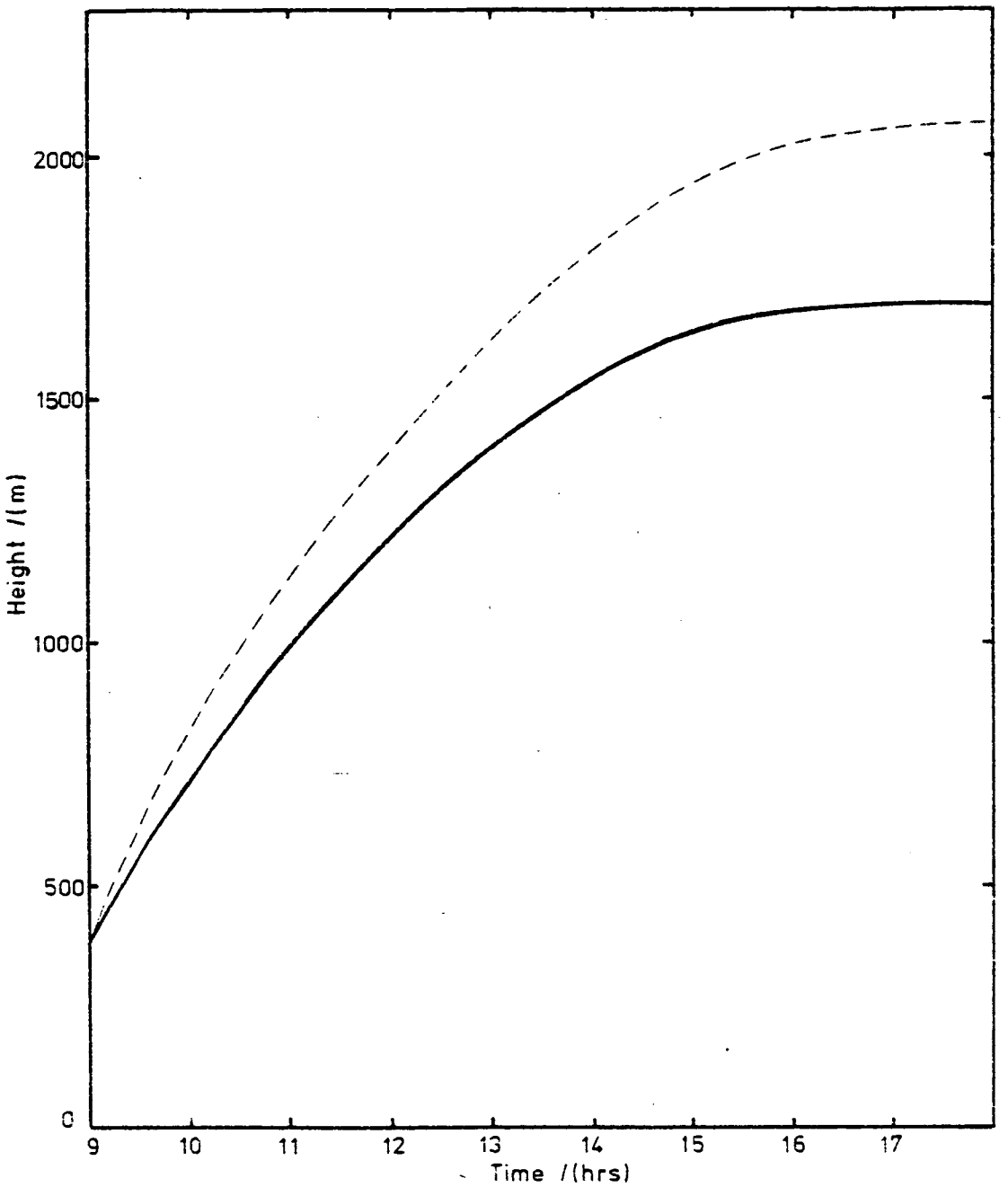

Figure 4.7 The Mixed Layer Depth Calculated by the Model for Mixed Layer Optical Depths of 0.0001 (---) and 0.3 (——)

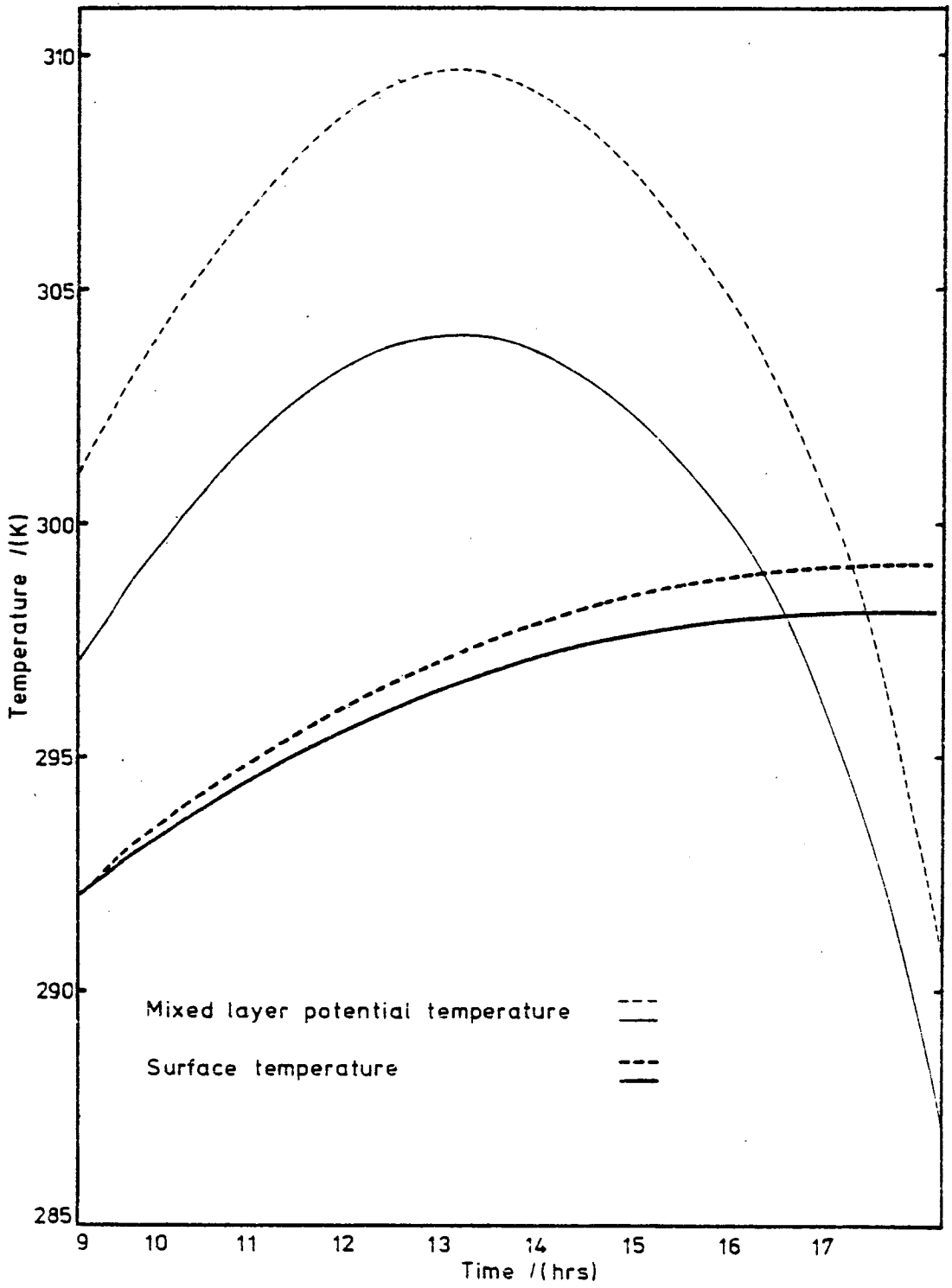

Figure 4.8 The Mixed Layer Potential Temperature and Surface Temperature Calculated by the Model for Mixed Layer Optical Depths of 0.0001 (---) and 0.3 (——)

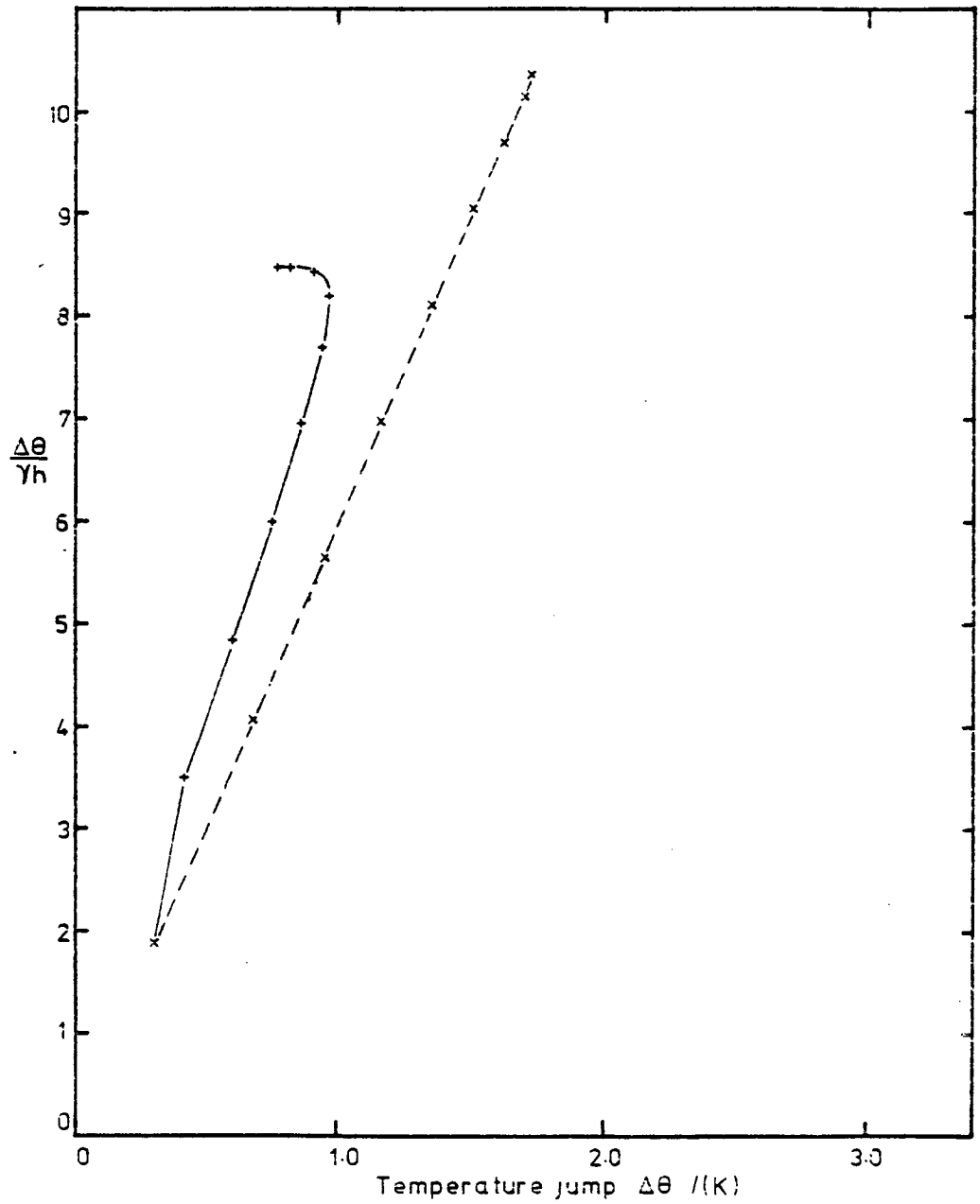

Figure 4.9 The Solutions Plotted in the $\Delta\theta$-γh Plane for Mixed Layer Optical Depths of 0.0001 (---) and 0.3 (——)

layer, and the consequent direct heating and stabilisation of the mixed layer, has on entrainment at the base of the capping inversion layer and growth of the mixed layer. The results from the analytic model show how the entrained flux ratio varies with the optical depth of the mixed layer given a non-scattering aerosol. It is to be expected from these results that during the course of a day the entrained flux ratio will increase to a maximum value towards noon, as the solar zenith angle decreases, and decrease thereafter. Since the mixed layer develops most quickly in the middle of the day the effect of this variation is likely to be minimised. Table 4.7 shows how the entrained flux ratio varies during the model integrations. The results from integrations with an increased value of the Halstead parameter are included as well. They will be discussed in more detail later. Results calculated for a mixed layer optical depth of 0.5 are also included.

Optical Depth Halstead Parameter Time/(hrs)	0.0001 0.01	0.3 0.01	0.3 0.1	0.5 0.1
09	0.25	0.23	0.20	0.06
10	0.25	0.23	0.22	0.10
11	0.25	0.23	0.22	0.15
12	0.25	0.23	0.22	0.15
13	0.25	0.23	0.22	0.13
14	0.25	0.23	0.21	0.08
15	0.25	0.21	0.14	-
16	0.25	0.20	-	-
17	0.06	-	-	-
18	-	-	-	-

Table 4.7 The Entrainment Heat Flux Ratio

The potential energy constraint described in chapter two applies to the numerical model as well as the analytic model. However because not all of the energy diverted from the surface by the aerosol heats the mixed layer in the numerical model it is a less stringent constraint. A check was kept to ensure that the energy condition was satisfied for all of the integrations described here.

In order to determine the overall effect of the variation of the entrained heat flux ratio the results from the numerical model were compared with those obtained by fixing the entrained heat flux ratio at the value appropriate to a non-turbid layer which, to be consistent with the previous results, was set at 0.25. When the mixed layer optical depth is 0.3 the calculated entrainment flux ratio is 0.23 between 09 and 14 hours after which it decreases rapidly. As a direct result the mixed layer deepens less quickly. The difference amounts to 20 m after six hours. The solutions are shown in Figure 4.10. The development of the mixed layer with an optical depth of 0.5 ceases about one hour earlier than the other examples quoted here, shortly after 1430 hours. After five hours the mixed layer depth calculated by the standard model, in which the entrainment heat flux ratio varies, is 50 m less than that calculated with a fixed entrainment heat flux ratio. The mixed layer temperatures agree to 0.25 K. These results suggest that for practical purposes the variation in the entrained heat flux ratio due to radiative convergence within the mixed layer can be neglected.

The partition of the available energy between the mixed layer and the soil layer, and the relative contributions of radiative and turbulent processes to the heating of the mixed layer were examined

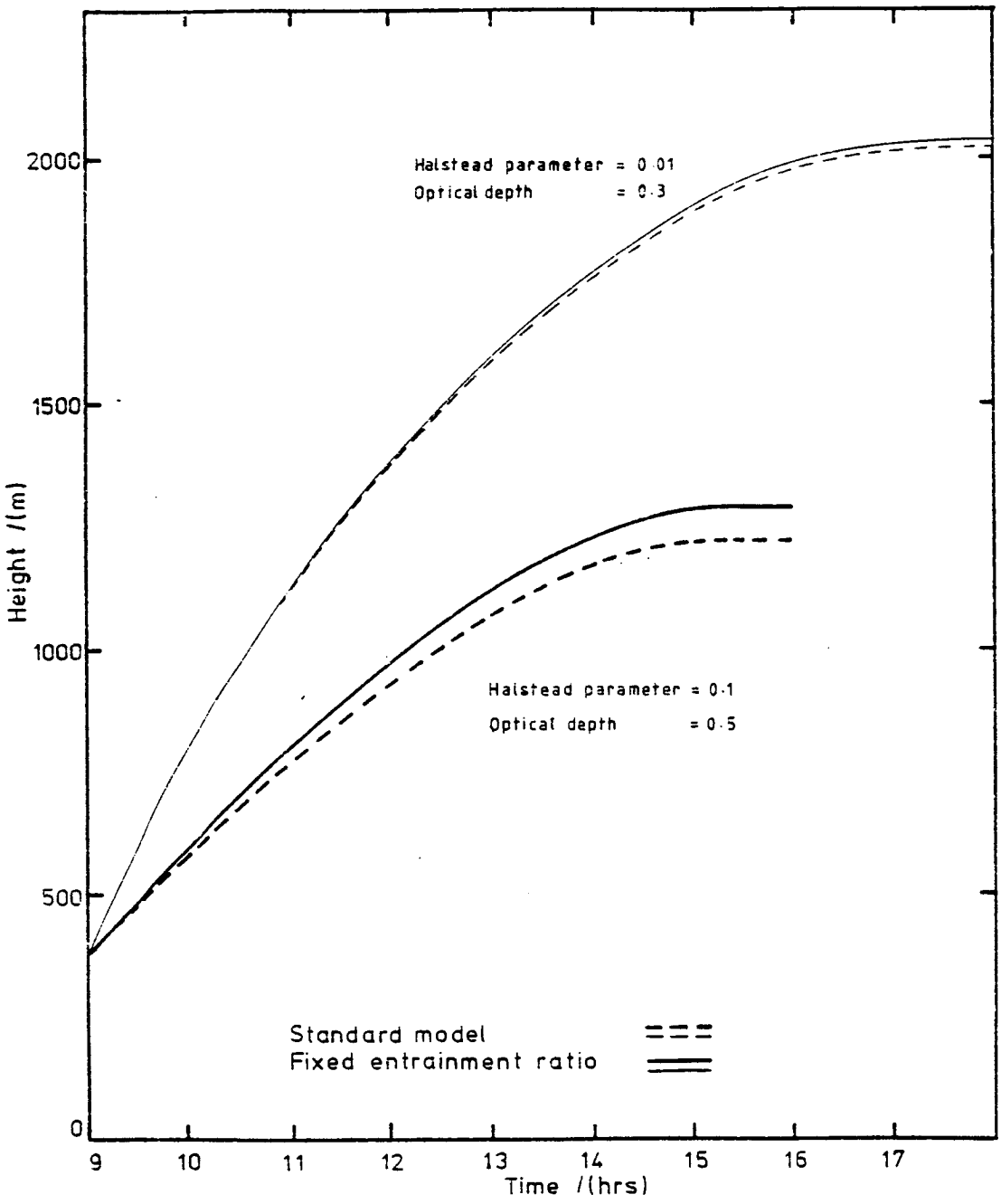

Figure 4.10 The Mixed Layer Depth Calculated by the Standard Model Compared to that Calculated with a Fixed Entrainment Flux Ratio of 0.25

by calculating the changes in the heat content of the mixed layer and soil layer over the six hours between 0900 and 1500. The model fluxes were numerically integrated over the same period. Since the values of the fluxes at sixty minute intervals were used for the latter calculation the results are accurate to no more than 2%.

The results, which are presented in Table 4.8 show that the total heating of the mixed layer decreases as the optical depth of the mixed layer increases; in fact, the total energy input to the mixed layer and soil layer decreases as the optical depth is increases. This is equivalent to saying that a greater fraction of the incoming energy is reflected away from the surface. The importance of the direct heating of the mixed layer can be seen to increase from less than 0.5% of the total, when the optical depth of the layer is 0.0001, to 30% when the optical depth is increases to 0.3.

Energy Input/(MJ)	Optical Depth	
	0.0001	0.3
Total sensible input to mixed layer	6.89	5.525
Latent input to mixed layer	0.497	0.314
Heat input to soil	0.997	0.651
Total	8.38	6.48
Turbulent heating of mixed layer	6.74	3.76
Radiative heating of mixed layer	0.001	1.59

Table 4.8 Calculated Energy Budget for the Mixed Layer and Soil over the Six Hours from 09 to 15 Hours for a 'Dry' Surface, Halstead Parameter = 0.01

It is easy to see that the effect of aerosol in the analytic model can only be to increase the energy input to the mixed layer, whereas, because the numerical model includes the effects of scattering of the incoming radiation, not all of the radiative energy intercepted by the aerosol before reaching the surface remains within the mixed layer. In other words, if the scattering is strong enough the addition of aerosol may lead to a decrease in the net heat input to the mixed layer and soil.

Meador and Weaver (1980) show that two stream radiation schemes yield solutions for a turbid layer above a black surface in which the overall albedo of the system increases with increasing optical depth. This implies that the addition of aerosol must decrease the heat input to the mixed layer and soil together and therefore addition of aerosol can only warm the mixed layer at the expense of the heat input to the soil.

Venkatram and Viskanta (1976) show that addition of aerosol to a convective boundary layer results in an overall heating or cooling of the mixed layer and soil, or a reduction in the albedo of the system, depending on the sign of the expression

$$(1 - wb)/wb - (1 - r_s^2)/2r_s$$

where w is the single scattering albedo of the aerosol, b the back-scattering coefficient and r_s the albedo of the surface, as in chapter 3.

The numerical model, as has already been suggested, cannot simulate conditions in which the addition of aerosol decreases the overall albedo of the mixed layer-soil system. This unanticipated

shortcoming arises from the omission of the effects of Rayleigh scattering within the mixed layer. The mean value of the Rayleigh optical depth, weighted by the solar spectral irradiance, over the solar spectrum, for the lowest kilometre of the atmosphere is of the order of 0.1. Since the phase function for Rayleigh scattering is symmetric in the forward and backward directions the backscattering coefficient for Rayleigh scattering is 0.5. Hence, in the real atmosphere, in the absence of aerosol a component of the incoming radiation is scattered away from the surface within the boundary layer. Addition of aerosol, which scatters strongly in the forward direction is then capable of reducing the overall albedo of the system.

The effect of the soil moisture on the model results was examined by repeating the integrations described above with the Halstead parameter increased by a factor of ten to 0.1. The results are very much as had been expected. The turbulent sensible heat flux is reduced and the latent energy flux increases. Because of the reduced sensible heat flux at the surface the development of the mixed layer proceeds at a slower rate, so that the nearly transparent mixed layer (τ = 0.0001) is, after six hours, 300 m shallower and 1 K cooler as a result of increasing the surface moisture. The surface temperatures generated with the increased soil moisture are as much as 5 K lower than those derived in drier conditions. The differences between the more turbid integrations are slightly smaller. The results are shown graphically in Figures 4.11, 4.12 and 4.13.

An analysis of the energy partition (see Table 4.9) reflects the changes to the sensible and latent heat fluxes and the reduced input of heat to the soil layer, which corresponds to the reduced

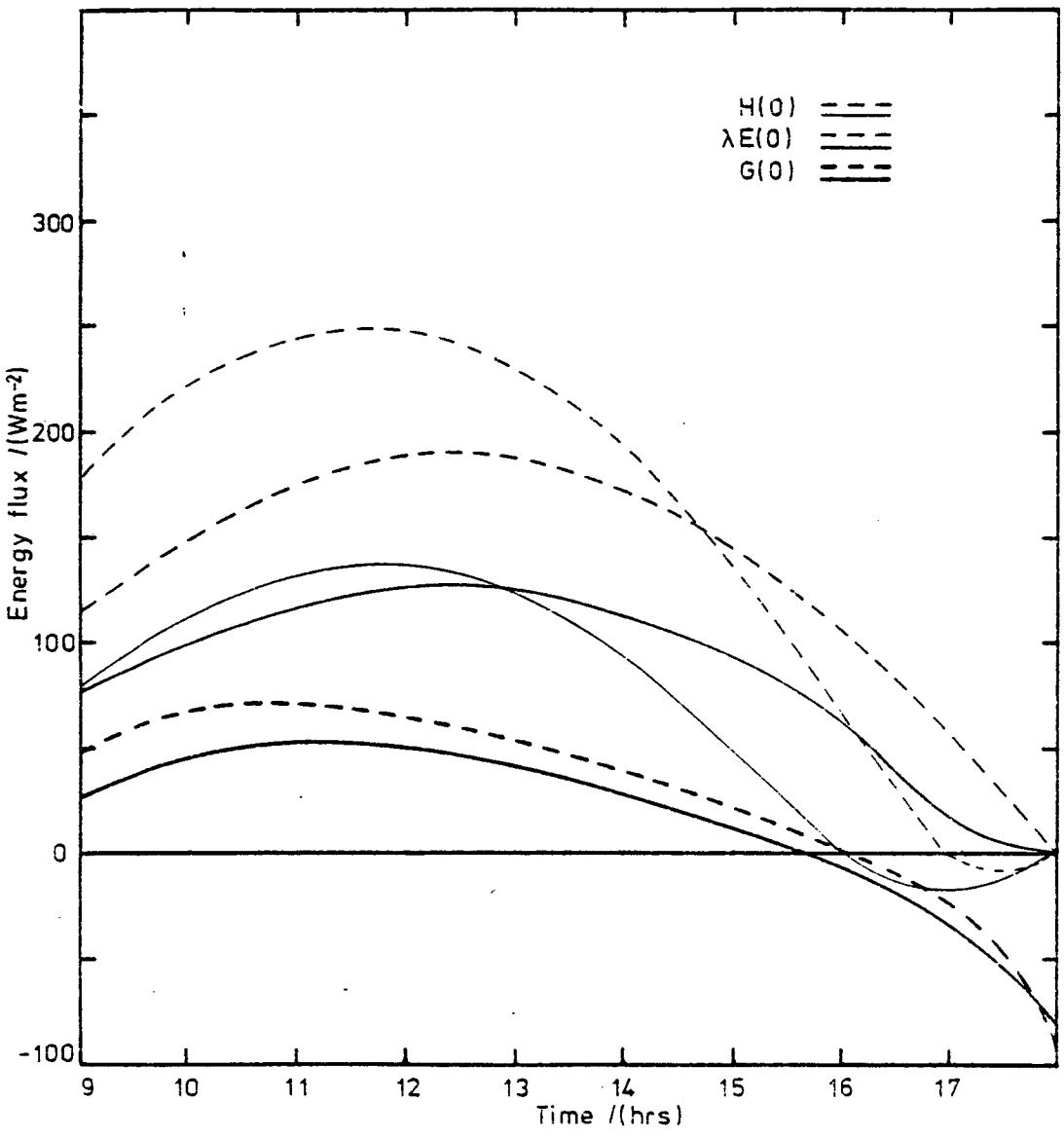

Figure 4.11 The Turbulent Fluxes and Soil Heat Flux Calculated by the Numerical Model for Mixed Layer Optical Depths of 0.0001 (---) and 0.3 (——) Over the Moist Surface (Halstead Parameter = 0.1)

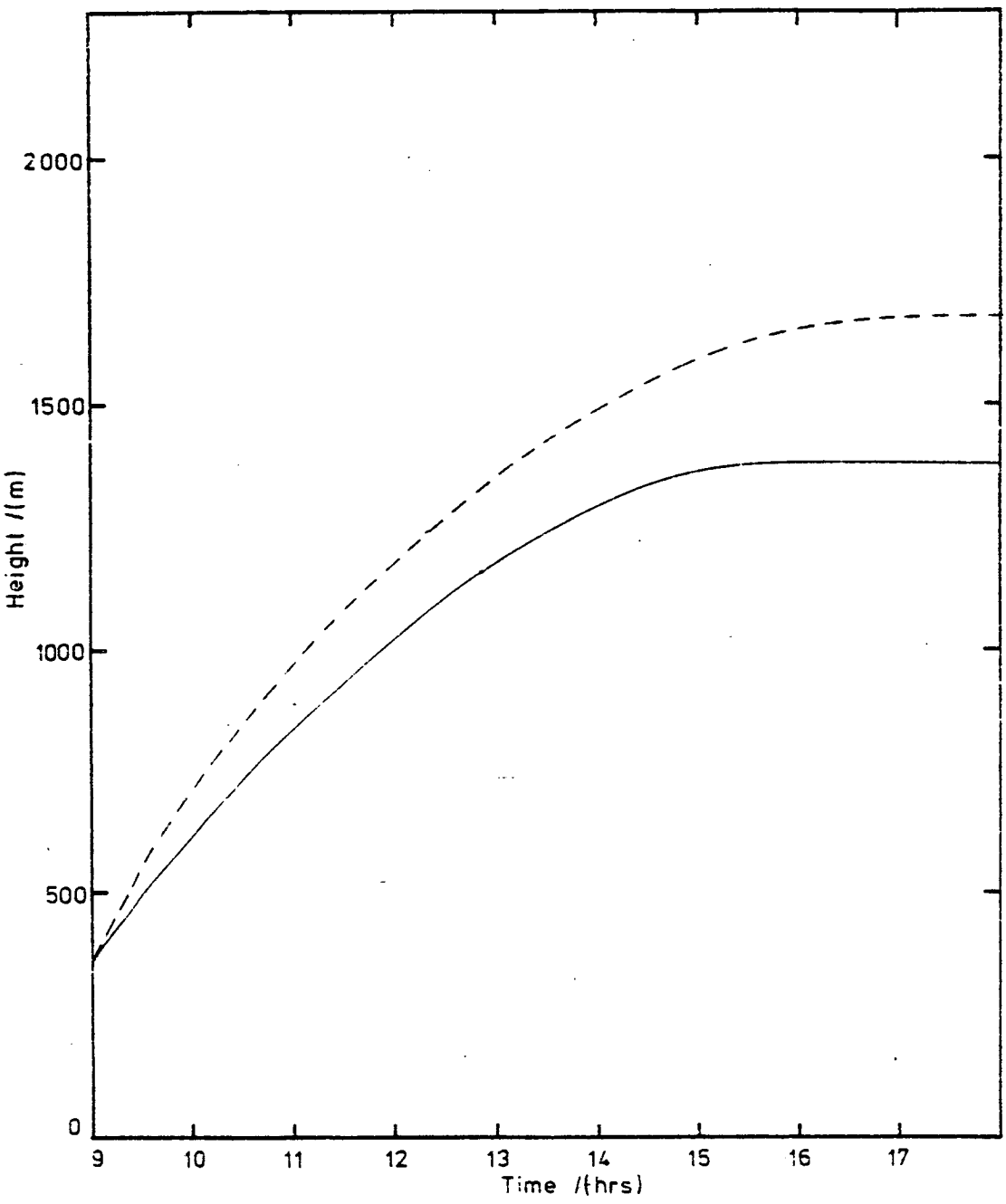

Figure 4.12 The Mixed Layer Depth Calculated by the Numerical Model for Mixed Layer Optical Depths of 0.0001 (---) and 0.3 (——) Over the Moist Surface (Halstead Parameter = 0.1)

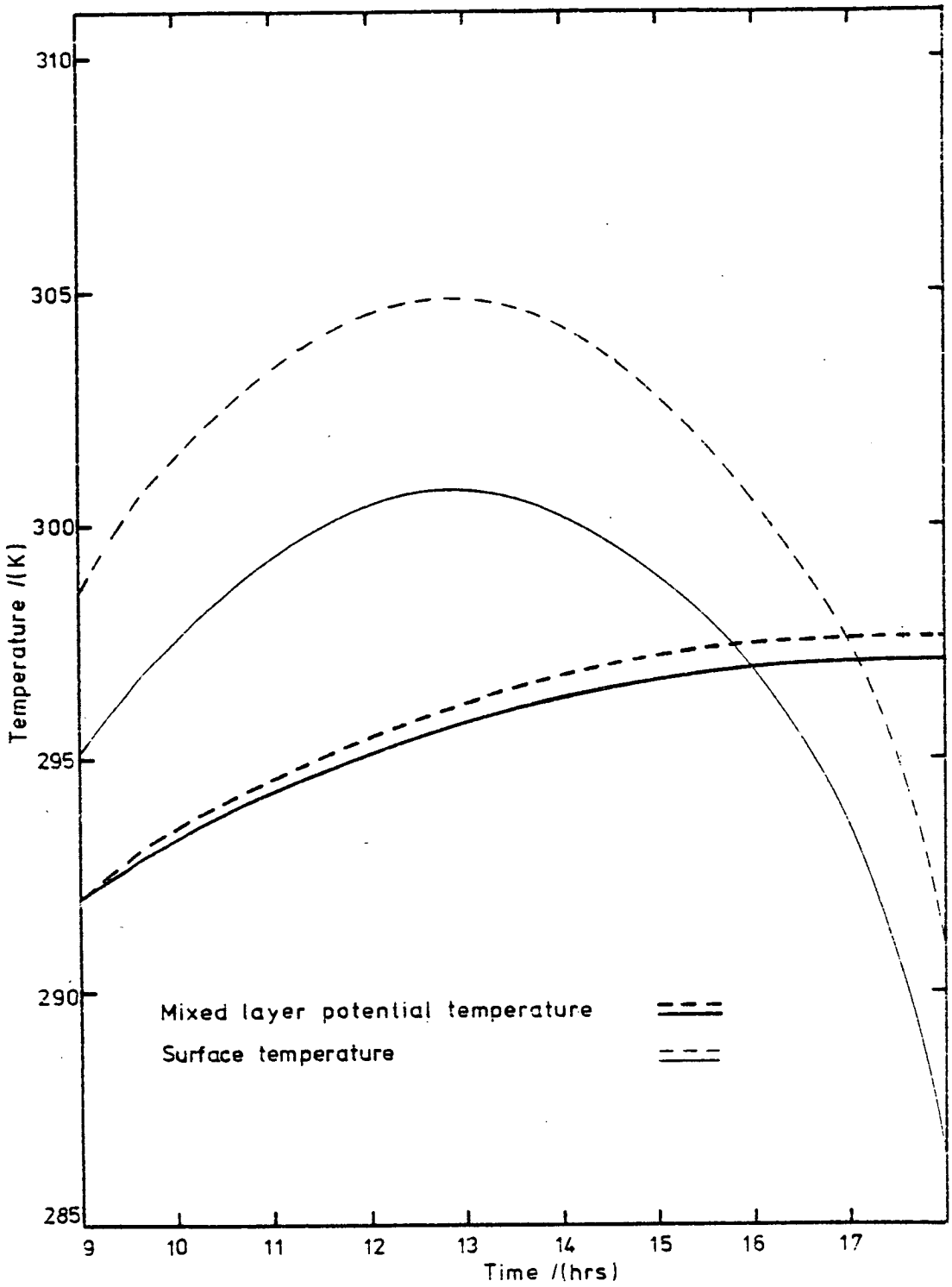

Figure 4.13 The Mixed Layer Potential Temperature and Surface Temperature Calculated by the Numerical Model for Mixed Layer Optical Depths of 0.0001 (---) and 0.3 (——) Over the Moist Surface (Halstead Parameter = 0.1)

Energy Input/(MJ)	Optical Depth	
	0.0001	0.3
Sensible heat to mixed layer	4.70	4.15
Latent heat to mixed layer	3.61	2.40
Heat to soil	0.79	0.49
Total	9.10	7.04
Turbulent heating of mixed layer	4.65	2.39
Radiative heating of mixed layer	0.001	1.59

Table 4.9 Calculated Energy Budget for the Mixed Layer and Soil Over the Six Hours from 09 to 15 Hours for a 'Moist' Surface, Halstead Parameter = 0.1

surface temperatures mentioned above. A further consequence of the reduced surface temperatures is a reduced loss of energy from the surface by longwave emission which results in an increase to the total input to the mixed layer and soil layer over the six hours. A comparison of the results from the two moderately turbid integrations (τ = 0.3) shows that the radiative heating, which accounts for a greater proportion of the total sensible heat input to the mixed layer when the surface is more moist, tends to reduce the effects of the increased surface moisture on the total heating of the mixed layer. This can be regarded, alternatively as the reduction of the sensible heat input to the mixed layer (caused by an increase in the optical depth of that layer) is itself smaller when the earth's surface is more moist.

4.6 CONCLUDING REMARKS

The effect of absorption of solar radiation by aerosol within a convective boundary layer on entrainment at the top of the layer has been examined using two theoretical models. The hypothesis that the stabilising effect of the absorption would, given the simple parameterization of the turbulent kinetic energy budget within the mixed layer, lead to a decrease in the entrained heat flux ratio has been shown to be correct.

Results from the analytic model show that addition of an absorbing aerosol to the mixed layer results in a reduction of the entrained heat flux ratio and of the sensible heat flux at the surface, but that the overall effect of the absorption is likely to be to increase the rates at which the mixed layer deepens and warms up. The same

model was used to show that the possible range over which the entrained flux ratio could vary as a result of aerosol absorption is restricted by a constraint on the change in the mixed layer potential energy due to direct heating and the buoyancy generated turbulent kinetic energy. The importance of the initial mixed layer depth and potential temperature to the subsequent development were also examined, and it was found that the solutions to the model equations tend towards a form which depends only on the potential temperature gradient above the mixed layer, the optical depth of the mixed layer and the ratio of the sensible heat flux at the surface to the absorbed shortwave energy. Nevertheless, initial conditions which are far removed from the asymptotic solution retard the development of the mixed layer.

The results from the numerical model predict that addition of aerosol leads to shallower, cooler mixed layers, in contrast to the results from the analytic model. This apparent inconsistency between the two sets of results stems from two causes. The inclusion of scattering of incoming radiation in the numerical model means that, for a given mixed layer optical depth, the absorption calculated by the numerical model is less than that implied in the analytic model, and the shortwave energy absorbed at the surface is greater. At the same time scattering reduces the total energy input to the mixed layer and soil. Secondly the assumption made in the derivation of the analytic model that the ratio of the sensible heat flux at the surface to the solar energy absorbed there is independent of the optical depth of the mixed layer is not made in the numerical model and the results show that increasing the optical depth from 0.0001 to 0.3 reduces this ratio to about 80% of its original value. These two effects

both imply a reduction in the rate of growth of a turbid mixed layer and, in fact, the numerical results are consistent with the analytic model in the sense that the criterion derived in chapter two (page 81) to determine whether or not a turbid mixed layer deepens more slowly than a comparable non-turbid layer is fulfilled.

It has been shown that, due to the absorption of radiation by aerosol, the entrained heat flux ratio varies during the day, increasing to a broad maximum towards noon and decreasing again in the afternoon. However the overall effect of this variation on the development of the mixed layer is relatively small.

The numerical model described here suffers from a number of shortcomings. The two-stream approximation used to calculate the shortwave fluxes within the mixed layer could be improved, at small solar zenith angles especially, by using the hybrid approximation described by Meador and Weaver (1980) instead of the quadrature approximation. It would then, perhaps, be of interest to include a more detailed specification of the optical properties of the aerosol, particularly their dependence on the relative humidity. The major deficiency which has already been mentioned, is the neglect of Rayleigh scattering within the mixed layer. Because the total effect of shortwave convergence on the entrainment ratio and growth of the mixed layer is small this neglect should not affect the conclusion that the variation of the entrainment ratio is small enough to be ignored and these modifications while permitting a more accurate simulation of real atmospheric boundary layers, are unlikely to necessitate modification of this conclusion.

The results described here, obtained from a one-dimensional, Boussinesq, mixed layer model, are applicable to lightly polluted, dry, convective boundary layers over dry surfaces. The entrainment model is formulated in terms of the virtual potential temperature and could, therefore, be used to model much moister layers. However, no check is made to ensure that the mixed layer remains unsaturated. Extending the model to include partly, or totally, cloudy layers would require extensive modification and a number of difficulties would have to be solved, in particular that of determining the cloud fraction.

The Halstead parameter is not a widely used measure of surface evaporation, and it would be preferable to parameterise the surface latent heat flux in terms of a quantity which can be related more directly to the physical state of the surface. An obvious possibility would be to use the resistance formalism.

The entrained heat flux at the bottom of the capping inversion has been parameterised in the simplest possible way. The partitioning of turbulent kinetic energy between the various processes which are important at the top of the mixed layer is not well understood, and results from the various, more sophisticated, entrainment parameterisations do not differ greatly over the range of interest of the governing variables. However, the available turbulent kinetic energy determines the development of a turbid layer, particularly in governing when the well-mixed profiles can no longer be maintained.

The radiation scheme used here could be improved in a number of ways. Radiative absorption at visible and infra-red wavelengths by atmospheric gases is ignored in the present model. Since water-vapour is the most important absorber in the infra-red part of the spectrum, the effect of neglecting long-wave absorption will be small in the integrations described here, which were all carried out for very dry mixed layers. Gaseous absorption of visible energy, which has also been neglected, would be likely

to have a qualitatively similar effect on the development of the convective boundary layer to that of aerosol. The contribution of gaseous absorption could be included in the model by redefining the optical parameters of the mixed layer, optical depth, backscattering ratio, and single scattering albedo, to be appropriately weighted means of those for the aerosol and absorbing gases individually.

The accuracy of the radiation scheme would be further improved, particularly at greater optical depths, by using the hybrid approximation referred to in chapter three, and by treating the mixed layer as several slabs within each of which the radiative transfer equation is solved. This would allow the optical parameters to be varied through the depth of the mixed layer. Although the representation of the aerosol is very much simplified, the assumptions made in other parts of the radiation scheme are likely to be of greater consequence and, in any development of the model should be examined and, if possible, improved first.

APPENDIX 1

RADIATION IN A CLEAN DRY RAYLEIGH ATMOSPHERE

The function $S(\tau)$ defined by Diermendjian and Sekara (1954), where is the optical depth in a clean dry Rayleigh atmosphere, is approximated by a sixth order polynomial

$$S(\tau) = a_0 + \sum_{n=1}^{6} a_n \tau^n$$

and the coefficients a_n are

$a_0 = -5.07343 \times 10^{-4}$

a_1	= 1.02812	a_4	= - 15.64559
a_2	= - 2.40796	a_5	= - 15.59665
a_3	= 7.74740	a_6	= - 5.91781

The function $Z(\tau,\mu)$ is calculated by linear interpolation between the values held in the accompanying table. The second variable, μ, represents the cosine of the solar zenith angle.

VALUES OF $Z(\tau,\mu)$

μ	Optical Depth, τ									
	0	0.01	0.02	0.04	0.06	0.08	0.1	0.12	0.14	0.16
0.0	1.000	0.4865	0.4763	0.4601	0.4466	0.4348	0.4242	0.4145	0.4056	0.3973
0.025	1.000	0.8353	0.7230	0.5932	0.5284	0.4930	0.4711	0.4557	0.4437	0.4335
0.05	1.000	0.9098	0.8347	0.7219	0.6437	0.5883	0.5482	0.5185	0.4957	0.4776
0.075	1.000	0.9529	0.9092	0.8343	0.7721	0.7202	0.6766	0.6397	0.6083	0.5814
0.1	1.000	0.9762	0.9524	0.9091	0.8698	0.8339	0.8010	0.7709	0.7433	0.7179
0.3	1.000	0.9842	0.9677	0.9375	0.9091	0.8824	0.8573	0.8336	0.8112	0.7901
0.4	1.000	0.9882	0.9756	0.9524	0.9302	0.9091	0.8889	0.8677	0.8511	0.8334
0.5	1.000	0.9907	0.9804	0.9615	0.9434	0.9259	0.9091	0.8928	0.8771	0.8620
0.6	1.000	0.9926	0.9836	0.9677	0.9524	0.9375	0.9231	0.9091	0.8955	0.8823
0.7	1.000	0.9935	0.9859	0.9722	0.9589	0.9459	0.9333	0.9211	0.9091	0.8985
0.8	1.000	0.9944	0.9876	0.9756	0.9669	0.9524	0.9412	0.9303	0.9196	0.9092
0.9	1.000	0.9950	0.9890	0.9783	0.9677	0.9575	0.9474	0.9376	0.9279	0.9185
1.0	1.000	0.9956	0.9901	0.9804	0.9709	0.9616	0.9524	0.9435	0.9347	0.9261
	0.18	0.2	0.3	0.4	0.5	0.6	0.7	0.8	0.9	1.0
0.0	0.3895	0.3823	0.3511	0.3263	0.3060	0.2897	0.2726	0.2591	0.2479	0.2362
0.025	0.4244	0.4161	0.3815	0.3521	0.3300	0.3111	0.2946	0.2800	0.2667	0.2544
0.05	0.4630	0.4506	0.4072	0.3770	0.3527	0.3322	0.3145	0.2989	0.2850	0.2714
0.075	0.5109	0.4937	0.4356	0.3996	0.3727	0.3506	0.3317	0.3152	0.3005	0.2873
0.1	0.5581	0.5379	0.4672	0.4238	0.3960	0.3687	0.3484	0.3308	0.3153	0.3104
0.2	0.6945	0.6729	0.5863	0.5250	0.4796	0.4444	0.4162	0.3928	0.3729	0.3555
0.3	0.7702	0.7513	0.6706	0.6077	0.5576	0.5169	0.4832	0.4548	0.4305	0.4093
0.4	0.8164	0.8002	0.7283	0.6691	0.6197	0.5777	0.5422	0.5113	0.4844	0.4606
0.5	0.8474	0.8333	0.7695	0.7150	0.6681	0.6274	0.5917	0.5602	0.5323	0.5072
0.6	0.8695	0.8571	0.8001	0.7503	0.7062	0.6676	0.6329	0.6018	0.5738	0.5483
0.7	0.8861	0.8751	0.8237	0.7780	0.7372	0.7005	0.6673	0.6371	0.6096	0.5845
0.8	0.8990	0.8890	0.8424	0.8004	0.7624	0.7279	0.6963	0.6672	0.6405	0.6157
0.9	0.9092	0.9002	0.8576	0.8188	0.7834	0.7509	0.7209	0.6931	0.6673	0.6432
1.0	0.9176	0.9094	0.8701	0.8342	0.8011	0.7705	0.7420	0.7155	0.6907	0.6674

APPENDIX 2

THE TWO STREAM APPROXIMATION: THE QUADRATURE METHOD

The quadrature method facilitates the solution of the two stream equations by replacing the integral of the scattering phase function and the integral of the product $p(\mu,\mu')I(\tau,\mu')$ by an expression based on a two point Gaussian quadrature.

$$\int_0^1 p(\mu,\mu')d\mu' = p(\mu,\mu_1)$$

$$\int_0^1 p(\mu,\mu')I(\tau,\mu')d\mu' = p(\mu\ \mu_1)I(\tau\ \mu_1) + p(\mu-\mu_1)I(\tau-\mu_1)$$

where $\mu_1 = 1/\sqrt{3}$

Then the hemispheric integrals $I^{\pm}(\tau)$ can be written as

$$I^{\pm}(\tau) = \int_0^1 \mu I(\tau,\pm\mu)d\mu = \mu_1 I(\tau,\mu_1)$$

and the integral which occurs in the definition of $\frac{dI^{\pm}}{d\tau}(\tau)$ is written

$$\int_0^1\int_{-1}^1 p(\mu,\mu')I(\tau,\mu')d\mu'd\mu = \frac{2w_o}{\mu_1}\left[(1-\beta_1)I^{+}(\tau) + \beta_1 I^{-}(\tau)\right]$$

where $\beta_1 = \frac{1}{2w_o}\int_0^1 p(\mu_1,-\mu')d\mu' = \frac{1}{2w_o}p(\mu_1,-\mu_1)$

similarly that occurring in the definition of the derivative of $I^{-}(\tau)$ becomes

$$\int_0^1\int_1^1 p(\mu,-\mu')I(\tau,\mu')d\mu'd\mu' = \frac{2w_o}{\mu_1}\left[\beta_1 I^{+}(\tau) + (1-\beta_1)I^{-}(\tau)\right]$$

The standard quadrature method, which has been used here, makes

use of one further simplication. The scattering phase function may be expanded into a series of Legendre polynomials of which only the first two terms are retained so that the phase function is written

$$p(\mu,\mu') = w_o(1 + 3g\mu\mu')$$

so that $\beta_1 = \frac{1}{2}(1 - g)$

Meador and Weaver (1980) demonstrate that the accuracy of the solutions is increased, especially for large optical depths, if the phase function is evaluated without truncating the series.

The constants in equations 3.4 and 3.5 can, using the relations presented here, be evaluated as follows:

$$\gamma_1 = \frac{1}{\mu_1}[1 - w_o(1-\beta_1)] \qquad \gamma_2 = w_o\beta_1/\mu_1$$

$$\gamma_3 = \frac{1}{2w_o} p(\mu_o - \mu_1) \qquad \gamma_4 = 1 - \gamma_3$$

$$\alpha^2 = (\gamma_1^2 - \gamma_2^2)$$

$$\alpha_1^2 = \frac{\gamma_2}{\gamma_1+\alpha} \qquad \alpha_2^2 = \frac{\gamma_2}{\gamma_1-\alpha}$$

$$\beta_1 = -\pi F w_o \frac{\gamma_2\gamma_3 + \gamma_2\gamma_4 - \gamma_3/\mu_o}{1/\mu_o^2 - \alpha^2}$$

$$\beta_2 = -\pi F w_o \frac{\gamma_2\gamma_3 + \gamma_2\gamma_4 - \gamma_4/\mu_o}{1/\mu_o^2 - \alpha^2}$$

APPENDIX 3

SOLAR GEOMETRY

The daily variation of the solar zenith angle at a particular latitude Φ is calculated from the sun's declination which varies by a maximum of $\frac{1}{2}°$ over the course of 24 hours. The sun's declination, δ, depends only on the time of year and is calculated from the formula (see Paltridge and Platt, 1976).

$$\begin{aligned}\delta = {} & 0.006918 - 0.39912\cos\theta + 0.070257\sin\theta \\ & - 0.006758\cos 2\theta + 0.000907\sin 2\theta \\ & - 0.002697\cos 3\theta + 0.001480\sin 3\theta\end{aligned}$$

where the angle θ is defined by

$$\theta = \frac{2\pi}{365} \times \text{day number}$$

The day number is defined as 1 on January 1st and increased by one each day to a maximum of 365 on December 31st.

This formula is accurate to better than three minutes of arc.

Once the solar declination for a particular day is known, the zenith angle θ at latitude Φ and local solar time t (hours) is

$$\theta = \cos^{-1}\left[\sin\delta\sin\Phi + \cos\delta\cos\Phi\cos\left(\frac{2\pi}{360}\,15(t-12)\right)\right]$$

The corrections, for longitude and the ellipticity of the earth's orbit (quantified in the 'Equation of time') are relatively simple but were not felt to be needed.

REFERENCES

ARTAZ, M. A. and ANDRÉ, J. C. (1980). Similarity Studies of Entrainment in Convective Mixed Layers. Boundary Layer Meteorology, 19, 51-56.

ATWATER, M. A. (1971). Radiative Effects of Pollutants in the Atmospheric Boundary. Journal of the Atmospheric Sciences, 28, 1367-1373.

BALL, F. K. (1960). Control of Inversion Height by Surface Heating. Quarterly Journal of the Royal Meteorological Society, 86, 483-494.

BARKER, E. J. and BAXTER, T. L. (1975). A Note on the Computation of Atmospheric Surface Layer Fluxes for Use in Numerical Models. Journal of Applied Meteorology, 14, 620-622.

BENOIT, R. (1976). A Comprehensive Parameterization of the Atmospheric Boundary Layer for General Circulation Models. Ph.D. thesis, McGill University and N.C.A.R.

BUSINGER, J. A., WYNGAARD, J. C., IZUMI, Y. and BRADLEY, E. F. (1971). Flux Profile Relationships in the Atmospheric Surface Layer. Journal of the Atmospheric Sciences, 28, 181-189.

CARSON, D. J. (1973). The Development of a Dry Inversion-Capped Convectively Unstable Boundary Layer. Quarterly Journal of the Royal Meteorological Society, 99, 450-467.

CARSON, D. J. and SMITH, F. B. (1974). Thermodynamic Model for the Development of a Convectively Unstable Boundary Layer. Advances in Geophysics, 18A, 111-124.

CATTLE, H. and WESTON, K. J. (1975). Budget Studies of Heat Flux Profiles in the Convective Boundary Layer over Land. Quarterly Journal of the Royal Meteorological Society, 101, 353-363.

CAUGHEY, S. J. and KAIMAL, J. C. (1977). Heat Flux in the Convective Boundary Layer. Quarterly Journal of the Royal Meteorological Society, 103, 811-815.

CAUGHEY, S. J. and PALMER, S. G. (1979). Some Aspects of Turbulence Structure through the Depth of the Convective Boundary Layer. Quarterly Journal of the Royal Meteorological Society, 105, 811-827.

CAUGHEY, S. J. and WYNGAARD, J. C. (1979). The Turbulence Kinetic Energy Budget in Convective Conditions. Quarterly Journal of the Royal Meteorological Society, 105, 231-239.

CHANDRASEKHAR and ELBERT, D. W. (1954).The Illumination and Polarization of the Sunlit Sky on Rayleigh Scattering. Transactions of the American Philosophical Society, 44,

CHOU, Ming-Dah and ARKING, A. (1980). Computation of Infra-Red Cooling Rates in the Water Vapour Bands. Journal of the Atmospheric Sciences, 37, 855-867.

CLARKE, R. H., DYER, A. J., BROOK, R. R., REID, D. G. and TROUP, A. J. (1971). The Wangara Experiment: Boundary Layer Data. CSIRO Div. of Meteorological Physics, Technical Paper No.19.

CURRAN, (1978). Comment on the paper 'Vertical Heat Flux in the Convective Boundary Layer' by S. J. Caughey and J. C. Kaimal. Quarterly Journal of the Royal Meteorological Society, 104, 1003-1004.

DEARDORFF, J. W. (1972). Parameterization of the Planetary Boundary Layer for Use in General Circulation Models. Monthly Weather Review, 100, 93-106.

DEARDORFF, J. W. (1974). Three Dimensional Numerical Study of the Height and Mean Structure of a Heated Planetary Boundary Layer. Boundary Layer Meteorology, 7, 81-106.

DEARDORFF, J. W. (1980). Cloudtop Entrainment Instability. Journal of the Atmospheric Sciences, 37, 131-147.

DEACON, E. L. (1969). Physical Processes Near the Surface of the Earth. In World Survey of Climatology. H. Flohn (ed), Academic Press.

DIERMENDJIAN, D. and SEKARA, Z. (1954). Global Radiation Resulting from Multiple Scattering in a Rayleigh Atmosphere. Tellus, 6, 382-398.

DUBOSCLARD, G. (1980). Comparison between Observed and Predicted Values for the Entrainment Coefficient in the Planetary Boundary Layer. Boundary Layer Meteorology, 18, 473-483.

DYER, A. J. (1974). A Review of Flux-Profile Relationships. Boundary Layer Meteorology, 7, 363-72.

DYER, A. J. and HICKS. B. B. (1970). Flux-Gradient Relationships in the Constant Flux Layer. Quarterly Journal of the Royal Meteorological Society, 96, 715-721.

ELTERMANN, L. and TOOLIN, R. B. (1965). Atmospheric Optics. In. Handbook of Geophysics and Space Environments. AFCRL, U.S. Airforce, Beford, Mass. S. L. Valley (ed).

GLAZIER, J., MONTEITH, J. L. and UNSWORTH, M. H. (1976). Effects of Aerosol on the Local Heat Budget of the Lower Atmosphere. Quarterly Journal of the Royal Meteorological Society, 102, 95-102.

GREEN, J.S.A. and DALU, G. A. (1980). Mesoscale Energy Generated in the Boundary Layer. Quarterly Journal of the Royal Meteorological Society, 106, 721-726.

HEIDT, F. D. (1977). The Growth of the Mixed Layer in a Stratified Fluid. Boundary Layer Meteorology, 12, 439-461.

HOUGHTON, J. T. (1974). The Physics of Atmospheres. Cambridge University Press.

KAHN, P. H. and BUSINGER, J. A. (1979). The Effect of Radiative Flux Divergence on Entrainment of a Saturated Convective Boundary Layer. Quarterly Journal of the Royal Meteorological Society, 105, 303-306.

KONDRATYEV, K. Ya. (1969). Radiation in the Atmosphere. Academic Press.

KONDRATYEV, K. Ya., WELCH, R. M., COX, S. K., GRISHECHKIN, V. S., IVANOV, V. A., PROKOFYEV, M. A., ZHVALEV, V. F. and VASILEJEV, O. B. (1981). Determination of Vertical Profiles of Aerosol Size Spectra from Aircraft Radiative Flux Measurements. Retrieval of Spherical Particle Size Distributions. Journal of Geophysical Research, 86, 9783-9793.

LACIS, A. A. and HANSEN, J. E. (1974). A Parameterization for the Absorption of Solar Radiation in the Earth's Atmosphere. Journal of the Atmospheric Sciences, 31, 118-133.

LENSCHOW, D. H. (1970). Airplane Measurements of Planetary Boundary Layer Structure. Journal of Applied Meteorology, 9, 874-84.

LENSCHOW, D. H. and JOHNSON, W. B. (1968). Concurrent Airplane and Balloon Measurements of Atmospheric Boundary-Layer Structure over a Forest. Journal of Applied Meteorology, 7, 79-89.

LETTAU, H. H. and DAVIDSON, B. (1957). Exploring the Atmosphere's First Mile: Vol. 2. Site Description and Data Tabulation. Pergamon Press.

LILLY, D. K. (1968). Models of Cloud Topped Mixed Layers under a Strong Inversion. Quarterly Journal of the Royal Meteorological Society, 98, 292-309.

MAGRAAF, W. A. and GRIGGS, M. (1969). Aircraft Measurements and Calculations of the Total Downward Flux of Solar Radiation as a Function of Altitude. Journal of the Atmospheric Sciences, 26, 469-477.

MAHRT, L. (1979). Penetrative Convection at the Top of a Growing Boundary Layer. Quarterly Journal of the Royal Meteorological Society, 105, 469-486.

MAHRT, L. and LENSCHOW, D. H. (1976). Growth Dynamics of the Convective Layer. Journal of the Atmospheric Sciences, 33, 41-51.

MANINS, P. C. and TURNER, J. S. (1978). The Relation between the Flux Ratio and Energy Ratio in Convectively Mixed Layers. Quarterly Journal of the Royal Meteorological Society, 104, 39-45.

MANTON, M. J. (1978). On Dry Penetrative Convection. Boundary Layer Meteorology, 14, 301-322.

MEADOR, W. E. and WEAVER, W. R. (1980). Two-Stream Approximations to Radiative Transfer in Planetary Atmospheres: A Unified Description of Existing Methods and a New Improvement. Journal of the Atmospheric Sciences, 37, 630-643.

MONTEITH, J. L. (1973). Principles of Environmental Physics. Edward Arnold.

MONTEITH, J. L. and SZIECZ, G. (1961). The Radiation Balance of Bare Soil and Vegetation. Quarterly Journal of the Royal Meteorological Society, 87, 159-170.

MOORES, W. H., CAUGHEY, J., READINGS, C. J., MILFORD, J. R., MANSFIELD, D. A., ABDULLA, S., GUYMER, T. H. and JOHNSTON, W. B. (1979). Measurements of Boundary Layer Structure and Development over S.E. England Using Aircraft and Tethered Balloon Instrumentation. Quaterly Journal of the Royal Meteorological Society, 105, 397-422.

MYRUP, L. O. (1969). A Numerical Model of the Urban Heat Island. Journal of Applied Meteorology, 10, 703-714.

NICHOLLS, S. (1977). Measurements of Turbulent by an Instrumented Aircraft in a Convective Atmospheric Boundary Layer over the Sea. Quarterly Journal of the Royal Meteorological Society, 104, 653-676.

PALTRIDGE. G. W. and PLATT, C.M.R. (1973). Absorption and Scattering of Radiation by an Aerosol Layer in the Free Atmosphere. Journal of the Atmospheric Sciences, 30, 734-735.

PALTRIDGE, G. W. and PLATT, C.M.R. (1976). Radiative Processes in Meteorology and Climatology. Elsevier.

PASQUILL, F. (1949). Eddy Diffusivity of Water Vapour and Heat Near the Ground. Proceeding of the Royal Society of London. Series A, 198, 116.

PAULSON, C. A. (1970). The Mathematical Representation of Wind Speed and Temperature Profiles in the Unstable Atmospheric Surface Layer. Journal of Applied Meteorology, 9, 857-861.

RAYMENT, R. and READINGS, C. J. (1974). A Case Study of the Structure and Energetics of an Inversion. Quaterly Journal of the Royal Meteorological Society, 100, 221-233.

READINGS, C. J., GOLTON, E. and BROWNING, K. A. (1973). Fine Scale Structure and Mixing within an Inversion. Boundary Layer Meteorology, 4, 275-287.

SELLERS, W. D. (1965). Physical Climatology. University of Chicago Press.

SMITH AND CARSON, D. J. (1977). Some Thoughts on the Specification of the Boundary Layer Relevant to Numerical Modelling. Boundary Layer Meteorology, 12, 307-330.

SMITH, F. B. and HUNT, R. D. (1978). Meteorological Aspects of the Transport of Pollution over Long Distances. Atmospheric Environment, 12, 461-467.

SNEDDON, I. (1956). Elements of Partial Differential Equations. McGraw-Hill.

STULL, R. B. (1973). Inversion Rise Model Based on Penetrative Convection. Journal of the Atmospheric Sciences, 30, 1092-1099.

STULL, R. B. (1976). The Energetics of Entrainment Across a Density Interface. Journal of the Atmospheric Sciences, 33, 1260-1267.

SWINBANK, W. C. (1964). The Exponential Wind Profile. Quarterly Journal of the Royal Meteorological Society, 90, 119-135.

TENNEKES, H. and LUMLEY, J. L. (1969). A First Course in Turbulence. M.I.T. Press.

TENNEKES, H. (1973). A Model for the Dynamics of an Inversion Above a Convective Boundary Layer. Journal of the Atmospheric Sciences, 30, 558-567.

THEKAEKARA, M. P. and DRUMMOND, A. J. (1971). Standard Values for the Solar Constant and its Spectral Components. Nature, Physical Science, 229, 6-9.

TOWNSEND, A. A. (1956). The Structure of Turbulent Shear Flows. Cambridge University Press.

TURNER, S. (1973). Buoyancy Effects in Fluids. Cambridge University Press.

TWOMEY, S. (1977). Atmospheric Aerosols. Elsevier.

VENKATRAM, A. and VISKANTA, R. (1977). Effects of Aerosol-Induced Heating on the Convective Boundary Layer. Journal of the Atmospheric Sciences, 34, 1918-1933.

WELCH, R. and ZDUNKOWSKI, W. (1976). A Radiation Model of the Polluted Atmospheric Boundary Layer. Journal of the Atmospheric Sciences, 33, 2170-2184.

WOOD, N.L.H. (1977). A Field Study on the Representativeness of Turbulent Fluxes of Heat and Water Vapour at Various Sites in Southern England. Quarterly Journal of the Royal Meteorological Society, 103, 617-624.

ZEMAN, O. and TENNEKES, H. (1977). Parameterization of the Turbulent Energy Budget at the Top of the Daytime Atmospheric Boundary Layer. Journal of the Atmospheric Sciences, 34, 111-123.

ZILITINKEVICH. (1970). The Dynamics of the Atmospheric Boundary Layer Leningrad. (Meteorological Office translation No. 647).

ZDUNKOWSKI, W. F., WELCH, R. M. and PAEGLE, J. (1976). One-Dimensional Numerical Simulation of the Effects of Air Pollution on the Planetary Boundary Layer. Journal of the Atmospheric Sciences, 33, 2399-2414.